In Vitro Evaluation of Amaryllidaceae Alkaloids Identifies Pseudolycorine as an Antifibrotic Lead for Arthrofibrosis Following Total Knee Arthroplasty

Sara Alzaanin

November 2026

A thesis submitted for the degree of Master of Philosophy of
The Australian National University

© Copyright by Sara Alzaanin 2026
All Rights Reserved

Declaration

This thesis contains no material which has been accepted for the award of any other degree or diploma in any university. To the best of the author's knowledge, it contains no material previously published or written by another person, except where due reference is made in the text.

Sara Alzaanin

November 2026

Acknowledgements

First and foremost, I would like to praise Allah, Lord of the Universe, who has given me the strength and guidance to complete this thesis.

I am profoundly grateful to my primary supervisor, Associate Professor Rachel Li, for her unwavering support throughout this project. Whenever I faced difficulties in my experiments, she offered insightful suggestions that helped me find my way forward. More than a supervisor, she has been a source of encouragement and growth, always creating opportunities for me to develop my skills both professionally and personally. Outside the laboratory, her warmth, kindness, and conversations brought me comfort and joy, and I will always treasure the time I have spent under her guidance.

I would also like to express my heartfelt thanks to Dr. Donghai Zhang, who helped me build my laboratory skills. His calm reassurance and willingness to help made a lasting impression on me, and I am fortunate to have had him as a mentor.

My sincere gratitude goes to Professor Paul Smith AM, Chair of my supervisory panel, for his invaluable clinical insight, his enduring commitment to advancing orthopaedic research, and his encouragement throughout this journey.

I am also deeply thankful to Dr. Arash Dastjerdi, whose passion for research inspired and motivated me throughout this project.

I would also like to thank Associate Professor Amee George, Dr. Jinshu He, and Dr. Koula Diamandis of the ANU Centre for Therapeutic Discovery for their generous assistance with the Opera Phenix high-content imaging system. I am truly grateful for the time and invaluable technical advice they shared with me.

Finally, I am grateful to all members of the Trauma and Orthopaedic Research Unit (TORU) for their support, camaraderie, and insightful suggestions.

Abstract

Arthrofibrosis following total knee arthroplasty (TKA) is a debilitating fibroproliferative condition characterised by excessive periarticular and intra-articular scar tissue formation, leading to persistent pain, restricted range of motion, and ultimately significant deterioration in quality of life. Despite affecting an estimated 3–10% of TKA patients, no pharmacological therapy is currently available, and existing mechanical and surgical interventions are associated with unpredictable outcomes and significant risks. With TKA rates projected to rise substantially in coming decades, there is an urgent and unmet clinical need for targeted pharmacological therapies capable of modulating the underlying fibrotic signalling pathways.

This study evaluated the in vitro antifibrotic activity of four Amaryllidaceae alkaloids (galanthine, lycorenine, pseudolycorine, and powelline) isolated from Amazonian bulbs, using the Scar-in-a-Jar phenotypic assay. Compounds were screened at 1 µM and 10 µM for their capacity to inhibit collagen type I (Col-I) deposition and α-smooth muscle actin (α-SMA) expression in fibroblasts, the two hallmark markers of the fibrotic phenotype. Pseudolycorine demonstrated the most consistent and potent inhibitory activity across both fibrotic markers and both concentrations tested. Dose-response analysis under Scar-in-a-Jar conditions established an IC_{50} of 1.84 µM for α-SMA inhibition. To elucidate the potential mechanism of action, pseudolycorine-treated and vehicle control fibroblasts were profiled using the RT^2 Profiler Human Fibrosis PCR Array, targeting 84 fibrosis-associated genes. Pseudolycorine produced a selective transcriptional response characterised by significant downregulation of *MMP14, TIMP4, PLAU, CCL11*, and *CCR2*, and a marked upregulation of *CEBPB*.

The downregulation of *MMP14* and *PLAU* suggests that pseudolycorine may attenuate pericellular proteolysis and latent TGF-β1 activation. Concurrently, the reduction in *CCL11* expression points to a suppression of TGF-β-independent fibroblast stimulation and the recruitment of inflammatory cells. Furthermore, the downregulation of *CCR2*

likely limits the trafficking of fibrogenic precursors and disrupts the autocrine pro-fibrotic loops that sustain the fibrotic niche. Most strikingly, pseudolycorine markedly upregulated *CEBPB*, which encodes the transcription factor C/EBPβ, a critical and context-dependent regulator of both inflammatory and fibrosis-associated gene networks. The selective nature of the transcriptional response, with most ECM remodelling genes and all TGF-β/SMAD pathway transcripts remaining unchanged, suggests a defined rather than generalised mechanism of action.

To the best of the author's knowledge, this is the first study to report the antifibrotic potential of pseudolycorine. The identification of pseudolycorine as an antifibrotic alkaloid provides proof-of-concept for the Amaryllidaceae family as a source of pharmacological leads for fibrosis, a disease area where therapeutic options remain severely limited. Future work should prioritise protein-level confirmation of the transcriptomic findings and, ultimately, in vivo assessment in an established animal model of post-surgical arthrofibrosis. Such steps are essential to establish pseudolycorine as a viable therapeutic candidate for post-TKA arthrofibrosis.

List of Abbreviations

TKA: Total Knee Arthroplasty

TGF-β: Transforming Growth Factor-β

ECM: Extracellular Matrix

IFP: Infrapatellar Fat Pad

MAPK: Mitogen-Activated Protein Kinase

PI3K: Phosphatidylinositol 3-Kinase

MUA: Manipulation Under Anaesthesia

AD: Arthroscopic Debridement

OD: Open Debridement

pTKA: Primary Total Knee Arthroplasty

rTKA: Revision Total Knee Arthroplasty

PASS: Patient-Actuated Serial Stretch

α-SMA: Alpha-Smooth Muscle Actin

ROM: Range of Motion

DMEM: Dulbecco's Modified Eagle Medium

PBS: Phosphate-Buffered Saline

FBS: Fetal Bovine Serum

PSN: Penicillin-Streptomycin-Neomycin

MMC: Macromolecular Crowding

Col-I: Collagen Type I

RT-qPCR: Reverse-Transcription Quantitative Polymerase Chain Reaction

cDNA: complementary DNA

DMSO: Dimethyl Sulfoxide

GAPDH: Glyceraldehyde-3-phosphate dehydrogenase

ROS: Reactive Oxygen Species

PDGF: Platelet-Derived Growth Factor

Interleukin: IL

MFI: Mean Fluorescence Intensity

ROI: Region of Interest

CEBPB: CCAAT/enhancer-binding protein beta

CCL11: Chemokine (C-C motif) Ligand 11

CCR2: C-C motif Chemokine Receptor 2

TIMP: Tissue Inhibitor of Metalloproteinase

MMP: Matrix Metalloproteinase

PLAU: Plasminogen Activator, Urokinase

uPA: Urokinase Plasminogen Activator

OA: Osteoarthritis

IC_{50}: Half-Maximal Inhibitory Concentration

RT: Room Temperature

NSAIDs: Non-Steroidal Anti-Inflammatory Drugs

BCL2: B-cell CLL/Lymphoma 2

FASLG: Fas Ligand

Table of Contents

Declaration ..... **i**
Acknowledgements ..... **ii**
Abstract ..... **iv**
List of Abbreviations ..... **vi**
Table of Contents ..... **ix**
List of Figures ..... **xiii**
List of Tables ..... **xvi**
Chapter 1 Introduction **17**
1.1 Thesis outline 18
1.2 Arthrofibrosis 18
1.3 Arthrofibrosis rates post-TKA 20
1.4 Arthrofibrosis pathogenesis 21
1.4.1 Arthrofibrosis as a dysregulated wound healing response 21
1.4.2 TGF-β and associated fibrogenic mediators 22
1.4.3 Effector cells in arthrofibrosis 23
1.5 Risk factors for arthrofibrosis 26
1.5.1 Preoperative risk factors 26
1.5.2 Intraoperative risk factors 28
1.5.3 Postoperative risk factors 29
1.6 Conservative treatment of arthrofibrosis 29
1.6.1 Postoperative physiotherapy 29
1.6.2 Adjuncts to physiotherapy 32
1.7 Surgical management of arthrofibrosis 34
1.7.1 Manipulation under anaesthesia (MUA) 34
1.7.2 Arthroscopic Debridement (AD) 38
1.7.3 Open Debridement (OD) 40
1.7.4 Revision TKA (rTKA) 42
1.8 Summary 44
Chapter 2 Research Objectives and Significance **47**
2.1 Rationale for candidate compound selection 47
2.1.1 Amaryllidaceae alkaloids as a chemically distinct and pharmacologically diverse family 47

2.1.2 Candidate compounds: Galanthine, lycorenine, pseudolycorine, and powelline 48
2.2 Hypothesis 49
2.3 Aims 49
2.4 Research questions 50
2.5 Research plan 50
2.6 Significance 51
2.7 Summary 52
Chapter 3 Materials and Methods 55
3.1 Materials 55
3.1.1 Candidate alkaloids 55
3.1.2 Cell culture 55
3.1.3 Scar-in-a-Jar assay 56
3.1.4 RT-qPCR 57
3.2 Methods 58
3.2.1 Routine cell culture 58
3.2.2 Scar-in-a-Jar assay 59
3.2.3 Pseudolycorine dose-response assay 65
3.2.4 RT-qPCR array profiling of fibrosis-associated genes 66
3.2.5 Statistical analysis 72
3.2.6 Sample size determination 72
3.3 Summary 72
Chapter 4 Results 75
4.1 Scar-in-a-Jar assay optimisation 75
4.1.1 Scar-in-a-Jar v1: Sub-optimal cellular yield and attachment 75
4.1.2 Cell density optimisation for Scar-in-a-Jar v2 77
4.1.3 Scar-in-a-Jar v2: Refinement of cell density and identification of cellular aggregation 79
4.1.4 Scar-in-a-Jar v3: Persistence of cellular aggregation despite procedural modifications 80
4.1.5 Identification of low serum concentration as the primary driver of cellular aggregation 82
4.1.6 Serum conditioning (10%→0.4% FBS) yields a uniform cell monolayer 86
4.1.7 Scar-in-a-Jar v4: Background-level fibrotic marker staining 88

4.1.8 Scar-in-a-Jar v5: Permeabilisation and fluorophore refinements insufficient to resolve background-level staining 91
4.1.9 Scar-in-a-Jar v6: Identification of poor antibody quality as the primary barrier to signal detection 93
4.1.10 Scar-in-a-Jar v7: Successful fibrotic marker staining and assay validation 98
4.2 Pseudolycorine demonstrated the strongest antifibrotic activity among the candidate alkaloids 102
4.3 Pseudolycorine exhibited an IC_{50} of 1.84 μM against α-SMA expression 108
4.4 RT-qPCR array analysis of 84 fibrosis-related genes to elucidate pseudolycorine's mechanism of action 110
4.4.1 Validation of RNA integrity and quality 110
4.4.2 Categorisation of the 84 fibrosis-related genes evaluated by RT-qPCR array 111
4.4.3 Pseudolycorine significantly reduced the expression of the pro-fibrotic gene *CCL11* 112
4.4.4 Pseudolycorine significantly reduced the expression of ECM remodelling genes: *MMP14*, *PLAU*, and *TIMP4* 113
4.4.5 Pseudolycorine significantly reduced the expression of inflammatory cytokine and chemokine genes: *CCR2* and *CCL11* 114
4.4.6 Pseudolycorine did not significantly alter the expression of growth factor genes 115
4.4.7 Pseudolycorine significantly increased the expression of the transcription factor *CEBPB* 116
4.4.8 Pseudolycorine did not significantly affect the expression of epithelial-to-mesenchymal transition genes 117
4.4.9 Pseudolycorine did not significantly alter the expression of apoptosis-regulatory genes 118
4.5 Summary 119
Chapter 5 Discussion 121
5.1 Established pharmacological profile of pseudolycorine 121
5.2 Targeted disruption of the pericellular matrix-remodelling axis 122
5.3 Reconciling SMAD transcript stability with pathway inhibition 123
5.4 Immunomodulatory effects 123
5.5 The context-dependent role of *CEBPB* upregulation 125
5.6 Post-translational regulation of collagen deposition 126
5.7 A mechanistic framework for preclinical evaluation 126

5.8 Study limitations 127
5.9 Future research directions 128
Chapter 6 Conclusion 130
Bibliography 132

List of Figures

Figure 1-1 Schematic illustration of knee joint range of motion. 20
Figure 1-2 Overview of the cellular and molecular mechanisms driving arthrofibrosis.. 25
Figure 1-3 Treatment algorithm for arthrofibrosis following total knee arthroplasty (TKA). 46
Figure 2-1 Chemical structures of the candidate Amaryllidaceae alkaloids, grouped by skeletal type. 48
Figure 3-1 Automated image analysis pipeline for fibrotic marker quantification. 64
Figure 4-1 Representative images from the v1 Scar-in-a-Jar assay. 76
Figure 4-2 Brightfield images of 1BR3 human fibroblasts seeded at decreasing densities under Scar-in-a-Jar assay conditions. 78
Figure 4-3 Representative images from the v2 Scar-in-a-Jar assay. 80
Figure 4-4 Brightfield images following optimisation of cell handling and seeding procedures. 82
Figure 4-5 Time-lapse brightfield imaging of 1BR3 human fibroblasts cultured under Scar-in-a-Jar conditions. 83
Figure 4-6 Effect of serum concentration on cell distribution and morphology following seeding. 84
Figure 4-7 Effect of increasing serum concentration on fibroblast morphology and spreading. 86
Figure 4-8 Fibroblast morphology during attachment and subsequent serum starvation. 88
Figure 4-9 Comparison of secondary-only control and full antibody staining for α-smooth muscle actin and collagen type I in the v4 Scar-in-a-Jar assay. 89
Figure 4-10 Representative images of positive and negative controls in the v4 Scar-in-a-Jar assay. 90
Figure 4-11 Comparison of secondary-only and full antibody staining for α-smooth muscle actin and collagen type I in the v5 Scar-in-a-Jar assay..... 92

Figure 4-12 Comparison of secondary-only and full antibody staining for α-smooth muscle actin and collagen type I in the v6 Scar-in-a-Jar assay. 94
Figure 4-13 Titration of α-smooth muscle actin (α-SMA) antibodies from Cell Signaling Technology (Cat. #19245) and Proteintech (Cat. #67735-1-Ig). 96
Figure 4-14 Titration of collagen type I antibody from Proteintech (Cat. #83752-5-RR). 97
Figure 4-15 Titration of collagen type I antibody from Sigma-Aldrich (Cat. #C2456). 98
Figure 4-16 Cell seeding density optimisation for the v7 Scar-in-a-Jar assay. 99
Figure 4-17 Comparison of secondary-only and full antibody staining for α-smooth muscle actin and collagen type I in the v7 Scar-in-a-Jar assay. 101
Figure 4-18 Representative images from the v7 Scar-in-a-Jar assay. 102
Figure 4-19 Immunocytochemical staining and quantification of fibrotic markers in the Scar-in-a-Jar model following treatment with test compounds at 1 µM. 105
Figure 4-20 Immunocytochemical staining and quantification of fibrotic markers in the Scar-in-a-Jar model following treatment with test compounds at 10 µM. 107
Figure 4-21 Dose-response analysis of pseudolycorine in the Scar-in-a-Jar model. ... 109
Figure 4-22 RNA quality analysis using the Agilent 4200 TapeStation system. 111
Figure 4-23 Relative expression of pro-fibrotic and anti-fibrotic genes in pseudolycorine-treated 1BR3 fibroblasts in the Scar-in-a-Jar model. 113
Figure 4-24 Relative expression of extracellular matrix (ECM) and cell adhesion molecule genes in pseudolycorine-treated fibroblasts in the Scar-in-a-Jar model. 114
Figure 4-25 Relative expression of inflammatory cytokine and chemokine genes in pseudolycorine-treated fibroblasts in the Scar-in-a-Jar model. 115
Figure 4-26 Relative expression of growth factor genes in pseudolycorine-treated fibroblasts in the Scar-in-a-Jar model. 116
Figure 4-27 Relative expression of signal transduction genes in pseudolycorine-treated fibroblasts in the Scar-in-a-Jar model. 117
Figure 4-28 Relative expression of epithelial-to-mesenchymal transition genes in pseudolycorine-treated fibroblasts in the Scar-in-a-Jar model. 118
Figure 4-29 Relative expression of other fibrosis-associated genes in pseudolycorine-treated fibroblasts in the Scar-in-a-Jar model. 119

List of Tables

Table 1 QIAGEN Genomic DNA elimination mix 68
Table 2 QIAGEN Reverse-transcription mix 69
Table 3 PCR components mix 69
Table 4 QuantStudio 12K Flex Real-Time PCR System thermal cycling programme 70
Table 5 Functional classification of genes in the RT^2 Profiler PCR Array Human Fibrosis panel, as defined by the manufacturer (QIAGEN) 112

Chapter 1 Introduction

Total knee arthroplasty (TKA), also known as total knee replacement, is one of the most successful and cost-effective orthopaedic procedures for relieving joint pain and restoring function in patients with debilitating, end-stage osteoarthritis (1). However, a small subset of patients develop an exaggerated inflammatory response following TKA, leading to excessive scar tissue formation that restricts normal range of motion (ROM) (2,3). This fibrotic joint disorder is known as knee arthrofibrosis. At the cellular level, arthrofibrosis is driven by the pathological persistence of myofibroblasts, which in normal wound healing coordinate spatially restricted, time-limited scar formation before undergoing apoptosis (4). In arthrofibrosis, however, these cells remain active through pro-inflammatory positive feedback loops, with transforming growth factor-β (TGF-β) as a central mediator (5). Persisting myofibroblasts overproduce, adhere to, and contract collagen and extracellular matrix (ECM) proteins within the knee joint and surrounding tissues, leading to tissue contraction, restricted joint mobility, pain, and ultimately significant deterioration in quality of life (6,7). The plausible aetiology of arthrofibrosis is considered multifactorial, encompassing both biological and mechanical influences that sustain a pro-inflammatory environment (8,9).

Arthrofibrosis is initially managed conservatively through physiotherapy, anti-inflammatory medications, and orthoses, though these modalities are not always effective and may exacerbate symptoms in some cases (10–12). When conservative treatment fails, surgical intervention is considered, escalating in invasiveness from manipulation under anaesthesia (MUA) to arthroscopic debridement (AD), open debridement (OD), and, in refractory cases, revision TKA (rTKA), each associated with variable success rates and potential complications (13–15). The limitations of current treatments highlight an urgent need for safe, effective, and affordable pharmacological therapies targeting the underlying fibrotic pathways. The present study aims to address this clinical need by evaluating the antifibrotic potential of a panel of Amaryllidaceae alkaloids isolated from Amazonian rainforest bulbs, namely galanthine, lycorenine, pseudolycorine, and powelline.

1.1 Thesis outline

This thesis is organised into six chapters. Chapter 1 reviews the definition, incidence, pathogenesis, and risk factors of arthrofibrosis, before examining current treatment strategies from least to most invasive, with attention to their efficacy, timing, and complications. Chapter 2 establishes the scientific foundation of the study, presenting the hypothesis, aims, and research questions, centred on the in vitro antifibrotic activity of the candidate alkaloids, the potency of the lead compound, and its mechanism of action, alongside the research plan and significance of the investigation. Chapter 3 details the materials and methods employed to address the research questions, encompassing the Scar-in-a-Jar assay, dose-response analysis, and a reverse-transcription quantitative PCR (RT-qPCR) array profiling 84 fibrosis-associated gene targets. Chapter 4 presents the corresponding results, addressing the in vitro antifibrotic activity of the candidate alkaloids, the half-maximal inhibitory concentration (IC_{50}) of the lead compound, and the gene expression changes it induced. Chapter 5 contextualises the RT-qPCR findings within the broader research landscape and proposes a mechanistic framework to guide future preclinical investigation, before addressing study limitations and prospective research directions. Chapter 6 presents the conclusions of the study and reflects on the wider implications of the findings**.**

1.2 Arthrofibrosis

The term arthrofibrosis is derived from the Greek roots arthro- ("joint"), fibro- ("fibrous"), and -osis (denoting a pathological process), collectively describing the excessive formation of fibrous tissue within a joint (16). Knee arthrofibrosis has historically been a poorly defined condition, hindering understanding of its aetiology, pathogenesis, prevalence, and treatment outcomes (13,16). To address this, an international expert panel undertook a formal consensus process in 2016, defining arthrofibrosis as a “limited ROM in extension and/or flexion” not attributable to infection, prosthetic malfunction, pain, or other identifiable causes, but rather to soft-tissue fibrosis that did not exist pre-operatively (17). As no definitive biomarkers currently exist, other causes of stiffness

must be excluded through radiographs, MRI, bone scans, and laboratory investigations (18,19). While normal knee flexion is approximately 140° (20), achieving 110–120° of flexion following TKA is generally considered sufficient for most daily activities (21,22). Based on these normative values, the expert panel graded arthrofibrosis severity as mild, moderate, or severe according to the degree of extension deficit (5–10°, 11–20°, >20°) and range of flexion (90–100°, 70–89°, <70°), respectively (17). These reductions in ROM correspond to progressive functional impairment, as fibrous tissue adhesions contract over time and pathologically bind intra-articular structures, causing pain, impairing normal joint kinematics, and predisposing the knee to degenerative changes (16). Figure 1-1 illustrates the knee joint at key angles of flexion and extension, providing a visual reference for these ROM thresholds.

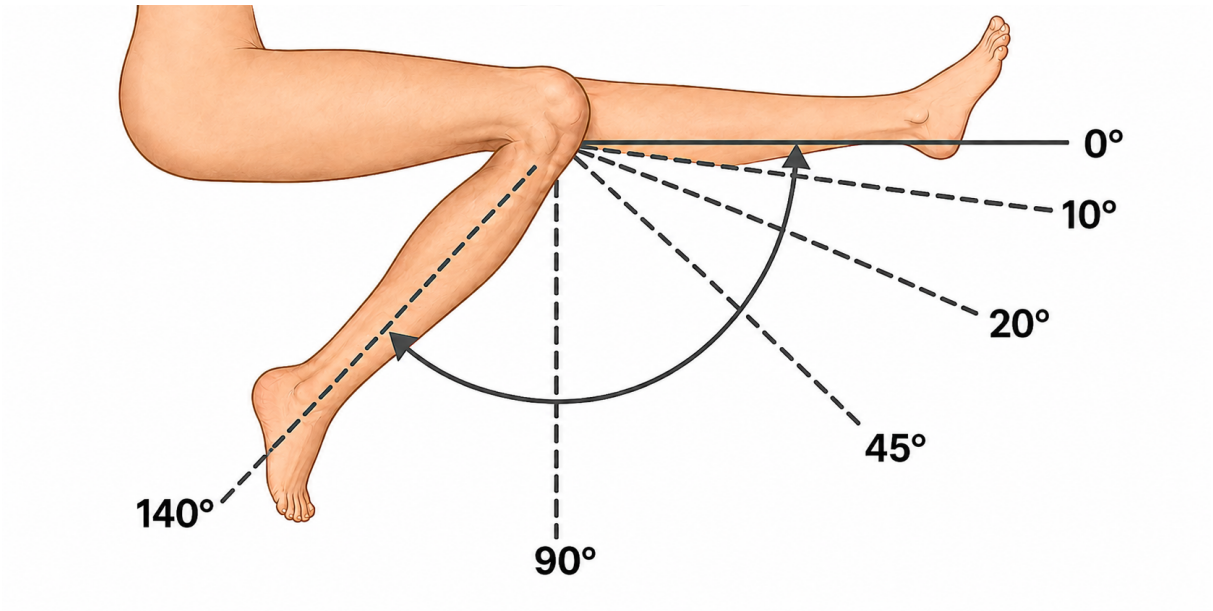

Figure 1-1 Schematic illustration of knee joint range of motion.
The diagram depicts key angles of knee flexion and extension, ranging from full extension (0°) through increasing degrees of flexion (10°, 20°, 45°, 90°) to maximum flexion (140°). These reference angles provide anatomical context for the range of motion thresholds used to classify arthrofibrosis severity following total knee arthroplasty.

1.3 Arthrofibrosis rates post-TKA

Knee arthrofibrosis represents a significant aetiology of TKA failure, with a reported failure rate of 14.1% in a prospective study of over 18,000 patients (23). Reported incidence rates vary considerably, ranging from 0.2% to 60% across the literature (e.g., 1,24–27), reflecting reporting bias from the exclusion of non-surgically treated cases from outcome registries (28,29), historical lack of standardised diagnostic criteria (10,17), and the inclusion of patients with normal transient postoperative stiffness in some studies (6,30). A recent critical review estimates the true incidence at approximately 3–4% (19). Notably, multiple projection studies predict this figure will rise sharply in parallel with increasing TKA demand in an ageing global population (e.g., 31–33).

1.4 Arthrofibrosis pathogenesis

1.4.1 Arthrofibrosis as a dysregulated wound healing response

Under normal physiological conditions, tissue injury activates the clotting cascade, induces local hypoxia, and triggers inflammasome activation, initiating a pro-inflammatory cascade characterised by the release of interleukin (IL)-1β, IL-18, platelet-derived growth factor (PDGF), TGF-β, and reactive oxygen species (ROS) (34). These mediators recruit and activate immune cells including mast cells, lymphocytes, and macrophages, which further amplify inflammation through the release of TNF-α, IL-1β, IL-6, and fibroblast growth factors (35). In response to inflammatory cues and mechanical strain, resident fibroblasts undergo a phenotypic shift characterised by increased migration and proliferation, augmented ECM synthesis, and eventual differentiation into myofibroblasts (36). These myofibroblasts drive the synthesis of reparative ECM proteins and, crucially, mediate ECM remodelling and wound contraction (37,38). Following successful repair, the inflammatory response is downregulated, myofibroblasts undergo apoptosis or dedifferentiate, and tissue homeostasis is restored (38).

In arthrofibrosis, however, the mechanisms responsible for resolving inflammation and terminating the wound healing response become dysregulated through complex, self-sustaining positive feedback loops, likely driven by a combination of environmental and genetic factors (9,39). This persistent dysregulation results in chronic inflammation and pathological ECM deposition, the hallmarks of fibrotic tissue remodelling (40). Fibrosis can therefore be regarded as an exaggerated and unresolved wound healing response (41,42). As it represents the final common pathway for numerous chronic inflammatory conditions and is a pathological hallmark across nearly all organ systems , mechanistic insights from fibrosis in other tissues have significantly informed the current understanding of arthrofibrosis pathophysiology (5).

1.4.2 TGF-β and associated fibrogenic mediators

TGF-β is the central initiator and mediator of arthrofibrosis, with TGF-β1 being the most functionally significant isoform in fibrotic pathology (43). Its pivotal role is demonstrated by the finding that TGF-β1 overexpression alone is sufficient to induce fibrosis (44–46), and by the identification of TGFβR1 as a promising biomarker of arthrofibrosis correlating with ROM loss, pain severity, and collagen deposition (47,48). Moreover, in vitro models of arthrofibrosis commonly involve the exogenous addition of TGF-β to induce a fibrotic phenotype in cultured cells (e.g., 49–51). Conversely, inhibition of TGF-β signalling at multiple downstream levels produces potent antifibrotic effects across various organ systems (e.g., 45,52).

TGF-β is secreted in a latent form and requires proteolytic cleavage or conformational change to become active, a process facilitated by ROS, low pH, specific proteases, integrins, and thrombospondin-1 (53,54). Enhanced activation of latent TGF-β is a hallmark of fibrotic conditions (55,56). TGF-β signals canonically through TGFβRII-mediated phosphorylation of TGFβRI, which activates SMAD2 and SMAD3, forming a complex with SMAD4 that translocates to the nucleus to regulate target gene transcription (56,57). Non-canonical SMAD-independent pathways, including mitogen-activated protein kinase (MAPK), phosphatidylinositol 3-kinase (PI3K)/AKT, and Rho-like GTPase cascades, further broaden the downstream signalling repertoire (43,44). Through both canonical and non-canonical pathways, TGF-β exerts pleiotropic pro-fibrotic effects by stimulating fibroblast-to-myofibroblast differentiation, inhibiting myofibroblast apoptosis, promoting ECM production, reducing ECM degradation through the downregulation of matrix metalloproteinases (MMPs) and upregulation of tissue inhibitors of metalloproteinases (TIMPs), and inducing pro-fibrotic epigenetic modifications (44,45,58). TGF-β further amplifies inflammation by upregulating pro-inflammatory cytokines (56), promoting a shift from anti-fibrotic Th1 to pro-inflammatory Th17 cells, (59), and activating inflammasomes via ROS (60–62). Because ROS and inflammatory cytokines in turn enhance TGF-β production, this creates a self-reinforcing feedback loop that perpetuates chronic inflammation and fibrosis (56,63).

Other pro-fibrotic mediators implicated in arthrofibrosis pathogenesis include PDGF, TNF-α, connective tissue growth factor, Substance P, and interleukins IL-1, IL-6, and IL-17, which collectively amplify TGF-β signalling, stimulate ROS generation, promote ECM deposition, and engage self-sustaining feedback loops that perpetuate inflammation and fibrosis (5,64,65). Hypoxia further compounds this by stabilising hypoxia-inducible factor-1, enhancing SMAD3 and TGF-β signalling, increasing α-SMA expression, and promoting lactic acid accumulation that activates both myofibroblasts and latent TGF-β (66–68). As fibrotic tissue is poorly vascularised, it remains chronically hypoxic, establishing yet another self-reinforcing loop that perpetuates disease progression (9).

1.4.3 Effector cells in arthrofibrosis

Myofibroblasts are the central effector cells in arthrofibrosis (69,70). In response to TGF-β and mechanical stress from the ECM, fibroblasts differentiate into myofibroblasts, which are specialised contractile cells characterised by α-SMA fibres that traverse their length and secretion of dense ECM, primarily composed of non-elastic type I collagen (Col-I; 22). These α-SMA fibres terminate at focal adhesion complexes composed of integrins and cadherin-based junctions; these complexes anchor the cell to the ECM and adjacent cells, respectively, thereby enabling direct force transmission during contraction (71,72). In the absence of regulatory inhibition, focal adhesions become increasingly complex and extensive collagen crosslinking transforms the ECM into a rigid, contractile scaffold that drives progressive tissue contraction and resists degradation (73). This mature ECM perpetuates fibrosis by promoting continued fibroblast-to-myofibroblast differentiation through mechanical stress (4). Myofibroblasts further amplify the fibrotic response by synthesising and secreting TGF-β, mechanically activating its latent ECM-bound form, and releasing pro-inflammatory mediators including IL-6, IL-1β, PDGF, and ROS (5,63). Together, these activities reinforce a pathological feedback loop in which myofibroblasts adopt an apoptosis-resistant, hyperproliferative phenotype that sustains their activation and amplifies ECM deposition (5,73).

Several immune and stromal cell types, including macrophages, mast cells, and Th2 lymphocytes, also play pivotal roles in sustaining chronic inflammation and fibrosis by serving as major sources of pro-fibrotic mediators such as TGF-β, TNF-α, PDGF, and IL-1β, and engaging in positive feedback loops that amplify the fibrotic response (5,74). An overview of the cellular and molecular mechanisms driving arthrofibrosis are presented in Figure 1-2.

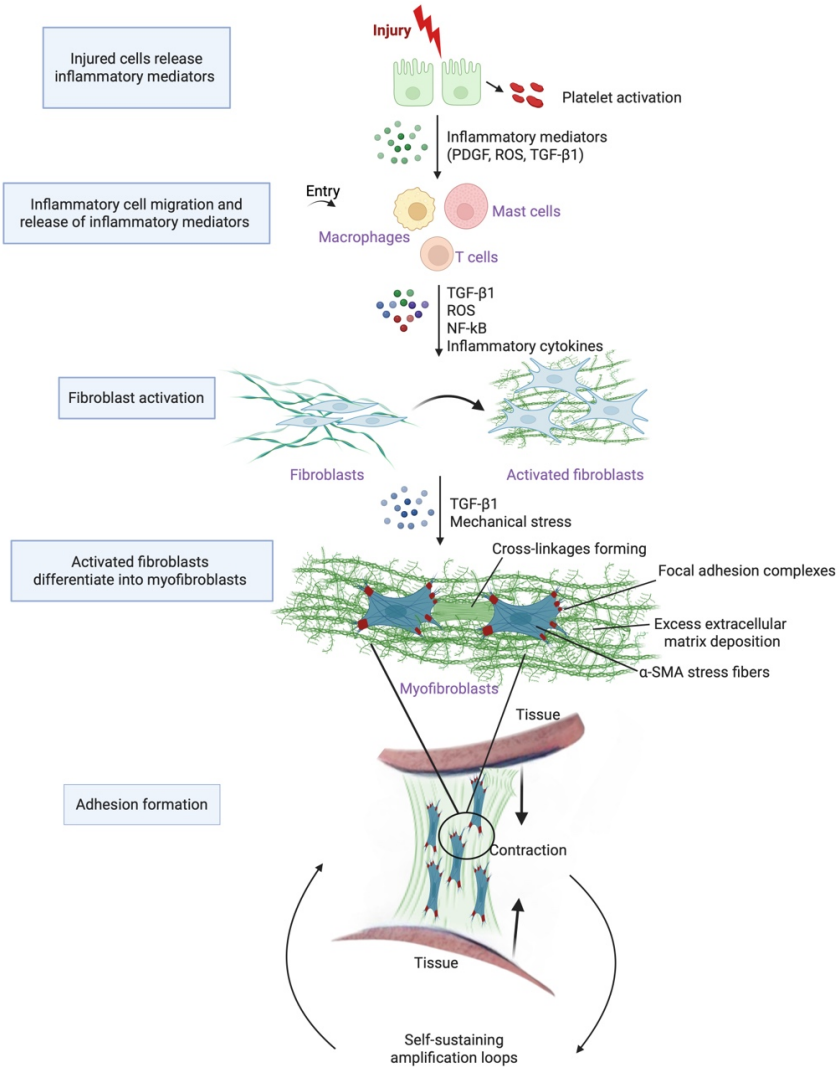

Figure 1-2 Overview of the cellular and molecular mechanisms driving arthrofibrosis.

Tissue injury triggers the release of inflammatory mediators such as reactive oxygen species (ROS), platelet derived growth factor (PDGF), transforming growth factor beta (TGFβ), and various cytokines. These signals activate immune cells, amplifying inflammation and initiating a cascade that stimulates fibroblast proliferation and extracellular matrix production. The combination of mechanical stress and TGFβ promotes fibroblast differentiation into myofibroblasts, which are key effector cells in arthrofibrosis. These cells are characterised by contractile alpha smooth muscle actin (αSMA) fibres that terminate in focal adhesion complexes. These complexes, composed of integrins and cadherin-based junctions, anchor the cell to the ECM and adjacent cells, enabling force transmission during contraction. As fibrosis progresses, focal adhesions become more complex and collagen crosslinking intensifies, transforming the ECM into a contractile scaffold that drives tissue stiffening and contraction. Myofibroblasts adopt a hyperproliferative, apoptosis-resistant phenotype through secretion of TGFβ, proinflammatory cytokines (e.g., IL6, IL1β), PDGF, ROS, and other paracrine signals, creating a self-amplifying fibrotic loop.

1.5 Risk factors for arthrofibrosis

1.5.1 Preoperative risk factors

1.5.1.1 Genetic predisposition

Some patients may have a genetic predisposition to developing arthrofibrosis, with susceptibility influenced by mutations in genes related to immune function, collagen synthesis and degradation, TGF-β signalling, fibroblast proliferation, and ROS metabolism, all of which can promote excessive ECM production (13,75,76). Supporting this, a potential link has been identified between specific human leukocyte antigen haplotypes and postoperative arthrofibrosis risk, including the presence of HLA-Cw08 and absence of HLA-Cw07 and DQB1*06 (77), though this finding is limited by a small sample size of 17 patients from an anterior cruciate ligament reconstruction cohort and requires validation in TKA populations.

1.5.1.2 Childhood adversity

Childhood adversity, such as abuse or neglect, has been identified as a risk factor for arthrofibrosis post-TKA, likely through its association with chronic inflammation (5,78). Specifically, adverse childhood experiences are associated with elevated Th17 cell counts, a heightened IL-6 response to stress, and increased susceptibility to autoimmune and inflammatory diseases (79).

1.5.1.3 Mental health status

Preoperative mental health status has been implicated in arthrofibrosis risk post-TKA, with both emotional illness and a history of depression associated with significantly poorer TKA outcomes at one-year follow-up (80,81). Depression may contribute by hindering patient motivation and engagement with postoperative rehabilitation, which is critical for functional recovery and arthrofibrosis prevention (26,81). The bidirectional relationship between inflammation and depression may further compound this risk (82,83).

1.5.1.4 Early-onset osteoarthritis (OA)

Early-onset OA, defined as onset before the age of 50, has been identified as a potential preoperative risk factor for arthrofibrosis (5,84). Synovial fibrosis has been reported in over half of OA patients (85–87), likely reflecting the central role of chronic inflammation in OA pathogenesis (88). Pro-inflammatory cytokines including TNF-α and IL-6 are upregulated in the synovial fluid of OA patients, and TGF-β, a potent driver of fibrosis, is overexpressed in synovial cells and subchondral bone, collectively fostering a pro-fibrotic joint environment (85,89,90). OA further amplifies this inflammatory milieu through a pro-inflammatory lipid profile within the IFP, activation of resident immune cells including T cells, B cells, mast cells, and macrophages upon surgical insult, and the induction of uncontrolled oxidative stress (91–93).

1.5.1.5 History of knee injury or surgery

A history of knee injury is a recognised risk factor for arthrofibrosis post-TKA, as trauma elevates pro-inflammatory cytokines such as TNF-α and IL-1β in synovial fluid, with the extent of tissue damage and time since injury further amplifying these levels (94). Previous knee surgery carries similarly elevated risk, with odds ratios of 2.4 for prior arthroscopy and 4.6 for prior arthrotomy relative to matched controls (81), consistent with a cumulative effect of tissue injury observed across fibrotic disorders (95). A key proposed mechanism involves epigenetic reprogramming of myofibroblasts following the initial fibrotic response; although inflammation may resolve clinically, a subset of fibroblasts retain pro-fibrotic epigenetic alterations and are more readily reactivated upon subsequent surgical insult, effectively serving as a cellular memory of prior injury (5,96,97).

1.5.1.6 Systemic comorbidities and inflammatory conditions

Preoperative comorbidities, including cardiac disease and chronic lung disease, have been identified as significant risk factors for arthrofibrosis, likely by promoting systemic inflammation and limiting the capacity for postoperative rehabilitation (81,98). Other pre-

existing inflammatory conditions, including obesity (99,100), diabetes mellitus (e.g., 26,81,98,101), ankylosing spondylitis and juvenile rheumatoid arthritis (14,102), similarly elevate risk by fostering a chronic pro-inflammatory and pro-fibrotic state. In diabetes mellitus specifically, abnormal glycosylation of collagen may provide an additional fibrosis-promoting mechanism (26).

1.5.1.7 Range of motion

Low preoperative ROM is consistently identified as one of the most important risk factors for arthrofibrosis following TKA (e.g., 98, 103,104). Limited preoperative ROM often complicates surgical exposure, frequently necessitating aggressive IFP excision, which increases infrapatellar tendon traction and scarring risk; the resulting tendon shortening may manifest as a reduction in patellar height, which can serve as a prognostic indicator of arthrofibrosis (98,105). Causes of limited preoperative ROM include septic arthritis, post-traumatic arthrosis, obesity-related posterior impingement, and capsular or extensor mechanism contractures (14,27). Although preoperative physiotherapy has been recommended to maximise ROM prior to TKA (102,106), a randomised controlled trial of 131 patients found no significant difference in postoperative functional recovery between those who completed a preoperative exercise programme and those who did not (107).

1.5.2 Intraoperative risk factors

Intraoperative surgical errors represent a significant risk factor for arthrofibrosis, particularly those resulting in imbalanced flexion and extension gaps or incorrect sizing and malpositioning of prosthetic components (103,108,109). Specific contributing technical factors include failure to remove posterior osteophytes (27,108); insufficient restoration of the posterior condylar offset ratio (110–112); excessive femoral component hyperflexion (113,114); inadequate tibial or femoral resection (18,110); malrotation of components (136,148); excessive joint line elevation (128,135); and failure to release a contracted posterior capsule (18,115). These errors disrupt normal knee kinematics, generating repetitive microtrauma that triggers an inflammatory response

and promotes fibrosis (14,113). Greater surgical complexity, reflected in prolonged operative time, increased soft tissue trauma, and haemarthrosis, further amplifies postoperative inflammation and arthrofibrosis risk (13,27). Accordingly, surgeons should ensure adequate surgical exposure, minimise soft tissue trauma, control intraoperative bleeding, and achieve accurate component positioning and balanced gap kinematics (98).

1.5.3 Postoperative risk factors

Prolonged immobility following TKA is a critical postoperative risk factor for arthrofibrosis and a key contributor to the loss of ROM gains (2,113,116). Compliance with postoperative physiotherapy may be hindered by poor patient motivation, which may stem from poor mental health; insufficient preoperative education regarding the importance of rehabilitation and proper exercise techniques; preoperative deconditioning due to comorbidities; and poor pain tolerance due to inadequate analgesic treatment or individual sensitivity to pain (98,109,117,118).

1.6 Conservative treatment of arthrofibrosis

1.6.1 Postoperative physiotherapy

Physiotherapy constitutes the first-line treatment for arthrofibrosis, as it is a non-invasive and cost-effective approach that can inhibit fibrotic deposition and adhesion formation, break down existing scar tissue, promote plastic deformation of periarticular soft tissues, and modulate pain through neurophysiological mechanisms (e.g., 19, 119,120). Its effectiveness is well-supported; reduced physiotherapy exposure has been shown to double MUA rates (121), and 70% of patients with early stage arthrofibrosis successfully avoided MUA following a structured multimodal physiotherapy programme (122). However, physiotherapy is most effective in the early postoperative period, when fibrous bands are immature and more responsive to mechanical intervention (2,123). Once the knee has progressed to synovial hypertrophy, fibrous tissue proliferation, or cyclops nodule formation, physiotherapy is unlikely to break down established scar tissue and

instead serves primarily to alleviate pain and maintain existing mobility (2,27,124). Accordingly, surgical intervention should be considered when conservative treatment fails to produce meaningful improvement after 6–12 weeks (14).

Essential components of a physiotherapy programme include patellar mobility exercises, passive and active-assisted ROM exercises, extensor mechanism training, and weight-bearing gait training (6,125,126). These components reflect the typical clinical presentation of arthrofibrosis, which is characterised by limited ROM proportional to fibrosis severity, an immobile patella, and a persistent sensation of tightness and stiffness (6,19,30). Despite their importance, there remains a lack of sufficiently detailed published protocols to enable consistent clinical replication, resulting in considerable variability in exercise prescription (6,30,127).

Critically, physiotherapy intensity must be carefully titrated to each patient's inflammatory response (6,16,17). Overly aggressive protocols that exceed the individual's pain threshold can perpetuate inflammatory responses and myofibroblast activation through mechanical stress, thereby worsening fibrosis and risking joint contracture, tendon rupture, or patellar fracture (14,125,128). Current best practice therefore emphasises gentle passive and active ROM exercises within a pain-free range, with therapist supervision to monitor for signs of persistent inflammation, the so-called "hot knee" (13,125). As this approach reflects, effective physiotherapy should ultimately be guided by the cellular, cytokine-based model of arthrofibrosis pathogenesis, rather than relying solely on the traditional pathophysiological adhesion model (6).

1.6.1.1 Facilitators of patient adherence to physiotherapy

The effectiveness of physiotherapy is highly dependent on patient motivation and adherence, as gains in ROM can be quickly lost without consistent activity (6,13,117). Preoperative education sessions that emphasise the importance of rehabilitation, provide guidance on home exercise techniques and pain management, and set realistic functional expectations promote individualised care planning and encourage patients to

take an active role in their recovery (113,129,130). The effectiveness of such education is supported by evidence that patients who received preoperative education had a significantly lower risk of developing arthrofibrosis requiring MUA ($p < 0.001$) (131).

Another key strategy to improve patient adherence to physiotherapy post-TKA is effective postoperative pain control (102,116,117). Indeed, adequate analgesia has been shown to significantly reduce the need for MUA from 9% to 1% (132). Multimodal analgesia, which combines agents or techniques with different mechanisms targeting various pain pathways, is the most effective approach, as pain associated TKA surgery arises from both central and peripheral mechanisms, rendering monotherapy often inadequate (e.g., 118,133,134). The strategy encompasses three phases: pre-emptive analgesia administered prior to surgery to reduce central and peripheral sensitisation; intraoperative analgesia to block pain signal generation and transmission; and postoperative analgesia to provide sustained relief (135). The clinical impact of multimodal analgesia is substantial, with one multimodal protocol reporting a 47.1% reduction in MUA rates compared to a traditional opioid-based approach (136). Importantly, several analgesic agents appear to exert direct antifibrotic effects beyond pain control, with perioperative NSAIDs, corticosteroids, ACE inhibitors, and angiotensin II receptor blockers each associated with significantly reduced rates of MUA and AD in large patient cohorts (e.g., 137–139). With their effectiveness increasingly supported by the literature, multimodal pain management strategies are rapidly being adopted as standard care, particularly given the growing emphasis on narcotic-sparing approaches to minimise opioid-related adverse effects (118,134).

Cryotherapy, the application of ice, can also be used liberally after each exercise session and as needed throughout the day to reduce inflammation, swelling, and pain, further promoting patient comfort and adherence to rehabilitation protocols (116,125).

1.6.2 Adjuncts to physiotherapy

For physiotherapy to be effective following TKA, soft tissues must be stretched daily for at least 6 to 12 weeks postoperatively (125,140). However, constraints on healthcare resources, combined with the pain and difficulty of performing exercises at home, often limit the feasibility of daily manual physiotherapy, hindering the achievement of plastic deformation and resulting in only modest improvements (28,141,142). Medical stretching devices are therefore increasingly used to supplement recovery, offering economic advantages over standard physiotherapy, reduced re-operation rates, and the added benefit of freeing physiotherapists to focus on neuromuscular re-education and strengthening during clinical sessions (124,143). These devices operate through two primary mechanisms: applying a prolonged constant low-grade force to induce creep deformation, classified as load-control devices, or incrementally displacing tissues to a fixed degree based on patient tolerance to achieve stress relaxation, classified as displacement-control devices (142,144).

1.6.2.1 Load-control devices

Load-control devices apply a constant, low-grade stretching force through a spring-like mechanism or elastic bands that gradually displaces soft tissue and induces plastic deformation, resulting in permanent elongation (144). Most commercially available devices require a minimum of 8 hours of daily wear, though custom-designed models may allow shorter sessions of 30–45 minutes two to three times daily, and overall treatment duration ranges from several weeks to months depending on individual response (145,146). The requirement for prolonged daily use, combined with the obtrusive and uncomfortable nature of the devices, represents a key limitation that may reduce patient compliance (144). Studies consistently report favourable outcomes with load-control devices in patients unresponsive to standard physiotherapy, with success rates of up to 90% and mean ROM improvements of approximately 25° (146,147).

1.6.2.2 Displacement-control devices

Displacement-control devices hold the knee at a constant displacement beyond its active ROM and gradually increase this displacement at timed intervals as soft tissue resistance decreases (144). Studies consistently report mean ROM improvements of 17°–25° with high patient satisfaction (10,147,148). Moreover, a randomised trial found that static progressive stretching produced outcomes comparable to MUA in terms of flexion ROM, with superior extension ROM gains and without the need for anaesthesia or hospitalisation (115). The authors hypothesised that the device repeatedly brings tissues into the end-elastic to early-plastic deformation range, where controlled micro-ruptures of stiff collagen fibres initiate a remodelling response, potentially explaining the durability of improvements observed (115).

Displacement-control devices are further classified into patient-actuated serial stretch (PASS) devices, in which patients actively stretch to end-range flexion in repeated cycles, and externally actuated devices, which apply a fixed external force. Pooled data from five studies reported a 29% greater ROM improvement with PASS devices compared to externally actuated devices (142), and a retrospective review of over 11,000 patients reported that more than 90% achieved greater than 90° of flexion, comparable to outcomes achieved with open surgical release (143).

Comparing displacement-control and load-control devices, a systematic review (142) found both to be effective in improving ROM ($p < 0.001$) in the treatment of knee arthrofibrosis, with displacement-control devices achieving comparable gains to load-control devices with less treatment time and minimal physiotherapy.

1.6.2.3 Continuous passive motion (CPM)

A third category of orthotic device, CPM, provides repetitive joint cycling through a defined ROM by utilising the principles of stress relaxation and creep loading to facilitate the controlled, non-fatiguing stretching of periarticular tissues (142). CPM has been a clinical staple for over 25 years, typically initiated immediately following TKA to prevent

arthrofibrosis and promote articular tissue healing (15,125,149). However, multiple systematic reviews and meta-analyses (e.g., 144,150–152) over the past 20 years have consistently found that while CPM may offer a modest improvement in active knee flexion of 2–4° in the early postoperative period, this advantage does not persist beyond the first few postoperative days and confers no long-term benefit over physiotherapy alone in ROM, pain, quality of life, or function following TKA. Furthermore, CPM does not reduce hospital length of stay and in some cases may prolong it, while incurring substantial equipment and labour costs (e.g., 153,154). Consequently, several institutions have discontinued its routine use following TKA, and it is increasingly being excluded from modern rehabilitation protocols (153,155).

1.7 Surgical management of arthrofibrosis

1.7.1 Manipulation under anaesthesia (MUA)

1.7.1.1 MUA incidence

If patients fail to achieve functional gains through physiotherapy within the first 4 to 6 weeks, such as failing to reach 90° of knee flexion, MUA is typically the first-line surgical intervention, once other causes of stiffness including technical errors, complex regional pain syndrome, and infection have been excluded (e.g., 28,113, 156). Reported incidence rates vary widely, ranging from 0.5% to 22.7%, largely reflecting the absence of a universally accepted ROM threshold for MUA indication and differences in patient populations, institutional protocols, and surgeon preferences (e.g., 157–159). Thresholds used in the literature range from less than 90° to greater than 105° of flexion (e.g., 95, 131,156,160), while some practitioners rely on case-by-case clinical assessment without a strict cutoff (e.g., 161).

1.7.1.2 MUA risk factors

Both computer-assisted and robotic-assisted TKA have been associated with significantly reduced MUA risk compared to conventional TKA, with non-robotic patients showing approximately twice the odds of requiring MUA at 90 days and one year

postoperatively (162,163). Younger age is a consistently identified demographic risk factor, with patients under 65 more than twice as likely to undergo MUA compared to older patients, likely reflecting higher physical demands and lower tolerance for limited ROM (e.g., 159, 164–166). Other reported risk factors include female sex (e.g., 160,165), limited pre-operative ROM (167), prior knee surgery (166), sickle cell disease (165), smoking (166), and non-white ethnicity (e.g., 163,165,166). Notably, patients requiring MUA following a first TKA face a 14-fold increased risk of requiring MUA after contralateral TKA, further supporting a role for genetic predisposition in arthrofibrosis susceptibility (164).

1.7.1.3 MUA technique

MUA is performed under general anaesthesia with the patient in the supine position (156). With the patient appropriately muscle-relaxed, the surgeon flexes the ipsilateral hip to 90° and applies slow, gentle pressure to the proximal tibia until a firm endpoint is reached or at least 100° of flexion is obtained, often accompanied by a palpable and audible release of adhesions (25). This position is then held for 20 to 30 seconds. Patellar mobilisation may also be performed to address adhesions in the suprapatellar pouch (14). Physiotherapy is initiated immediately post-procedure to minimise adhesion reformation, supported by an adductor canal block or epidural catheter for 24 to 48 hours to facilitate postoperative pain management (14,25).

1.7.1.4 MUA timing

While no universal consensus exists regarding the optimal timing for MUA, most studies agree that it is most effective when performed within 6–12 weeks following the index procedure, as this timeframe corresponds to a period of relative tissue immaturity when adhesions are more amenable to mechanical disruption (e.g., 161, 168–170). A systematic review (170) of 14 studies involving 13,445 knees found that the mean gain in flexion was nearly twice as high in the early intervention group (within three months) compared to the delayed group (32.0° vs 19.2°). Interestingly, however, absolute post-MUA ROM was comparable between groups, likely attributable to the significantly higher

pre-MUA knee flexion observed in the delayed group (p = .003), reflecting a less severe baseline. These findings suggest that studies reporting no significant difference in absolute post-MUA ROM between early and late intervention groups, and by extension concluding that timing does not influence outcomes, may be confounded by differences in baseline severity (e.g., 161, 171).

Performing MUA too early, however, carries its own risks. MUA within the first few weeks post-TKA increases the likelihood of wound dehiscence, soft tissue damage, and exacerbation of the inflammatory response, potentially worsening fibrotic changes (5,122). Most authors therefore recommend deferring MUA until at least three weeks post-TKA to balance efficacy with safety (e.g., 14, 122).

Beyond 12 weeks, fibrous adhesions develop high tensile strength, becoming increasingly rigid and resistant to disruption, raising the risk of serious complications including extensor mechanism rupture and periprosthetic fracture (14,125). A systematic review (170) reported significantly higher rates of rTKA and surgical complications in patients who underwent late MUA compared to those treated earlier (p = .002 and p < .001, respectively). Nevertheless, some studies suggest MUA can still yield meaningful improvements beyond three months, particularly in patients who have not yet achieved 80° of flexion (e.g., 161, 172–174), and it should not be categorically withheld on the basis of timing alone.

1.7.1.5 MUA Effectiveness

The literature reports a mean flexion gain following MUA ranging from 24.7° to 48.9° (e.g., 122,161,172), and a systematic review (175) of 22 studies found that mean post-MUA ROM at final follow-up exceeded 90° in all but two studies, suggesting that MUA can provide clinically meaningful improvements in ROM for most patients. However, if the initial MUA fails, subsequent attempts are associated with markedly reduced success rates, with failure rates approaching 50% following a second attempt (122,175). Furthermore, patients who underwent MUA within one year of primary TKA (pTKA) had a

five-fold increased risk of subsequent revision compared to those who did not (176), and demonstrated smaller long-term improvements in ROM and functional scores at ten-year follow-up (167).

Despite these initial gains, ROM improvements following MUA are often not sustained, declining significantly within the first postoperative week, and in some cases, final ROM at long-term follow-up is no greater than that observed in non-manipulated knees (e.g., 25,115, 177). MUA may therefore serve more as a therapeutic adjunct to support postoperative rehabilitation in patients with painful, limited knee motion, rather than as a definitive solution for ROM deficits (e.g., 25,102,117). The decline is thought to reflect two contributing mechanisms: insufficient postoperative physiotherapy to consolidate intraoperative gains, and the procedure itself exacerbating the underlying abnormal inflammatory response, as the rapid forceful disruption of fibrous bands induces mechanical stress that can sustain myofibroblast activation and perpetuate the fibrotic cycle (6,115,122). Adjunct strategies such as maintaining the knee in 90° flexion post-procedure and administering intra-articular local anaesthetic and steroid injections at the time of MUA have been proposed to help preserve ROM gains (102,178).

1.7.1.6 MUA Complications

Although uncommon, MUA carries a risk of serious complications, particularly when performed with excessive force (6). Reported adverse events include haemarthrosis (18,117,177); posterior cruciate ligament rupture (102,115,179); wound dehiscence (18,117,177); patellar tendon rupture (9); chondral injury (9,125,129); mechanical loosening (163); complex regional pain syndrome (123,180); periprosthetic fracture (e.g., 2,9,129); pulmonary embolism (18,115); and heterotopic ossification (117). Fractures and tendon ruptures often necessitate further surgical intervention followed by immobilisation, which can itself exacerbate arthrofibrosis (13,181). Failure rates range from 4% to 26% (e.g., 30,122, 174), with most surgeons defining failure as a flexion ROM of less than 90°, and a cumulative 10-year revision risk of 10% following MUA has been reported, double that of the general TKA population (159).

1.7.2 Arthroscopic Debridement (AD)

1.7.2.1 AD technique

AD is a minimally invasive surgical technique used to precisely remove fibrous scar tissue from specific compartments within the knee joint in patients who have not responded to more conservative treatments (15). It is often performed concurrently with MUA, with MUA typically preceding AD to facilitate instrument access; however, in severe arthrofibrosis or in patients with osteoporosis, AD may be performed first to comprehensively release adhesions before manipulation, thereby reducing the force required and minimising the risk of fracture (12,126).

The procedure employs an arthroscope connected to a high-resolution camera that transmits real-time images to a monitor, guiding the procedure visually (182). Standard arthroscopic access involves the creation of anterolateral and anteromedial portals, with additional accessory portals used as needed to enhance visualisation and instrument access across all knee compartments (129,183). A sterile irrigation system distends the contracted capsule, enhancing visualisation and facilitating adhesion lysis (129,149,183). Fibrotic tissue is debrided using powered shaver attachments and an arthroscopic radiofrequency probe, the latter of which reduces the risk of postoperative haemarthrosis and arthrofibrosis recurrence through controlled thermal ablation (129,183). Millett et al. (125) recommend a systematic nine-step evaluation of the arthrofibrotic knee, encompassing the suprapatellar pouch, medial and lateral gutters, IFP, retinacula, intercondylar notch, and posterior capsular insertions, to ensure comprehensive debridement of all accessible regions. Following the procedure, a suction drain may be placed and portals sutured, with effective multimodal analgesia initiated promptly to enable early intensive physiotherapy and maintain intraoperative ROM gains (126,129).

1.7.2.2 AD timing

Most studies recommend performing AD between 3–6 months postoperatively if 90° of flexion has not been achieved with conservative treatment (e.g., 12,102,184). Early AD (within 6 months) has been shown to result in significantly better functional scores and ROM than later interventions, with knee flexion of 120° or greater achieved in 75% of early cases compared to just 39% in the late AD group ($p < 0.05$) (126). This superiority is attributable to the progressive maturation and crosslinking of fibrous adhesions, which renders them increasingly resistant to debridement (5,126). Consequently, as functional improvements plateau when intervention is delayed, deferring AD beyond six months is generally discouraged (98).

1.7.2.3 AD effectiveness

Success rates for AD, typically defined as improvements in ROM without recurrence of arthrofibrosis, range from 63% to 94% across the literature, with reported ROM improvements of 18.5° to 61° (e.g., 28,170,185). This variability is likely influenced by multiple factors, including postoperative physiotherapy protocols, surgical technique, patient comorbidities, BMI, preoperative ROM, and the anatomical extent and location of fibrotic tissue (e.g., 5,184,185). Although AD is generally effective in improving ROM, gains tend to diminish over time, with intraoperative ROM consistently exceeding final ROM at follow-up across studies (e.g., 123,186,187). Notably, one study observed that patients lost approximately half of their immediate postoperative ROM gains by 12-month follow-up (24). Early intensive physiotherapy supported by adequate multimodal analgesia is therefore essential to consolidate intraoperative gains (129,186).

Despite this potential for ROM decline, AD offers several clinically meaningful advantages over more invasive alternatives. It allows direct visualisation and minimally invasive removal of scar tissue across multiple knee compartments, is associated with reduced morbidity and faster recovery, and enables early physiotherapy from postoperative day one (99,129,188). It also permits identification and treatment of intra-articular pathology, including loose bodies, retained foreign bodies, and focal lesions

contributing to persistent extension deficits, that would be unlikely to respond to MUA alone (15,129).

1.7.2.4 AD complications

While AD is generally considered a safe and minimally invasive option, with a systematic review reporting a complication rate of less than 2% (189), it is not without risks, some of which overlap with those associated with MUA. Reported complications include joint swelling, portal bleeding, haemarthrosis, pulmonary embolism, cartilage and ligament damage, neurovascular injury, infection, and scratching of polished implant surfaces that may accelerate polyethylene wear (e.g., 99,126,183). The risk of haemarthrosis may be mitigated by using electrocautery in highly vascular tissue and placing a surgical drain (149). Moreover, limiting the procedure to two or three portals minimises the risk of prosthetic damage and reduces the potential for infection (149,186,190).

Moreover, AD has important technical limitations. Access to the posterior knee compartment, essential for correcting extension deficits, remains technically challenging due to narrow instrument corridors and proximity to neurovascular structures, and is therefore generally reserved for experienced surgeons (14,15,191). Additionally, AD is less effective when motion loss arises from extra-articular factors or when severe ROM restriction of 60° or less is present, due to limited instrument access and the risk of instrument breakage in severely arthrofibrotic knees (12,102). Accordingly, AD is most appropriate for mild to moderate arthrofibrosis within 3–6 months post-TKA and is not recommended in more severe cases (102).

1.7.3 Open Debridement (OD)

1.7.3.1 OD technique

OD involves direct open surgical exposure of the knee joint, offering extensive visualisation and access to both the anterior and posterior compartments, making it particularly effective for patients with extensive intra-articular and periarticular fibrosis

not amenable to AD (9,113). The procedure begins with a midline skin incision and medial parapatellar arthrotomy, through which TKA components are inspected for malalignment or loosening before systematic debridement of scarring across the periarticular soft tissues, synovial lining, gutters, IFP, and suprapatellar pouch (27,192). Soft tissue releases, including quadsplasties such as quadriceps pie-crusting, V-Y plasties, or rectus snips, may be performed to address muscle contractures, and the polyethylene insert is temporarily removed to facilitate access to the posterior compartment, often replaced with a slightly thinner component to improve extension (193). A suction drain is routinely placed for 24 to 48 hours postoperatively to reduce haemarthrosis and arthrofibrosis recurrence risk, and epidural anaesthesia maintained for 48 to 72 hours, supplemented by femoral nerve blocks, to enable early intensive rehabilitation (27,125).

1.7.3.2 OD timing

OD for arthrofibrosis is typically performed after six months if patients fail to make meaningful progress despite intensive rehabilitation and reach a plateau in physiotherapy (e.g., 27,194,195). This timing allows postoperative inflammation to subside and ensures that less invasive interventions, such as MUA or AD, have been adequately attempted before resorting to open surgery (5).

1.7.3.3 OD effectiveness

As with other treatments for arthrofibrosis, outcomes following OD are variable. Reported ROM gains range from 19.4° to 61.5°, with most studies supporting its effectiveness in improving joint mobility (e.g., 192, 196,197). However, functional outcomes are less consistently achieved, with some studies reporting declines in Knee Society functional scores despite improvements in ROM, and recurrent arthrofibrosis requiring further surgery reported in a subset of patients (27,197).

The comparative effectiveness of OD relative to other surgical interventions remains debated. An earlier systematic review (28) suggested OD yields inferior ROM improvements compared to MUA and AD, while a more recent review (198) of 25 studies

concluded that OD may offer the greatest ROM benefit, with a mean gain of 43.4° compared to 36.2° for AD and 38.4° for MUA. Both reviews, however, emphasise the need for high-quality randomised controlled trials, as the current literature is largely limited to case series with inherent methodological weaknesses.

1.7.3.4 OD complications

The open surgical approach carries an inherent risk of postoperative wound infection and arthrofibrosis recurrence, as the surgical trauma activates wound-healing pathways including increased ECM synthesis and inflammation, and may trigger immune memory responses or reinforce existing pro-fibrotic feedback loops, a risk further amplified when focal adhesions close to the articular surface are released (5,12). Additional complications include a high incidence of patellofemoral arthritis and patellar tendon shortening of approximately 6 mm (192). While AD offers advantages over OD in terms of reduced blood loss, faster recovery, and lower wound complication rates, it does not permit adequate access to periarticular soft tissues or the posterior compartment, and OD should therefore be reserved for cases where AD is insufficient rather than used as a first-line intervention (12,199).

1.7.4 Revision TKA (rTKA)

1.7.4.1 rTKA technique

rTKA is regarded as the final treatment option for persistent ROM limitation when all previous interventions have failed, and accounts for 7–18% of revision procedures depending on the series (200–202). The procedure mirrors the surgical approach used in OD, beginning with a midline incision and medial parapatellar arthrotomy, followed by thorough synovectomy and removal of fibrotic tissue from the extensor mechanism and knee gutters (14,93). Additional exposure may be achieved via quadriceps snip, V-Y plasty, or tibial tubercle osteotomy where required (93,203). Surgeons subsequently assess polyethylene wear, joint line variation, patellofemoral tracking, component stability, and overall alignment to determine whether full or partial component exchange

is necessary (14,204). As with other surgical treatments for arthrofibrosis, postoperative management includes structured physiotherapy and multimodal analgesia to facilitate recovery and optimise functional outcomes (3).

1.7.4.2 rTKA timing

Because rTKA is the most invasive, technically demanding, and costly treatment option for arthrofibrosis, it is reserved as a last-line intervention, often performed beyond one year post-TKA (e.g., 205,206).

1.7.4.3 Cost burden of rTKA

rTKA is significantly more costly than pTKA, which itself ranges from AUD $19,000 to $30,000 per patient (207). Revision prostheses are up to three times more expensive due to their specialised design, and the inherent complexity of addressing bone defects, instability, and soft-tissue damage results in longer operating times, extended hospital stays, and greater resource utilisation (208,209). Costs are further compounded by complications, with 90-day costs at least 80% higher in patients experiencing infectious or vascular complications compared to those without (209).

1.7.4.4 rTKA effectiveness

Research on rTKA suggests that functional outcomes are often unpredictable, and ROM restoration remains suboptimal even with accurate surgical technique and appropriate indications. Indeed, Greidanus et al. (1) assert that “most revision patients will never experience an outcome as favourable as their primary procedure.” A recent systematic review (120) reported that a postoperative arc of motion greater than 90° was achieved in only 30% of rTKA studies, compared to 71% of AD studies and 70% of MUA studies, with 43% of rTKA patients requiring further intervention compared to 25% and 17% in the AD and MUA groups, respectively. Another systematic review (198) similarly found that rTKA produced the smallest mean ROM gain among available surgical treatments, averaging only 24.7°. Individual studies report variable outcomes, with ROM gains ranging from

approximately 18° to 50°, though improvements frequently fall short of the functional threshold required for daily activities and are often accompanied by high rates of recurrent arthrofibrosis requiring re-intervention (e.g., 205, 211,212). When compared to rTKA performed for other indications such as instability, wear, or infection, rTKA for arthrofibrosis is consistently associated with poorer clinical outcomes, lower patient satisfaction, and higher complication rates (e.g., 213,214).

1.7.4.5 rTKA outcome predictors

Regarding outcome predictors, the literature is inconsistent. Some studies have identified earlier revision timing, fewer prior surgeries, and greater preoperative ROM restriction as favourable prognostic factors (205,215,216), while others found no significant demographic or operative predictors of success (204,217). These findings collectively demonstrate the unpredictable nature of rTKA for arthrofibrosis.

1.7.4.6 rTKA complications

rTKA carries a high risk of complications, including infection, periprosthetic fractures, neurovascular damage, patellar tendon rupture, patellar instability, pulmonary embolism, and wound-healing complications (e.g., 14,211,218,219). Arthrofibrosis recurrence is of particular concern, as patients undergoing rTKA for arthrofibrosis carry the highest risk of persistent severe fibrosis, with re-revision rates exceeding 25% and combined complication and reoperation rates approaching 49% in some series (206,220,221). Consequently, thorough preoperative counselling regarding the high complication risk and unpredictable functional outcomes is essential for all patients selected for rTKA (13,14,216).

1.8 Summary

Chapter 1 provided a comprehensive review of knee arthrofibrosis following TKA, beginning with its definition as a pathological condition characterised by excessive periarticular and intraarticular scar tissue formation, leading to persistent pain, restricted joint motion, and diminished quality of life. Its pathogenesis involves

dysregulation of normal wound-healing pathways and chronic inflammation, with TGF-β acting as a central mediator sustaining the persistence of myofibroblasts, the key contractile effector cells in fibrosis. Risk factors were categorised into preoperative, intraoperative, and postoperative domains, collectively contributing to a pro-inflammatory environment that promotes fibrotic tissue formation.

Current treatment strategies were reviewed in a stepwise fashion, reflecting clinical escalation from conservative to surgical management (Figure 1-3). Physiotherapy remains the first-line intervention and is most effective in early-stage arthrofibrosis, when fibrous bands are immature and more responsive, though excessive mechanical stress can paradoxically worsen fibrosis by perpetuating myofibroblast activation and inflammatory responses. Standard rehabilitation can also be accompanied by displacement- and load-control stretching devices to enhance ROM outcomes. Conversely, CPM offers no proven long-term benefit for ROM, showing inconsistent clinical outcomes, and is consequently being excluded from modern rehabilitation protocols. Where conservative measures fail, clinical management escalates to surgical intervention. MUA is most effective within 6–12 weeks post-surgery; earlier attempts increase the risk of wound dehiscence and soft-tissue damage, while delayed procedures encounter stiffer, more resistant adhesions that are harder to break and raise the risk of tendon rupture or bone fracture. Subsequent escalations include AD, typically performed between 3–6 months postoperatively. Across both MUA and AD, improvements in ROM are often partial and tend to diminish over time. Beyond six months, OD is considered, offering a larger surgical field that enables more extensive release of adhesions, though its open approach carries higher risks of complications and arthrofibrosis recurrence compared to less invasive techniques. RTKA is regarded as a salvage procedure and remains the most invasive, technically demanding, and costly option, with functional outcomes that remain unpredictable.

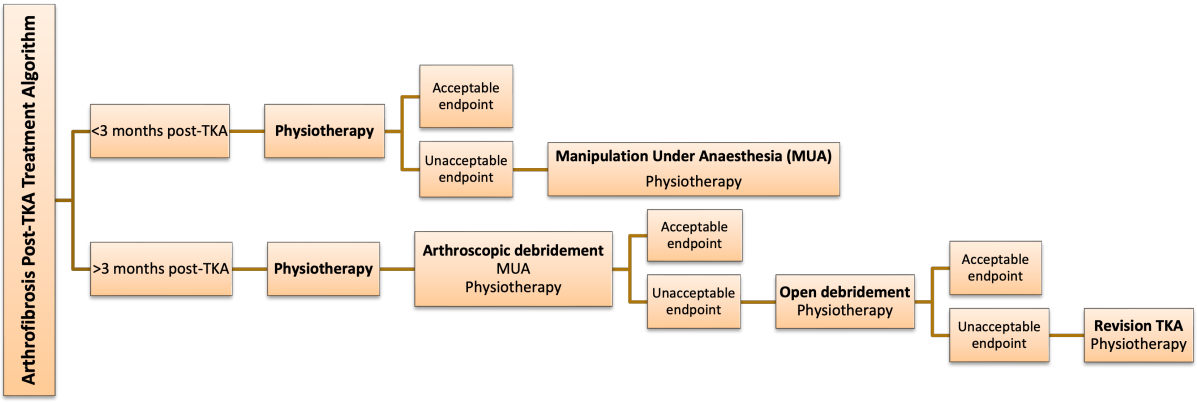

Figure 1-3 Treatment algorithm for arthrofibrosis following total knee arthroplasty (TKA).
Patients presenting within 3 months post-TKA are initially managed with physiotherapy; if an acceptable endpoint is not achieved, manipulation under anaesthesia (MUA) is considered. Beyond 3 months, management continues with physiotherapy, with escalation to arthroscopic debridement, often combined with MUA, as higher tissue tensile strength at this stage increases the risk of complications with MUA alone. Persistent arthrofibrosis may require open debridement, which enables the release of adhesions in tissue compartments inaccessible arthroscopically. Revision TKA is considered a salvage procedure once all other treatment options have been exhausted. Physiotherapy follows all surgical interventions to maintain improvements in range of motion.

Ultimately, the unpredictable outcomes and inherent risks associated with these mechanical and surgical interventions highlight a critical need for targeted pharmacological therapies capable of modulating the underlying fibrotic signalling pathways. This need is further amplified by the expected rise in arthrofibrosis prevalence in parallel with increasing TKA rates, which will place a growing clinical and socioeconomic burden on patients and healthcare systems. The present study aims to address this need, with its specific aims, hypotheses, and significance outlined in the following chapter.

Chapter 2 Research Objectives and Significance

Initial conservative management of arthrofibrosis does not consistently alleviate pain and stiffness and may, in certain cases, worsen symptoms (6,222). When these measures fail, subsequent surgical interventions such as MUA and lysis of adhesions (arthroscopic or open) become necessary; however, they are costly and technically complex procedures with variable outcomes and inherent risks and complications (e.g., 13,14,19). Furthermore, these procedures are only appropriate within specific postoperative time windows. For instance, MUA is typically not recommended beyond 12 weeks after pTKA due to the elevated risk of patellar fracture or tendon rupture associated with the increased tensile strength of matured adhesions (163).

Clearly, there remains a critical unmet need for safe, clinically effective, and affordable treatments for arthrofibrosis following TKA. The present study seeks to address this gap through the in vitro investigation of Amazonian Amaryllidaceae alkaloids as candidate antifibrotic agents, with the hypothesis, aims, research questions, research plan, and significance of this work outlined in the present chapter.

2.1 Rationale for candidate compound selection

2.1.1 Amaryllidaceae alkaloids as a chemically distinct and pharmacologically diverse family

Alkaloids are a structurally diverse group of naturally occurring, nitrogen-containing organic compounds found primarily in plants, often possessing potent and wide-ranging biological activities (223). The Amaryllidaceae plant family is particularly distinguished by its alkaloid richness, having yielded more than 636 unique alkaloids (224). Biosynthetically, all Amaryllidaceae alkaloids share a common precursor, norbelladine, formed from the condensation of the amino acids phenylalanine and tyrosine (225). Oxidative coupling of norbelladine at different positions gives rise to the structurally distinct carbon skeletons found exclusively within this plant family, including the lycorine, homolycorine, crinine, haemanthamine, narciclasine, tazettine, montanine,

and galanthamine skeletal types (224). From these foundational scaffolds, a complex network of enzymatic transformations, in which one alkaloid frequently serves as the biosynthetic precursor to another, generates a broad spectrum of structurally diverse compounds (226,227). This remarkable structural diversity is reflected in a potent and wide-ranging array of bioactivities, including anti-viral (228), anti-bacterial (229), anti-tumour (230), anti-fungal (231), antimalarial (232), anti-cholinesterase (229), and analgesic effects (1). Consequently, Amaryllidaceae alkaloids are attracting considerable and increasing interest as promising molecular scaffolds for drug discovery and clinical development (226).

2.1.2 Candidate compounds: Galanthine, lycorenine, pseudolycorine, and powelline

The four alkaloids selected for investigation in the present study (galanthine, lycorenine, pseudolycorine, and powelline) were isolated from the bulbs of Amazonian Amaryllidaceae species. The compounds represent three structurally distinct alkaloid subclasses within the Amaryllidaceae family: galanthine and pseudolycorine are both lycorine-type alkaloids, lycorenine belongs to the homolycorine skeleton type, and powelline is a crinine-type alkaloid (Figure 2-1; 224). This structural diversity across lycorine-, homolycorine-, and crinine-type scaffolds encompasses pharmacologically distinct subclasses within the broader Amaryllidaceae alkaloid family, making them collectively well-suited to a comparative antifibrotic screen (233–235).

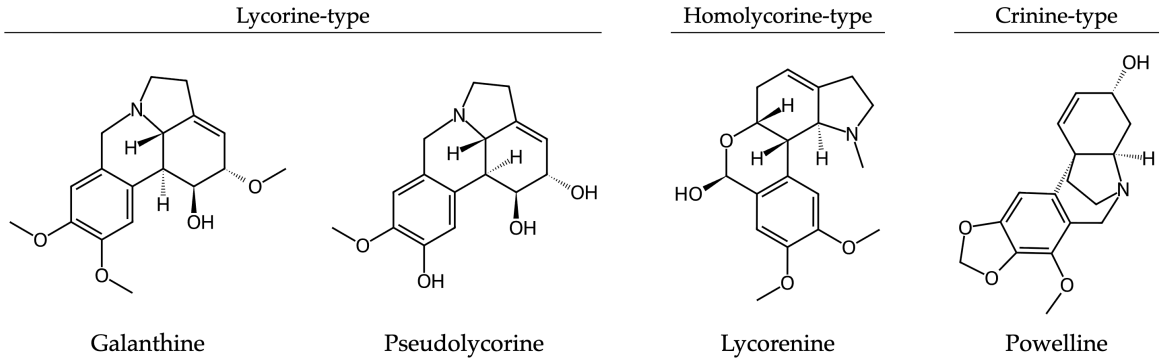

Figure 2-1 Chemical structures of the candidate Amaryllidaceae alkaloids, grouped by skeletal type.

The existing fibrosis-relevant pharmacological literature on these four specific compounds is limited. Pseudolycorine has demonstrated direct anti-inflammatory

activity relevant to fibrotic disease, having been shown to inhibit the dose-dependent expression of the pro-inflammatory cytokines TNF-α and IL-1β in human peripheral blood mononuclear cells (236). For powelline, structurally related cripowellin-type crinine alkaloids have demonstrated inhibition of COX-2 inflammatory enzymes, as well as antimicrobial, antioxidant, and anti-inflammatory activities, providing indirect structural support for its potential bioactivity (237). Galanthine was identified as one of the alkaloids with the highest statistical weight in a regression model of Amaryllidaceae alkaloid-containing extracts for pro-inflammatory IL-6 production in UVB-exposed keratinocytes, suggesting a meaningful contribution to IL-6 reduction (238). The genus Lycoris, from which lycorenine is isolated, has been identified as a source of alkaloids with potent anti-inflammatory activities, supported by evidence from both in vitro and in vivo models as well as traditional medicinal use (239). Taken together, the structural diversity of the four candidate compounds, the anti-inflammatory properties demonstrated by some of the compounds, and their largely uncharacterised activities in the context of fibrosis collectively provide the rationale for their evaluation as candidate antifibrotic agents in the present study.

2.2 Hypothesis

It is hypothesised that galanthine, lycorenine, pseudolycorine, and powelline, Amaryllidaceae alkaloids isolated from Amazonian bulbs, possess in vitro antifibrotic activity, and that a lead compound can be identified and characterised through dose-response analysis. Furthermore, it is hypothesised that the antifibrotic effect of the lead compound is mediated through a defined and selective transcriptional mechanism involving the differential regulation of fibrosis-associated gene networks.

2.3 Aims

1. Evaluate the in vitro antifibrotic activity of galanthine, lycorenine, pseudolycorine, and powelline by quantifying their effects on the hallmark markers of the fibrotic

phenotype: α-SMA expression as a measure of fibroblast-to-myofibroblast activation, and Col-I deposition as a marker of pathological ECM accumulation.

2. Determine the IC_{50} of the lead compound identified in Aim 1, to characterise its potency and establish an appropriate treatment concentration for subsequent mechanistic investigation.

3. Elucidate the potential mechanism of action of the lead compound by evaluating treatment-induced changes across a broad panel of fibrosis-associated gene targets, with the goal of identifying the transcriptional pathways that underlie its antifibrotic activity.

2.4 Research questions

1. Do galanthine, lycorenine, pseudolycorine, and powelline exhibit in vitro antifibrotic activity, as reflected by reductions in α-SMA expression and Col-I deposition?

2. Which compound demonstrates the greatest antifibrotic potency, and at what concentration does it exert half-maximal inhibitory activity?

3. What is the mechanism of action underlying the antifibrotic activity of the lead compound?

2.5 Research plan

The three research questions outlined above will be addressed sequentially, with each experimental phase informing the next. The experimental workflow is summarised below.

To address Research Question 1, the in vitro antifibrotic activity of galanthine, lycorenine, pseudolycorine, and powelline will be evaluated using the Scar-in-a-Jar assay, a phenotypic high-content imaging platform that quantifies fibrotic marker deposition

under conditions that closely replicate the in vivo ECM environment. Compounds will be screened at two concentrations (1 μM and 10 μM) and their effects on Col-I deposition and α-SMA expression quantified by immunofluorescence to identify a lead antifibrotic candidate.

To address Research Question 2, the potency of the lead compound identified in the first phase will be characterised through a dose-response experiment under Scar-in-a-Jar conditions across a nine-point concentration range. The resulting IC_{50} value will serve as the basis for selecting the treatment concentration used in subsequent gene expression analyses.

To address Research Question 3, the potential mechanism of action of the lead compound will be investigated by profiling treatment-induced changes in fibrosis-associated gene expression using an RT-qPCR array targeting 84 genes implicated in fibrotic signalling pathways. This will enable identification of the transcriptional networks through which the lead compound exerts its antifibrotic activity and generate mechanistic hypotheses to guide future preclinical investigation

2.6 Significance

Arthrofibrosis following TKA is poorly tolerated by patients due to the development of adherent, contractile scar tissue; this pathology manifests as persistent knee stiffness, chronic pain, and quadriceps weakness, often accompanied by gait abnormalities, crepitus, and periarticular swelling (9). These symptoms collectively impair function and significantly deteriorate quality of life (6,7). Biomechanical studies have shown that even a loss of as little as 5° of knee extension can impair gait, while reduced flexion limits the ability to sit, climb stairs, drive, and perform basic daily activities (5,8). Although arthrofibrosis is often described in the literature as a "disappointing" or "frustrating" outcome for both patients and surgeons (e.g., 7, 14,240), such descriptors understate its true impact. Indeed, many patients find arthrofibrosis more debilitating than the original degenerative condition or injury that necessitated the TKA (241,242). Semi-structured

interviews have revealed that symptoms exert an overwhelming impact on daily activities, social functioning, and mental and emotional well-being, and can even result in job loss (5,7).

Historically, a lack of consensus on the definition of arthrofibrosis has significantly impeded research into its aetiology, pathogenesis, prevalence, and treatment outcomes (13). Nevertheless, the burden of arthrofibrosis is expected to rise sharply in parallel with increasing TKA demand in an ageing global population (23). In Australia, the incidence of TKA for osteoarthritis is expected to rise by 276% by 2030 from the current annual rate of over 53,500 procedures (207), while in the United States, annual TKA volumes are projected to exceed one million by 2040 (33). This growing incidence of arthrofibrosis following TKA is expected to diminish the quality of life for an increasing number of patients and their families, while placing a substantial societal and economic burden through lost productivity and increased healthcare costs associated with operating theatre use, surgeon and staff time, specialised equipment, and postoperative high-dependency care (1,26,103). Arthrofibrosis accounts for approximately 28% of surgical readmissions within 90 days of TKA (243) and 7–15% of all rTKAs (200,201,222), each of which costs more than three times as much as a primary procedure, itself ranging from AUD $19,000 to $30,000 per patient (207,244). These pressures will be compounded by an ageing orthopaedic workforce, with over one-third of Australian orthopaedic surgeons approaching retirement (245) and 60% of United States orthopaedic surgeons projected to be over 65 by 2031 (246). The far-reaching impact of arthrofibrosis stems largely from the lack of safe, consistently effective, and affordable treatments. By aiming to address this gap, the present research seeks to improve quality of life for patients affected by arthrofibrosis while reducing the broader socioeconomic burden.

2.7 Summary

Chapter 2 detailed the study's hypothesis, aims, research questions, and research plan, while highlighting its significance in addressing the unmet clinical demand for safe, effective, and affordable post-TKA arthrofibrosis treatments. Specifically, the in vitro

antifibrotic activity of four candidate Amaryllidaceae alkaloids (galanthine, lycorenine, pseudolycorine, and powelline) will be evaluated, after which the potency of the lead compound will be characterised through IC_{50} determination, and its potential mechanism of action investigated through analysis of treatment-induced changes in fibrosis-associated gene expression. Chapter 3 details the methodology designed to address the research questions.

Chapter 3 Materials and Methods

This chapter details the materials and methods employed to address the three research questions outlined in Chapter 2. The first research question, concerning whether the four candidate alkaloids exhibit in vitro antifibrotic activity, is addressed through immunofluorescence-based screening of the fibrotic markers Col-I and α-SMA using the Scar-in-a-Jar assay. The second, concerning the potency of the lead compound, pseudolycorine, is addressed through a dose-response experiment under Scar-in-a-Jar conditions to establish its IC_{50} value. The third, concerning the mechanism of action of pseudolycorine, is addressed through an RT-qPCR array profiling treatment-induced changes across 84 fibrosis-associated gene targets.

3.1 Materials

3.1.1 Candidate alkaloids

The four candidate alkaloids (galanthine, lycorenine, pseudolycorine and powelline) were obtained from the Amaryllidaceae Alkaloid Repository, held for research use at the Research School of Chemistry, Australian National University (Canberra, ACT, Australia). The repository material was acquired under a material transfer agreement from the laboratory of Henry M. Fales, PhD, Laboratory of Applied Mass Spectrometry, National Heart, Lung and Blood Institute, National Institutes of Health (Bethesda, MD, USA), and was originally isolated from the bulbs of Amazonian Amaryllidaceae species. All four were supplied at ≥98% purity, prepared as 10 mM stock solutions in dimethyl sulfoxide (DMSO), and stored at −80 °C protected from light.

3.1.2 Cell culture

- 1BR3 Fibroblast Cell Line (Sigma-Aldrich, Australia, Cat. #90011801-1VL)
- Phosphate-Buffered Saline (PBS; JCSMR, Australia)
- TrypLE™ Express Enzyme, no phenol red (Gibco, Australia, Cat. #12604013)

- Dulbecco's Modified Eagle Medium (DMEM), high glucose, GlutaMAX™ Supplement, pyruvate (DMEM; Gibco, Australia, Cat. #10569044)

- Fetal Bovine Serum (FBS; Sigma-Aldrich, Australia, Cat. #12003C)

- Penicillin-Streptomycin-Neomycin (PSN) Antibiotic Mixture (Gibco, Australia, Cat. #15640055)

- T25 Nunc EasYFlask Cell Culture Flasks (Thermo Scientific, Australia, Cat. #156367)

- T75 Nunc EasYFlask Cell Culture Flasks (Thermo Scientific, Australia, Cat. #156499)

- Serological Pipettes, Stripette Paper/Plastic-Wrapped Disposable Polystyrene, Sterile (Corning, USA, Cat. #4488 & #4489)

3.1.3 Scar-in-a-Jar assay

- PhenoPlate 96-well, black, optically clear flat-bottom, tissue-culture treated (Revvity, Australia, Cat. #6055302)

- L-Ascorbic acid 2-phosphate sesquimagnesium salt hydrate (Sigma-Aldrich, Australia, Cat. #A8960)

- Human TGF-beta 1 Recombinant Protein, PeproTech (Cat. #100-21)

- SB-525334 (ProbeChem, China, Cat. #PC-42858),

- PXS-5505 dihydrochloride monohydrate (ProbeChem, China, Cat. #PC-21385)

- DMSO (Univar Solutions, Australia, Cat. #16186025)

- PVP40 (Merck, Australia, Cat. #PVP40)

- Paraformaldehyde (Sigma-Aldrich, Australia, Cat. #158127)

- TWEEN 20 (Merck, Australia, Cat. #P1379)

- Triton X-100 (Sigma-Aldrich, Australia, Cat. #T8787)

- Alpha-Smooth Muscle Actin (D4K9N) Rabbit Monoclonal Antibody (Cell Signaling Technology, USA, Cat. #19245, Lot: 6)

- Anti-Collagen Type I (COL1A1) Antibody mouse monoclonal, COL-1, (Sigma-Aldrich, Australia, Cat. #C2456, Lot: 0000278884)

- Goat anti-Rabbit IgG (H+L) Highly Cross-Adsorbed Secondary Antibody, Alexa Fluor™ Plus 647 (Invitrogen, Australia, Cat. #A32733TR)

- Goat anti-Mouse IgG (H+L) Highly Cross-Adsorbed Secondary Antibody, Alexa Fluor™ Plus 488 (Invitrogen, Australia, Cat. #A32723TR)

- CellMask Plasma Membrane Stains (Invitrogen, Australia, Cat. #C10045)

- Hoechst 33342 (Thermo Scientific, Australia, Cat. #62249)

- Aluminium foil (Confoil, Australia)

- Revvity Opera Phenix High-Content Imaging Microscope (Revvity, Australia, Cat. #HH14001000)

3.1.4 RT-qPCR

- RNeasy Mini Kit (QIAGEN, Australia, Cat. #74104)

- RNA ScreenTape (Agilent, Australia, Cat. #5067-5576)

- RNA ScreenTape Sample Buffer (Agilent, Australia, Cat. #5067-5577)

- Agilent 4200 TapeStation system (Agilent, Australia, Cat. #G2991AA)

- 10 ml Luer Lock Terumo Syringes (Terumo, Australia, Cat. #SS-10L)

- Terumo AGANI Hypodermic Needles 23G x 16mm (Terumo, Australia, Cat. #AN*2316R1)

- RNase AWAY (Sigma-Aldrich, Australia, Cat. #83931)

- 0.2 ml PCR Tubes with Flat Caps, high profile, clear (Bio-Rad, USA, Cat. #TFI0201)

- Axygen MaxyClear Snaplock Microtubes, 1.5 mL (Axygen, China, Cat. #14-222-155)
- 1000 µl Universal Barrier Tip (Neptune, USA, Cat. #63300749)
- Axygen 10 µL Microvolume Pipette Tips (Corning, USA, TXLF-10-R-S)
- Axygen 200 µL Universal Fit Filter Tips (Corning, USA, TF-200)
- RT^2 First Strand Kit (QIAGEN, Australia, Cat. #330401)
- Eppendorf Mastercycler ep gradient S (Eppendorf AG, Germany, Model 5345)
- Eppendorf Centrifuge 5418 (Eppendorf AG, Germany, Model 5418)
- RT^2 SYBR Green ROX qPCR Mastermix (QIAGEN, Australia, Cat. #330520)
- RT^2 Profiler PCR Array Human Fibrosis (QIAGEN, Australia, Cat. #330231)
- Ethanol Absolute (Ajax Finechem, Australia, Cat. #AJA5077-20PL)
- Universal 32 Benchtop Centrifuge (Hettich, Germany, Cat. #1605)
- QuantStudio 12K Flex Real-Time PCR System (Applied Biosystems, USA, Cat. #4471134)

3.2 Methods

3.2.1 Routine cell culture

The 1BR3 human fibroblast cell line was used for all experiments in this study and maintained according to standard mammalian cell culture procedures (247). Cultures were established by thawing a 1.5 mL vial of cryopreserved cells at 37 °C and transferring the suspension to a T25 flask. The cells were supplemented with 6 mL of DMEM culture medium containing 2 mM L-glutamine, 10% FBS, and 1% PSN, before being incubated in a humidified environment at 37 °C with 5% CO_2. After 24 hours, the medium containing non-adherent cells and residual cryoprotectant was aspirated, and the adherent cells were washed with culture medium to yield passage 0 cells. Routine maintenance was

performed in a humidified incubator at 37 °C with 5% CO_2, with the culture medium exchanged every 2 or 3 days. Cells were grown to approximately 80% confluence before passaging, which typically occurred every 5 to 7 days. To passage the cells, the medium was aspirated and the cell monolayer was washed briefly with PBS. The cells were then trypsinised using 0.7 mL of trypsin per 10 cm^2 for approximately three minutes at 37 °C. Once detached, an equal volume of culture medium was added to neutralise the trypsin. The resulting cell suspension was divided among T75 flasks at a 1:3 ratio, with fresh culture medium added to each flask to reach a final volume of 20 mL.

3.2.2 Scar-in-a-Jar assay

3.2.2.1 The Scar-in-a-Jar assay as an in vitro screening tool for antifibrotics

The Scar-in-a-Jar assay is a widely used in vitro fibrosis model for antifibrotic drug screening, first introduced in 2009 and subsequently optimised for medium-throughput 96-well applications (e.g., 50,51,248). A key feature is its ability to accelerate ECM deposition by culturing fibroblasts under macromolecular crowding (MMC) conditions in the presence of TGF-β1, which induces fibroblast-to-myofibroblast differentiation (50). MMC is generated using neutral carbohydrate-based macromolecules such as Ficoll and PVP40, which induce an excluded volume effect that reduces free extracellular volume, thereby enhancing enzyme-substrate interactions (249,250). Building on these molecular dynamics, MMC promotes Col-I deposition through three key mechanisms: (1) accelerating the enzymatic cleavage of the C-propeptide from procollagen to generate mature collagen; (2) enhancing the supramolecular assembly of collagen triple helices into fibrils by physically forcing them into closer proximity; and (3) facilitating ECM stabilisation by optimising the interaction between mature fibrils and cross-linking enzymes (50,251). The resulting pseudo-3D culture conditions more accurately reflect the in vivo ECM environment than conventional, highly dilute 2D systems (251,252).

Both TGF-β1 and MMC are essential components of the assay (248,250). TGF-β1 alone results in limited ECM fibril deposition, with most collagen remaining intracellular, while MMC alone has a negligible effect on mature Col-I formation; together, they increase Col-

I deposition approximately five-fold within three days, a level maintained for up to five days in culture (51). Ascorbic acid is also required, facilitating the post-translational hydroxylation of proline to hydroxyproline, which is necessary for collagen folding and stabilisation (49,251).

Compared to conventional collagen quantification methods such as hydroxyproline colorimetry and the Sircol assay, which suffer from poor specificity, labour intensity, and low throughput (253,254), the Scar-in-a-Jar assay offers a more streamlined and versatile platform for collagen quantification in vitro (51). It is highly compatible with high-content optical screening (51), enabling direct immunofluorescent quantification of ECM components including Col-I, fibronectin, α-SMA, and multiple collagen subtypes, normalised to nuclear count, without requiring matrix solubilisation or extraction (51). This format supports medium-throughput phenotypic screening for antifibrotic compounds with unknown mechanisms of action, capturing multiple aspects of ECM maturation beyond transcriptional readouts or soluble collagen assays (51). In one study, the assay was used to screen over 150 novel compounds with a success rate above 95%, a Z'-factor of approximately 0.5, and a coefficient of variation below 5% in positive controls (51).

3.2.2.2 Fibrotic model induction and compound treatment

The Scar-in-a-Jar assay was employed to evaluate the in vitro antifibrotic efficacy of the test compounds. The methodology was adapted from established protocols (e.g., 50, 51,251) and further optimised to suit the specific experimental requirements of this study. To prepare cells for the assay, fibroblast cells were cultured to confluence, after which the medium was aspirated, and the monolayer was briefly washed with PBS. Cells were trypsinised using 0.5 mL of trypsin per 10 cm^2 for approximately three minutes at 37 °C, followed by the addition of an equal volume of culture medium to neutralise the trypsin. The resulting cell suspension was centrifuged at 1,200 rpm for 6 minutes at 20 °C; the subsequent pellet was resuspended in fresh, pre-warmed culture medium, and the cell concentration was determined using a haemocytometer. Cells were seeded at

100 µL/well into black-walled 96-well imaging plates at a density of 1,350 cells per well in culture medium containing 10% FBS and 1% PSN, and incubated for 12 hours at 37 °C with 5% CO_2 to allow for cell attachment and monolayer formation. Unless otherwise stated, all subsequent incubation steps were performed under these conditions.

Following the initial incubation, the medium was replaced with 100 µL of low-serum culture medium (0.4% FBS DMEM) to serum-starve the cells for 12 hours. Treatment compounds (SB-525334, PXS-5505, galanthine, lycorenine, pseudolycorine, and powelline), originally prepared as 10 mM stock solutions in DMSO, were diluted to 2x working concentrations (20 µM and 2 µM) in Scar-in-a-Jar assay medium. This assay medium consisted of 0.4% FBS DMEM supplemented with TGF-β1 (1 ng/mL), PVP40 (21.5 mg/mL), and L-ascorbic acid phosphate magnesium salt n-hydrate (50 µg/mL). A 100 µL volume of each compound solution was added to the wells, yielding final concentrations of 10 µM and 1 µM. Each concentration was assessed in three biological replicates, with each replicate comprising three technical replicates. Control conditions comprised a negative control (no treatment), a vehicle control (0.1% DMSO), a positive control (SB-525334; a TGF-β receptor I/ALK5 inhibitor), and a pharmacological reference control (PXS-5505; a potent inhibitor of the lysyl oxidase family of enzymes responsible for collagen cross-linking, with established antifibrotic efficacy demonstrated across multiple organ fibrosis models (255)). After 72 hours, the medium was exchanged with freshly prepared Scar-in-a-Jar assay medium and the corresponding treatment compounds. Cells were then incubated for a further 72 hours prior to fixation and staining.

3.2.2.3 Immunocytochemistry

Following cell culture under Scar-in-a-Jar assay conditions and compound treatment, immunocytochemistry was performed to visualise the fibrotic markers Col-I and α-SMA. Unless otherwise specified, all wash steps consisted of three additions of 200 µL/well PBS-Tween (0.05% v/v), with the plate agitated on an orbital shaker (70–80 rpm) at room temperature (RT) during each step. Between additions, the liquid was removed by flicking

and blotting the plate. Moreover, all incubation steps were performed on an orbital shaker (70–80 rpm) at RT to ensure consistent reagent distribution. Fibroblast monolayers were initially washed once with 200 µL/well of PBS, then fixed in 100 µL/well of 4% paraformaldehyde in PBS for 10 minutes, followed by 5-minute washes. Cells were permeabilised with 100 µL/well of 0.1% Triton X-100 in PBS for 10 minutes, followed by 3-minute washes, and subsequently blocked with 200 µL/well of 3% BSA in PBS for 1 hour. Primary antibodies, anti-α-SMA (1:250) and anti-Col-I (1:1000), both diluted in 1% BSA/PBS, were applied as a mixture at 100 µL/well and incubated overnight at 4 °C, followed by 5-minute washes. Secondary antibodies (1:1000 each in 1% BSA/PBS) were applied as a mixture at 100 µL/well for 1 hour at RT, protected from light, followed by 3-minute washes. Nuclei were then stained with Hoechst 33342 (1:2000, 100 µL/well) for 10 minutes and washed. Plasma membranes were subsequently stained with CellMask Orange (1:5000, 100 µL/well) for 10 minutes and washed; both dye incubation steps were performed protected from light. Finally, wells were filled with 200 µL/well of PBS and protected from light prior to imaging. Staining controls were included in parallel to ensure assay validity: secondary antibody-only wells to confirm secondary antibody specificity; unstained wells to evaluate baseline cellular autofluorescence; and single-stain controls for each primary/secondary antibody pair to verify primary specificity, confirm appropriate localisation, and assess fluorescence bleed-through. Imaging was performed using the Opera Phenix High-Content Imaging System, acquiring 14 fields of view (FOV) per well at 20× magnification.

3.2.2.4 Image analysis

Immunocytochemical images from each well, acquired as separate channels for each stain alongside a merged composite, were analysed to quantify the fibrotic markers Col-I and α-SMA. Initial image processing was performed using Harmony high-content imaging and analysis software (version 5.2) for advanced flat-field and brightfield correction. Corrected images were then exported in TIFF format to ImageJ (version 2.16.0/1.54p) for automated analysis using a custom macro script; a representative portion of this macro script is illustrated in Figure 3-1a. Briefly, a Moments thresholding

algorithm was applied to the Hoechst channel to eliminate background signal and accurately segment individual nuclei (Figure 3-1b-c). To assess Col-I deposition, a circular mask was generated around each segmented nucleus and expanded outward by a 10-pixel radius (determined via CellMask plasma-membrane morphology) to capture the extracellular region, designating the primary region of interest (ROI; Figure 3-1c-e). This ROI was applied to the Alexa Fluor 488 channel to quantify Col-I mean fluorescence intensity (MFI; Figure 3-1f). Background fluorescence was subsequently determined by inverting the ROI selection, and this background MFI was subtracted from the primary ROI MFI to yield background-corrected values (Figure 3-1g). These values were subsequently divided by the number of nuclei in the respective well, as determined by Harmony 5.2 software using Hoechst staining, to account for variability in cell number per well. The same procedure was applied to quantify α-SMA MFI, with the exception that a cytoplasmic ROI was defined using an 8-pixel radius and applied to the Alexa Fluor 647 channel.

(a)

```
// ========== Folders ==========
HoechstDir  = "/Users/saraalzaanin/Documents/Hoechst/";
a488Dir  = "/Users/saraalzaanin/Documents/Alexa488/";

// ========== File lists ==========
HoechstList = getFileList(HoechstDir);
a488List = getFileList(a488Dir);

// ========== Prepare Results ==========
run("Clear Results");
if (isOpen("ROI Manager") == 0) run("ROI Manager...");
roiManager("Reset");

// ========== Loop over Hoechst images ==========
for (i = 0; i < HoechstList.length; i++) {

    HoechstName = HoechstList[i];
    ext = toLowerCase(HoechstName);

    if (!endsWith(ext, ".tif") && !endsWith(ext, ".tiff"))
        continue;

    // ---- Extract suffix (e.g. "_B10.tif") ----
    us = lastIndexOf(HoechstName, "_");
    if (us < 0) {
        print("Skipping (cannot parse well/FOV): " + HoechstName);
        continue;
    }
    suffix = substring(HoechstName, us);

    // ---- Find matching Alexa488 image ----
    a488Name = "";
    for (j = 0; j < a488List.length; j++) {
        cand = a488List[j];
        candExt = toLowerCase(cand);
        if (!endsWith(candExt, ".tif") && !endsWith(candExt, ".tiff"))
            continue;

        if (endsWith(cand, suffix)) {
            a488Name = cand;
            break;
        }
    }

    if (a488Name == "") {
        print("No Alexa488 match for " + HoechstName);
        continue;
    }

    // ------ Open Hoechst ------
    open(HoechstDir + HoechstName);
    HoechstID = getImageID();

    // Set scale once (global)
    if (i == 0)
        run("Set Scale...", "distance=1.74 known=1 unit=micron global");

    // ------ Process Hoechst (silent duplicate) ------
    run("Duplicate...", "title=Hoechst_proc_" + i);
    procID = getImageID();
    run("16-bit");
    setAutoThreshold("Moments dark");
    run("Maximum...", "radius=10");


    // Threshold and force it into a binary mask (this guarantees a selection can be made)

    setOption("BlackBackground", true);
    run("Convert to Mask");


    run("Create Selection");

    roiManager("Reset");
    roiManager("Add");

    // ------ Open Alexa488 ------
    open(a488Dir + a488Name);
    a488ID = getImageID();

    // ------ Measure ------
    roiManager("Select", 0);
    run("Measure");
    setResult("Hoechst_Image",  nResults-1, HoechstName);
    setResult("Alexa_Image", nResults-1, a488Name);


    // ------ Create and measure INVERSE ROI ------
    run("Make Inverse");
    roiManager("Add");        // ROI index 1
    roiManager("Select", 1);
    run("Measure");
    setResult("Region", nResults-1, "Inverse_ROI");
    setResult("Hoechst_Image",  nResults-1, HoechstName);
    setResult("Alexa_Image", nResults-1, a488Name);


    // ------ Cleanup for this iteration ------

    selectImage(procID); close();
    selectImage(HoechstID); close();
    selectImage(a488ID); close();
}

// ========== FINAL CLEANUP ==========
run("Close All");         // ensures no images remain open
roiManager("Reset");      // optional: clear ROIs
print("Batch processing complete.");
```

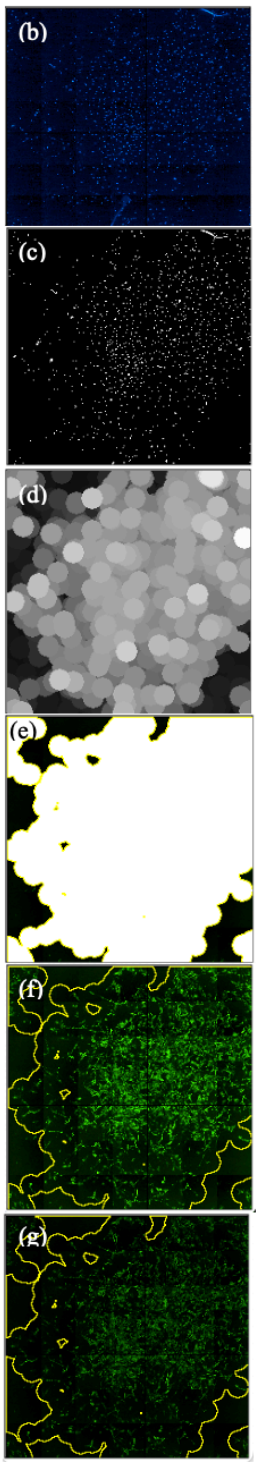

Figure 3-1 Automated image analysis pipeline for fibrotic marker quantification. (a) Representative ImageJ macro script utilised for automated processing. (b) Original Hoechst image; (c) 16-bit image thresholded using the Moments algorithm; (d) nuclear mask expanded by a defined pixel radius approximating cell diameter to delineate the extracellular region; (e) region of interest (ROI) defined from the expanded mask; (f) ROI applied to the Alexa Fluor 488 channel to quantify mean fluorescence intensity; (g) ROI inverted to measure background fluorescence for subtraction.

3.2.3 Pseudolycorine dose-response assay

To characterise the potency of pseudolycorine and establish an appropriate treatment concentration for subsequent RT-qPCR experiments, the response of fibroblasts to pseudolycorine was evaluated across nine concentrations using 3.16-fold serial dilutions ranging from 1 nM to 10 µM under Scar-in-a-Jar conditions. Concentrations were selected in accordance with established pharmacological protocols for robust curve fitting (256).

Cell seeding was performed as described in section 3.2.2.2. Briefly, 1BR3 fibroblasts were seeded at 100 µL/well into black-walled 96-well imaging plates at a density of 1,350 cells per well in culture medium containing 10% FBS and 1% PSN, and incubated for 12 hours at 37 °C with 5% CO_2. Following the initial incubation, the medium was replaced with 100 µL of low-serum culture medium (0.4% FBS DMEM) to serum-starve the cells for 12 hours (37 °C, 5% CO_2). Scar-in-a-Jar assay medium was prepared consisting of 0.4% FBS DMEM supplemented with TGF-β1 (1 ng/mL), PVP40 (21.5 mg/mL), L-ascorbic acid phosphate magnesium salt n-hydrate (50 µg/mL), and 0.2% DMSO. Pseudolycorine dilutions were prepared from a 10 mM stock via eight sequential 3.16-fold dilutions in Scar-in-a-Jar assay medium to yield concentrations ranging from 2 nM to 20 µM. A 100 µL volume of each dilution was then added to the existing 100 µL of medium in the wells, resulting in final concentrations of 1 nM to 10 µM (n = 3 per concentration). Vehicle control wells received 100 µL of diluent (n = 3), and basal control wells received 100 µL of medium lacking TGF-β1 to serve as basal α-SMA expression controls (n = 3). Cells were incubated for 72 hours at 37 °C with 5% CO_2, after which the medium was exchanged with freshly prepared Scar-in-a-Jar assay medium containing the corresponding treatment concentrations. Cells were then incubated for a further 72 hours under the same conditions. α-SMA staining and image analysis were performed as described in section 3.2.2.4.

Pseudolycorine concentrations were log-transformed and plotted against α-SMA MFI normalised to the vehicle control, and three-parameter non-linear regression dose-response curves were fitted in GraphPad Prism (v11.0.0) to determine the IC_{50}.

3.2.4 RT-qPCR array profiling of fibrosis-associated genes

3.2.4.1 Cell seeding and treatment for RT-qPCR

To investigate gene expression changes following treatment with the lead compound, RT-qPCR was performed using 1BR3 fibroblasts seeded at a density of 8,000 cells/cm^2 in eight T75 flasks. Cells were allowed to attach and form a monolayer for 12 hours, after which the culture medium was replaced with 15 mL culture medium supplemented with TGF-β1 (1 ng/mL), PVP40 (21.5 mg/mL), and L-ascorbic acid phosphate magnesium salt n-hydrate (50 µg/mL). A 10 mM DMSO stock solution of pseudolycorine was added to four flasks to achieve a final concentration of 1.84 µM, corresponding to the IC_{50} determined from the prior dose-response experiment, thereby ensuring that transcriptomic changes were evaluated at a pharmacologically relevant dose. In the remaining four flasks, an equivalent volume of DMSO was added to maintain the same final DMSO concentration, and these served as vehicle controls. Flasks were incubated at 37 °C in a humidified incubator with 5% CO_2. After 72 hours, the medium was exchanged with freshly prepared assay medium containing the corresponding treatments, and flasks were incubated for a further 48 hours, at which point cells had reached confluence and were harvested for RNA extraction.

3.2.4.2 RNA extraction

Total RNA was extracted from the treated 1BR3 fibroblasts using the QIAGEN RNeasy Mini Kit in accordance with the manufacturer's protocol (RNeasy Mini Handbook, 04/2023). The culture medium was aspirated and the monolayer briefly washed with PBS. Cells were trypsinised (0.5 mL trypsin per 10 cm^2) for approximately three minutes at 37 °C, after which an equal volume of culture medium was added to neutralise the trypsin. The resulting cell suspension from each flask was centrifuged at 1,200 rpm for 6 minutes at

20 °C. The supernatant was aspirated and the pellet disrupted by addition of 350 µL Buffer RLT. The lysate was homogenised by passing through a 23-gauge needle fitted to an RNase-free syringe five times, after which an equal volume of 70% ethanol was added and mixed by pipetting. Unless otherwise specified, all subsequent centrifugation steps were performed at 8,000 × g in an Eppendorf Centrifuge 5418, with flow-through discarded after each step.

The lysate was transferred to an RNeasy spin column placed in a 2 mL collection tube in 700 µL aliquots and centrifuged for 15 seconds. To wash the spin column membrane, 700 µL Buffer RW1 was added followed by centrifugation for 15 seconds. On-column DNase digestion was then performed: 10 µL DNase I stock solution was combined with 70 µL Buffer RDD per sample, mixed by gentle inversion, and 80 µL of the resulting solution was applied directly to the spin column membrane and incubated at RT for 15 minutes. A further 350 µL Buffer RW1 was added followed by centrifugation for 15 seconds. Buffer RPE (500 µL) was added and the column centrifuged for 15 seconds, after which a second 500 µL addition of Buffer RPE was applied followed by centrifugation for 2 minutes to dry the membrane. The spin column was transferred to a new 2 mL collection tube and centrifuged for 1 minute at 14,000 × g to remove residual wash contaminants. Finally, the spin column was placed in a new 1.5 mL collection tube, 35 µL RNase-free water was applied directly to the membrane, and RNA was eluted by centrifugation for 1 minute.

3.2.4.3 RNA quantification and quality control

RNA concentration, purity, and integrity were assessed using the Agilent 4200 TapeStation system prior to complementary DNA (cDNA) synthesis, according to the manufacturer's instructions. RNA Sample Buffer was equilibrated to RT for 30 minutes. For each sample, 1 µL of RNA was combined with 5 µL RNA Sample Buffer in a strip tube and vortexed at 2,000 rpm for 1 minute, heated to 72 °C for 3 minutes, then placed on ice for 2 minutes. Samples were loaded into the TapeStation instrument and analysed using an electronic RNA ladder. RNA concentration, purity, and integrity were recorded, with an

RNA Integrity Number (RIN) threshold of ≥ 7 applied as the minimum quality criterion for proceeding to cDNA synthesis. RNA was stored at −80 °C until use.

3.2.4.4 complementary DNA (cDNA) synthesis

Isolated total RNA was reverse transcribed to cDNA using the QIAGEN RT^2 First Strand Kit, according to the manufacturer's instructions (RT^2 Profiler PCR Array Handbook, 06/2019). A uniform input quantity of 400 ng RNA per sample was used, with concentrations determined from the Agilent 4200 TapeStation output (ng/µL). Prior to reverse transcription, a genomic DNA elimination mix was prepared for each sample as outlined in Table 1, to remove residual genomic DNA contamination. The mix was incubated at 42 °C for 5 minutes in an Eppendorf Mastercycler ep Gradient S, then placed immediately on ice for 1 minute.

Table 1 QIAGEN Genomic DNA elimination mix

Component	**Amount**
RNA	400 ng
Buffer GE	2 µL
RNase-free water	Variable
Total volume	**10 µL**

A reverse transcription mix was prepared sufficient for eight samples, and 10 µL was combined with 10 µL of each genomic DNA elimination mix per sample. The resulting mixture was incubated at 42 °C for exactly 15 minutes in an Eppendorf Mastercycler ep Gradient S to facilitate cDNA synthesis, after which the reaction was terminated by incubation at 95 °C for 5 minutes. Finally, 91 µL RNase-free water was added to each reaction and mixed by pipetting. Samples were stored at −80 °C until use.

Table 2 QIAGEN Reverse-transcription mix

Component	Amount
5x Buffer BC3	36 µL
Control P2	9 µL
RE3 Reverse Transcriptase Mix	18 µL
RNase-free water	27 µL
Total volume	**90 µL**

3.2.4.5 RT-qPCR

To quantify the expression of fibrosis-related genes in pseudolycorine-treated and vehicle control cells, RT-qPCR was performed on the synthesised cDNA using the QIAGEN RT^2 Profiler Human Fibrosis PCR Array (84 genes), according to the manufacturer's instructions (RT^2 Profiler PCR Array Handbook, 06/2019). The PCR components mix for each sample was prepared in a 1.5 mL tube as outlined in Table 3, in a darkened environment to minimise SYBR Green photodegradation.

Table 3 PCR components mix

Component	Amount
2x RT^2 SYBR Green Mastermix	650 µL
cDNA synthesis reaction	102 µL
RNase-free water	548 µL
Total volume of master mix	**1300 µL**

384 EZLoad Cover was applied to each plate to facilitate precise well alignment during pipetting, and 10 µL of the PCR components mix was loaded into each well of the RT^2

Profiler Human Fibrosis PCR Array using an 8-channel pipettor, with two vehicle control and two pseudolycorine-treated samples loaded per plate. The array plate was sealed with optical adhesive film and centrifuged at 1,000 × g for 1 minute at RT in a Universal 32 benchtop centrifuge to remove air bubbles. The plate was then placed into a QuantStudio 12K Flex Real-Time PCR System programmed with the cycling conditions outlined in Table 4. The initial heating step activated HotStart DNA Taq Polymerase, followed by amplification cycles during which fluorescence data were collected, and a final melt curve analysis to verify PCR product specificity.

Table 4 QuantStudio 12K Flex Real-Time PCR System thermal cycling programme

Stage	Cycle(s)	Duration	Temperature
Holding	1	10 min	95°C
Denaturation Annealing	40	15 s 1 min	95°C 60°C
Melt curve	Continuous	15 s 1 min 15 s	95°C 60°C 95°C

The baseline was determined using the adaptive baseline feature. A threshold value of 0.12 was defined manually using the log view of the amplification plots, set above the background signal and within the lower one-third to lower one-half of the linear amplification phase, and applied consistently across all plates. The resulting C_t values for all wells were exported to an Excel spreadsheet for further analysis.

3.2.4.6 RT-qPCR data analysis

RT-qPCR data analysis was conducted using the QIAGEN GeneGlobe Data Analysis Center. A default C_t cut-off of 35 was applied; all undetermined or exceeding C_t values

were replaced with this cut-off value prior to further calculations. Built-in positive PCR controls, reverse transcription controls, and genomic DNA contamination controls passed quality thresholds across all samples.

To identify the most appropriate reference gene for normalisation, the stability of the five candidate reference genes was evaluated using RefFinder, which integrates four major computational algorithms — geNorm, NormFinder, BestKeeper, and the comparative ΔC_t method — to rank candidate reference genes (257). Each program assigns a weighted score to individual genes, and the geometric mean of these weights determines the overall stability ranking. GAPDH was identified as the most stable reference gene and was used as the normalisation factor.

Fold changes in gene expression between pseudolycorine-treated and vehicle control groups were calculated using the $\Delta\Delta C_t$ method (258). ΔC_t values were first calculated for each gene of interest (GOI) by subtracting the reference gene C_t value from the GOI C_t value:

$$\Delta C_t = C_t(\text{GOI}) - C_t(\text{reference gene})$$

$\Delta\Delta C_t$ values were then calculated by subtracting the mean ΔC_t of the vehicle control group from the ΔC_t of each treatment sample:

$$\Delta\Delta C_t = \Delta C_t(\text{treatment}) - \text{mean } \Delta C_t(\text{control})$$

Fold change was calculated by converting $\Delta\Delta C_t$ from a $\log_2$ scale to a linear scale:

$$\text{Fold Change} = 2^{(-\Delta\Delta C_t)}$$

3.2.5 Statistical analysis

Background-corrected MFI values derived from immunocytochemical images for each treatment group in the Scar-in-a-Jar assay were exported to GraphPad Prism (version 11.0.0). Normality was confirmed using the Shapiro–Wilk test and homogeneity of variances using the Brown–Forsythe test. One-way analysis of variance (ANOVA) followed by Sidak's multiple comparisons test was used to compare each treatment group against its respective vehicle control. A p-value of < 0.05 was considered statistically significant. Results are expressed relative to vehicle control (0% inhibition) and as mean ± standard error of the mean (SEM).

Statistical differences in fibrosis-related gene expression between vehicle control and pseudolycorine-treated groups were assessed in the QIAGEN GeneGlobe Data Analysis Center using a two-tailed unpaired Student's t-test with equal variance, applied to the $2^{(-\Delta C_t)}$ values for each gene across biological replicates. Genes were considered differentially expressed if they met both a fold change threshold of ≥ 2 or ≤ 0.5 relative to the vehicle control and a statistically significant p-value of < 0.05. In GraphPad Prism (version 11.0.0), fold change values were log2-transformed and presented as mean ± standard deviation, with genes grouped into functional categories as defined by the RT^2 Profiler PCR Array Human Fibrosis manufacturer (QIAGEN).

3.2.6 Sample size determination

Sample sizes for the Scar-in-a-Jar assay and RT-qPCR experiments were determined based on standards established in prior studies, with a minimum of three biological replicates per treatment group to ensure sufficient statistical power for the detection of biologically meaningful differences (e.g., 51,251,259).

3.3 Summary

Chapter 3 outlined the methods used to address the study's aims. Briefly, the in vitro antifibrotic activity of the candidate alkaloids was evaluated using the high-content,

phenotypic Scar-in-a-Jar assay, which enables visualisation and quantification of the fibrotic markers Col-I and α-SMA. Subsequently, a dose-response experiment was conducted under Scar-in-a-Jar conditions to determine the IC_{50} of the lead compound, pseudolycorine; this value was used to define the treatment concentration for the subsequent gene expression analysis. Finally, an RT-qPCR array was used to profile 84 fibrosis-associated genes following treatment with pseudolycorine under Scar-in-a-Jar conditions, aimed at elucidating the potential mechanism of action for this compound. The following chapter presents the results of these experiments.

Chapter 4 Results

This chapter presents the results of the experiments described in Chapter 3, collectively aimed at addressing the three research questions outlined in Chapter 2. It begins with the systematic optimisation of the Scar-in-a-Jar assay, a prerequisite step to ensure a robust platform for high-content imaging. This is followed by the immunofluorescence-based screening of the four candidate alkaloids across two concentrations, addressing whether the compounds exhibit in vitro antifibrotic activity (Research Question 1). Subsequently, a dose-response analysis of pseudolycorine is presented to establish its IC_{50} value (Research Question 2). The chapter concludes with an analysis of RT-qPCR array data characterising the changes in fibrosis-associated gene expression induced by pseudolycorine treatment, aimed at elucidating its mechanism of action (Research Question 3).

4.1 Scar-in-a-Jar assay optimisation

4.1.1 Scar-in-a-Jar v1: Sub-optimal cellular yield and attachment

The Scar-in-a-Jar assay was initially performed based on the protocol described by Chen et al. (49), with the following modifications. Passage four primary human synovial fibroblasts obtained from TKA patients with full ethical consent (ETH.9.865) were seeded at a density of 2×10^3 cells per well. PVP40 was used as the macromolecular crowding agent in place of Ficoll, as it provides optimal conditions for antifibrotic drug screening (250). Compound screening of SB-525334, PXS-5505, and the four candidate alkaloids was conducted at 1 µM and 10 µM.

Cells were fixed with 4% paraformaldehyde, which was preferred over methanol fixation to better preserve cellular morphology and ECM structure for immunofluorescent detection of Col-I and α-SMA (260), followed by permeabilisation with 0.3% Tween-20 in PBS and blocking with 3% BSA in PBS. Anti-rabbit Col-I (Proteintech, Cat. #83752-5-RR; 1:400) and anti-mouse α-SMA (Proteintech, Cat. #67735-1-Ig; 1:300) primary antibodies were co-incubated, followed by sequential application of species-specific secondary

antibodies, both at 1:1000: goat anti-rabbit IgG Alexa Fluor Plus 488 (A32733) and goat anti-mouse IgG Alexa Fluor Plus 647 (A32723), with washing steps between incubations to minimise cross-reactivity. No nuclear counterstain was used as the Incucyte S3 system detects only green and red fluorescence channels; brightfield imaging was instead used for nuclei quantification to enable normalisation of fluorescence measurements. Images were acquired at 10× magnification, capturing two fields of view per well (Figure 4-1).

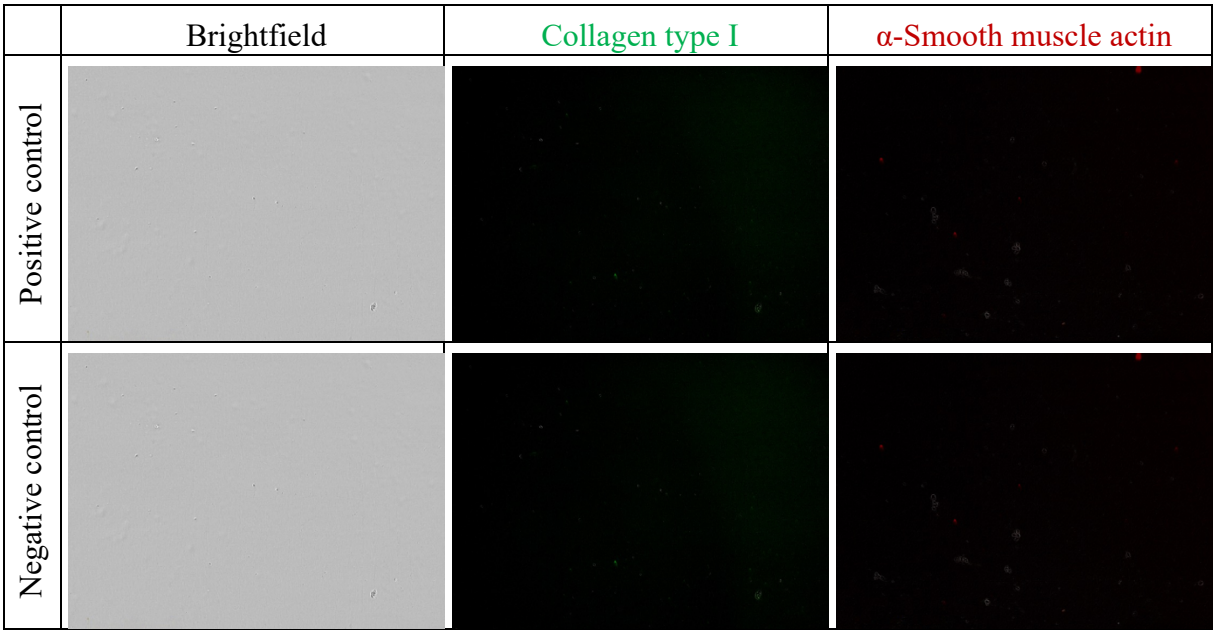

Figure 4-1 Representative images from the v1 Scar-in-a-Jar assay.
Images show the positive control (TGF-β1–treated) and negative control (TGF-β1–free) conditions. Within each row, images correspond to the same field of view and are presented as: brightfield, collagen type I (Alexa Fluor 488, green), and α-smooth muscle actin (α-SMA) (Alexa Fluor 647, red). Acquired on the Incucyte S3 system at 10× magnification. Scale bar = 100 µm.

In the initial Scar-in-a-Jar experiment, very few cells were observed, and those present displayed poor morphology consistent with loss of viability. Cells were sparsely distributed and difficult to identify by brightfield imaging. Consequently, meaningful fluorescence staining and quantitative analysis were not possible. The seeding density used in this experiment was selected based on previous experiments; however, given the substantially different culture conditions employed in the Scar-in-a-Jar assay, particularly reduced serum levels and the inclusion of additional components such as

PVP40 and TGF-β, it became apparent that this density had not been optimised for this specific context.

Furthermore, the use of primary synovial fibroblasts, which are inherently more sensitive to changes in culture conditions (e.g., serum starvation and the presence of DMSO) than immortalised cell lines (261), likely contributed to the poor cell survival observed. Primary cells also exhibit batch-to-batch variability, whereby cells derived from different donors can respond differently to the same stimuli due to genetic background and tissue heterogeneity, thereby making it difficult to achieve reproducible results across different experiments or batches of cells (262). Together, these factors highlighted the limited suitability of the experimental conditions for primary cells. Consequently, subsequent experiments incorporated a dedicated cell density optimisation step and the use of a fibroblast cell line, which provides greater robustness and reproducibility under the specialised conditions required for the Scar-in-a-Jar assay; however, this approach comes with the disadvantage that such models are more distant from the original disease context (261).

4.1.2 Cell density optimisation for Scar-in-a-Jar v2

A cell density optimisation experiment was performed using the 1BR3 human fibroblast cell line (Merck, Australia, Cat. #90011801) to establish appropriate seeding conditions for the Scar-in-a-Jar assay, as variations in density can influence drug sensitivity and introduce variability across experimental repeats, thereby acting as a confounding variable (263). A 1:2 serial dilution of cells was performed over eight steps, starting from an initial density of 50,000 cells per well. Cells were serum-starved in DMEM culture medium containing 0.4% FBS for 24 hours, followed by the addition of Scar-in-a-Jar assay components. Brightfield images were acquired to assess cell morphology, monolayer formation, and surface coverage at each seeding density (Figure 4-2).

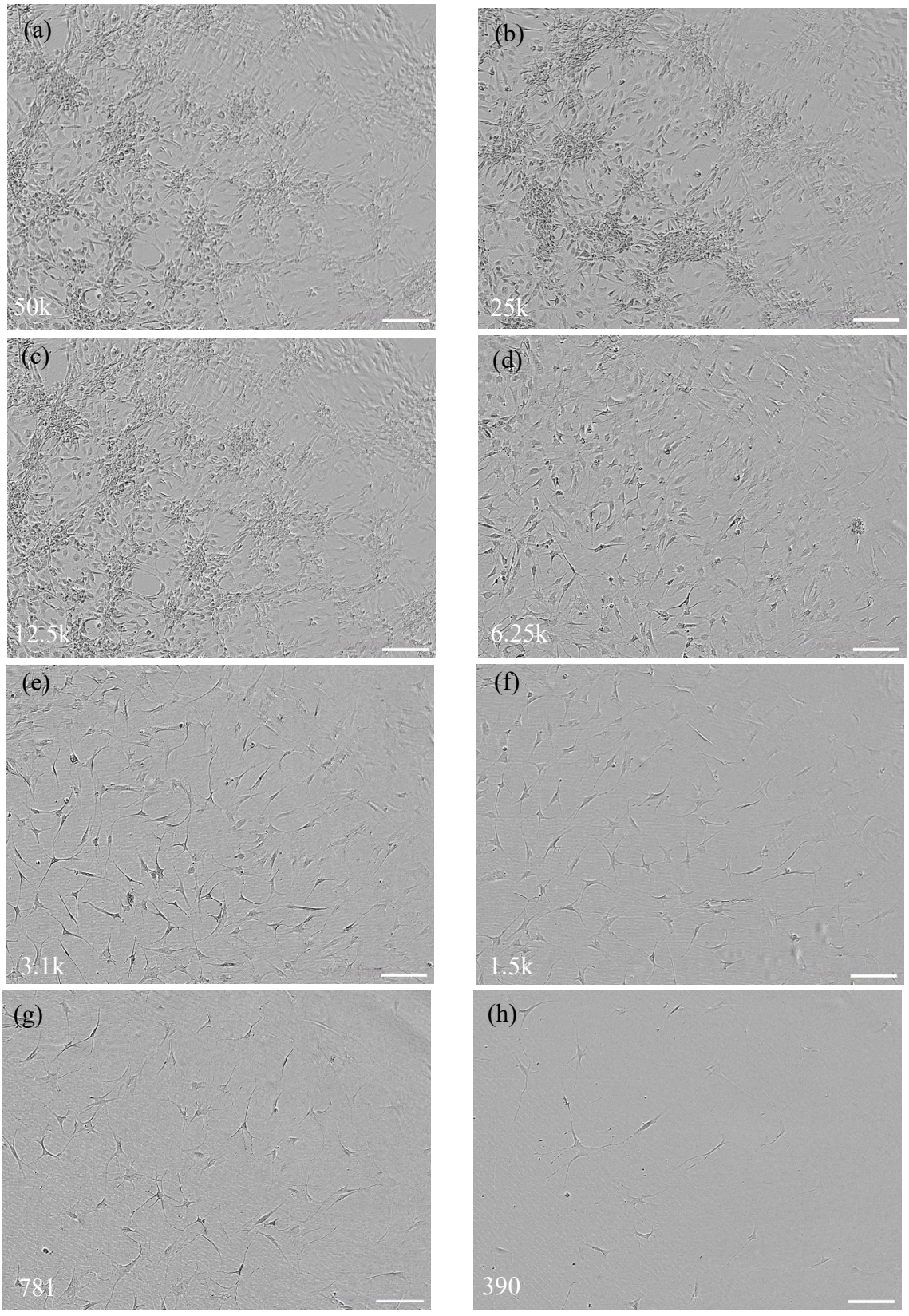

Figure 4-2 Brightfield images of 1BR3 human fibroblasts seeded at decreasing densities under Scar-in-a-Jar assay conditions.

Cells were seeded via 1:2 serial dilution across eight densities (50,000-390 cells per well). Brightfield images were acquired 48 hours after assay component addition on the Incucyte S3 system at 10× magnification. Representative images are shown for (a) 50,000, (b) 25,000, (c) 12,500, (d) 6,250, (e) 3,125, (f) 1,563, (g) 781, and (h) 390 cells per well. Scale bar = 100 µm.

At high seeding densities, cells rapidly reached near-complete confluence, exhibiting extensive cell–cell contact and evidence of overcrowding, which is commonly associated with contact inhibition and nutrient limitation (264). In contrast, low seeding densities resulted in poor cell growth, sparse coverage, and minimal cell–cell contact, leading to incomplete monolayer formation. Seeding densities between 12,500 and 6,250 cells per well produced a uniform monolayer with well-defined cell morphology and consistent cell–cell interactions. These intermediate densities corresponded to approximately 70% confluence, providing an optimal balance between active cell proliferation and sufficient cell–cell contact. Consequently, a seeding density of 8,000 cells per well was selected to support reproducible quantification in the Scar-in-a-Jar assay while avoiding full confluence and its associated negative consequences on cellular behaviour. This seeding density is also consistent with those used in previous studies (51,265).

4.1.3 Scar-in-a-Jar v2: Refinement of cell density and identification of cellular aggregation

A v2 Scar-in-a-Jar assay (see Figure 4-3) was performed using the same methodology as v1, with the exception that a seeding density of 8,000 1BR3 cells per well was used, based on the results of the preceding cell density optimisation experiment.

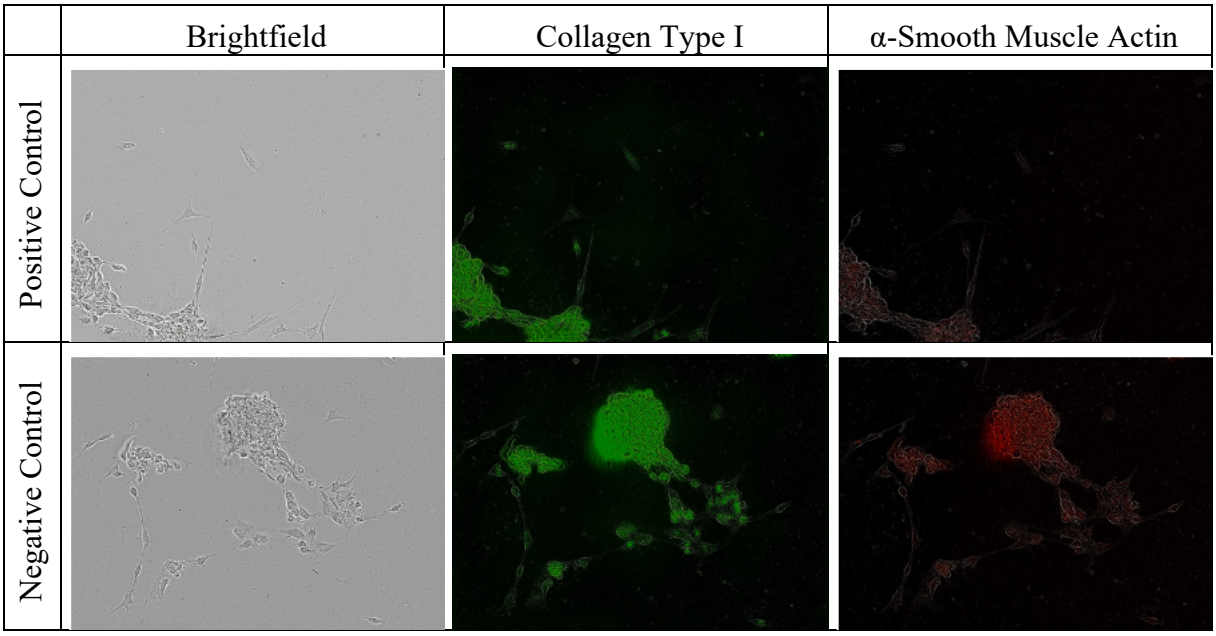

Figure 4-3 Representative images from the v2 Scar-in-a-Jar assay.
Images show the positive control (TGF-β1–treated) and negative control (TGF-β1–free) conditions. Within each row, images correspond to the same field of view and are presented as: brightfield, collagen type I (Alexa Fluor 488, green), and α-smooth muscle actin (α-SMA) (Alexa Fluor 647, red). Acquired 72 hours after assay component addition on the Incucyte S3 system at 20×. Scale bar = 100 µm.

In the v2 Scar-in-a-Jar assay, cells were clearly visible, representing an improvement over the v1 assay, and immunofluorescent staining above background levels was readily detectable. However, substantial cellular debris was present, and many viable cells appeared to aggregate and form clusters, resulting in regions of high cell density interspersed with areas devoid of cells ("cell deserts"). Uneven cell seeding can lead to variability in growth, assay outcomes, and drug responses, as densely populated regions may behave differently from sparsely populated areas (266). Such heterogeneity can obscure true biological effects; therefore, achieving uniform cell distribution at seeding is essential for generating reliable and reproducible data.

4.1.4 Scar-in-a-Jar v3: Persistence of cellular aggregation despite procedural modifications

To address cell clumping and promote uniform cell distribution, several modifications to the cell handling and seeding procedure were implemented. Trypsin exposure was minimised by reducing the volume applied to just cover the cell layer (0.5 mL per 10 cm^2

instead of 0.7 mL per 10 cm^2) and immediately inactivating the enzyme once cells were observed to have rounded and detached. Excessive trypsin exposure can result in over-digestion and the subsequent release of extracellular DNA, which promotes cell aggregation (267).

Following centrifugation, the use of a 23-gauge needle for cell resuspension was avoided to reduce shear stress–induced cell damage that can lead to the release of cell-free DNA and drive aggregation (267). Instead, cells were gently resuspended by sequential pipetting with a 1000 µL pipette tip followed by a 200 µL tip, applying minimal force sufficient to disperse clumps without damaging cell membranes.

Wells were pre-wetted prior to cell seeding by adding half of the culture medium volume before introducing the cell suspension. This approach reduces surface tension–driven localised aggregation (268). Moreover, cells were seeded by dispensing the suspension with a multichannel 200 µL pipette tip positioned against the side wall of the well just above the bottom surface and slowly releasing the suspension to encourage even lateral spreading. This was followed by five gentle pipetting steps to further improve distribution.

During and after plating, cells were gently redistributed using a cross-shake mixing technique, whereby the plate was moved in a gentle "+" pattern (left–right and forward–backward, repeated 5–6 times), rather than circular swirling, which can drive cells toward the centre of the well. Following plating, plates were left undisturbed in the biosafety cabinet at RT for 30 minutes to allow uniform cell settling and initial attachment prior to transfer to the 37 °C incubator (269). This step minimises thermal gradients that can arise when plates are immediately placed at 37 °C, which may otherwise generate convection currents within the well, redistributing cells toward the periphery and resulting in uneven seeding, particularly in edge wells (265).

Following implementation of the modified cell handling and seeding procedures, cellular distribution across the well was more uniform compared to the v2 Scar-in-a-Jar assay,

with a noticeable reduction in large aggregation zones (Figure 4-4). However, small cell clumps were still observed. In addition, most cells displayed suboptimal morphology, appearing less spread and more contracted than typically observed under standard culture conditions (e.g. in T75 flasks), suggesting reduced cell health or altered attachment behaviour under these assay conditions.

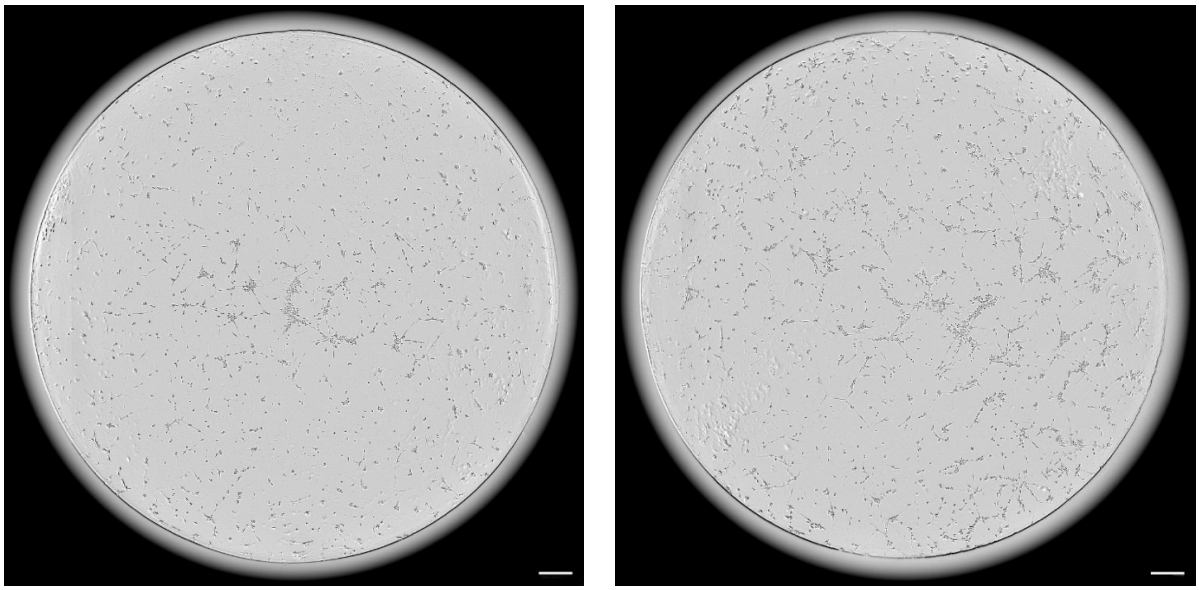

Figure 4-4 Brightfield images following optimisation of cell handling and seeding procedures.
1BR3 human fibroblasts imaged 72 hours after Scar-in-a-Jar assay component addition on the Incucyte S3 system at 4×. Scale bar = 400 µm.

Consequently, immunostaining was not pursued at this stage. Instead, further investigation was undertaken to identify potential causes underlying the persistent cell clumping and reduced cell spreading observed under these assay conditions.

4.1.5 Identification of low serum concentration as the primary driver of cellular aggregation

A time-lapse experiment was performed to determine whether cell clumping occurred before or after assay component addition (Figure 4-5). This distinction was important because, if clumping occurred prior to assay component addition, it would likely be attributable to the low serum concentration, which represents the primary difference from standard fibroblast culture conditions.

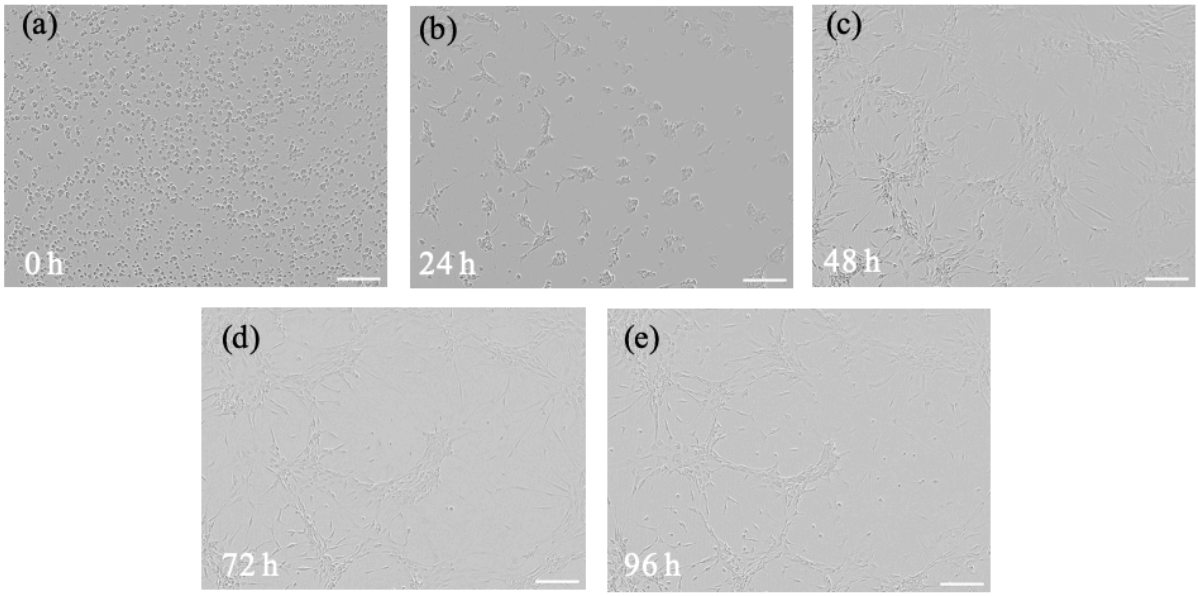

Figure 4-5 Time-lapse brightfield imaging of 1BR3 human fibroblasts cultured under Scar-in-a-Jar conditions.
Cells were cultured in 0.4% FBS DMEM with Scar-in-a-Jar assay components added at 24 h. Representative images acquired at (a) 0 h, (b) 24 h, (c) 48 h, (d) 72 h, and (e) 96 h on the Incucyte S3 system at 10×. Scale bar = 200 µm.

Time-lapse imaging revealed that cell clumping occurred prior to the addition of Scar-in-a-Jar assay components, indicating that aggregation was not induced by the assay components themselves. This observation suggested that cell clumping was likely attributable to the low-serum culture conditions (0.4% FBS). To confirm this, a comparative experiment was subsequently performed in which cells cultured under 10% FBS were directly compared with those maintained in 0.4% FBS (Figure 4-6).

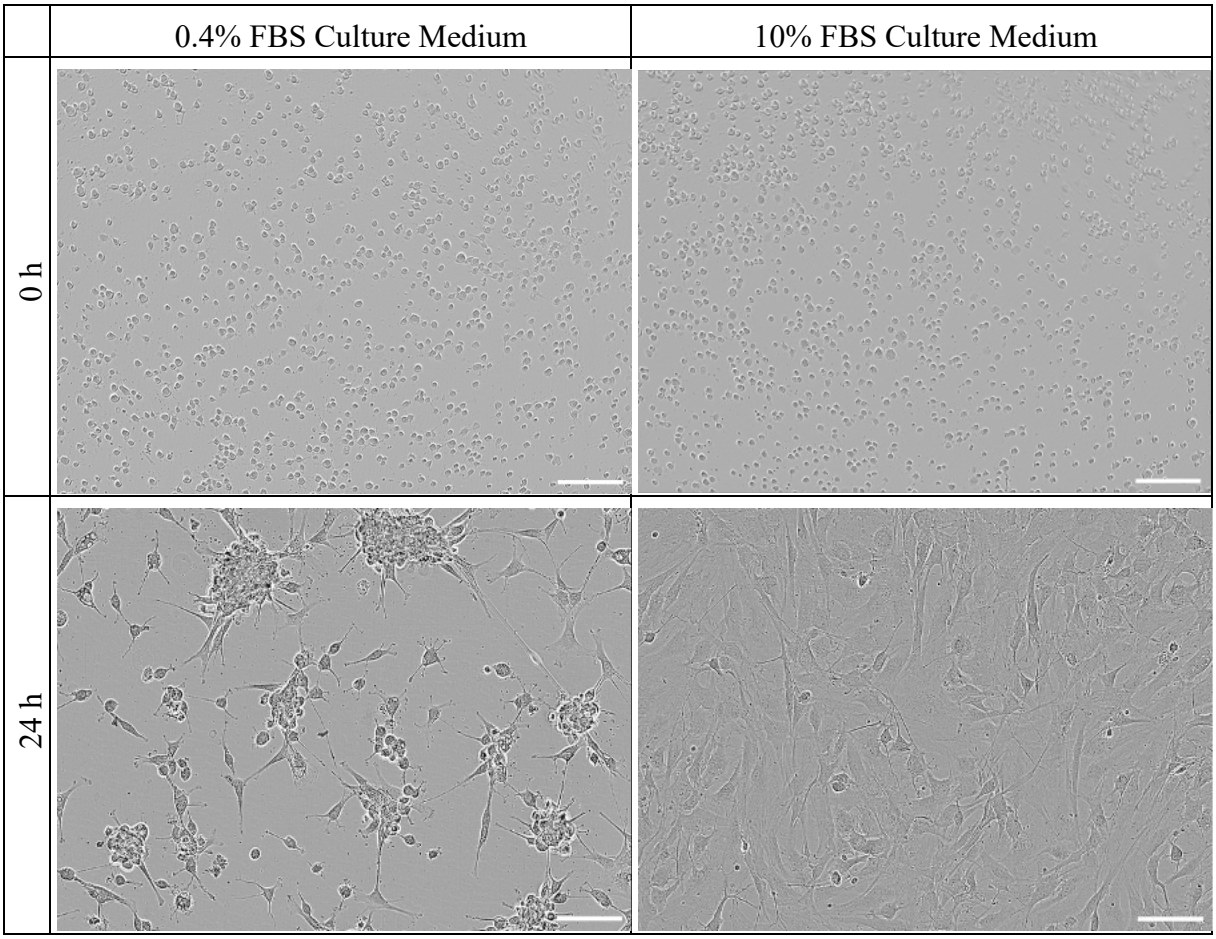

Figure 4-6 Effect of serum concentration on cell distribution and morphology following seeding.
Representative brightfield images of 1BR3 human fibroblasts seeded in 0.4% or 10% FBS, imaged immediately after seeding and at 24 hours. Upper panels: 10× magnification; lower panels: 20× magnification. Acquired on the Incucyte S3 system. Scale bar = 200 µm.

When comparing cells cultured in 10% FBS versus 0.4% FBS DMEM, cells in both conditions initially appeared rounded immediately after seeding. However, over time, cells cultured in 10% FBS exhibited robust attachment and spreading, forming a well-distributed monolayer with typical fibroblast morphology. In contrast, cells maintained in 0.4% FBS displayed limited spreading, with many cells remaining rounded and a pronounced tendency to form aggregates and clusters. These observations indicated that low-serum conditions impaired normal cell attachment and spreading, contributing to increased cell clumping.

A plausible explanation for the differences in cell morphology observed between the two serum conditions is that FBS normally supplies soluble ECM components, such as fibronectin, which adsorb to the culture surface and support integrin-mediated fibroblast attachment and spreading (270). Fibronectin provides integrin-binding sites, including RGD motifs, that are recognised by cell-surface integrins (271). Upon binding to these ECM proteins, integrins cluster to form focal adhesions, multiprotein complexes that connect the extracellular environment to the intracellular actin cytoskeleton (271). This linkage enables cells to generate traction forces, spread across the substrate, and adopt their characteristic fibroblast morphology (272).

Under low-serum conditions (0.4% FBS), reduced availability of fibronectin and other adhesion-promoting factors compromises integrin-mediated adhesion and focal adhesion assembly, thereby limiting cell spreading and stabilisation on the culture surface (273). As a result, fibroblasts exhibit reduced spreading, with many cells remaining rounded and preferentially engaging cadherin-mediated cell–cell adhesion, particularly via cadherin-11, a fibroblast-enriched cadherin strongly associated with fibroblast clustering and fibrotic tissue organisation (274). In contrast, cells cultured in 10% FBS benefit from sufficient attachment and spreading factors, promoting robust integrin-mediated adhesion, cytoskeletal organisation, and uniform cell spreading across the culture surface (273). This interpretation was further supported by experiments in which the FBS concentration was incrementally increased in 2% steps from 0% to 10%, and cell morphology was monitored (Figure 4-7).

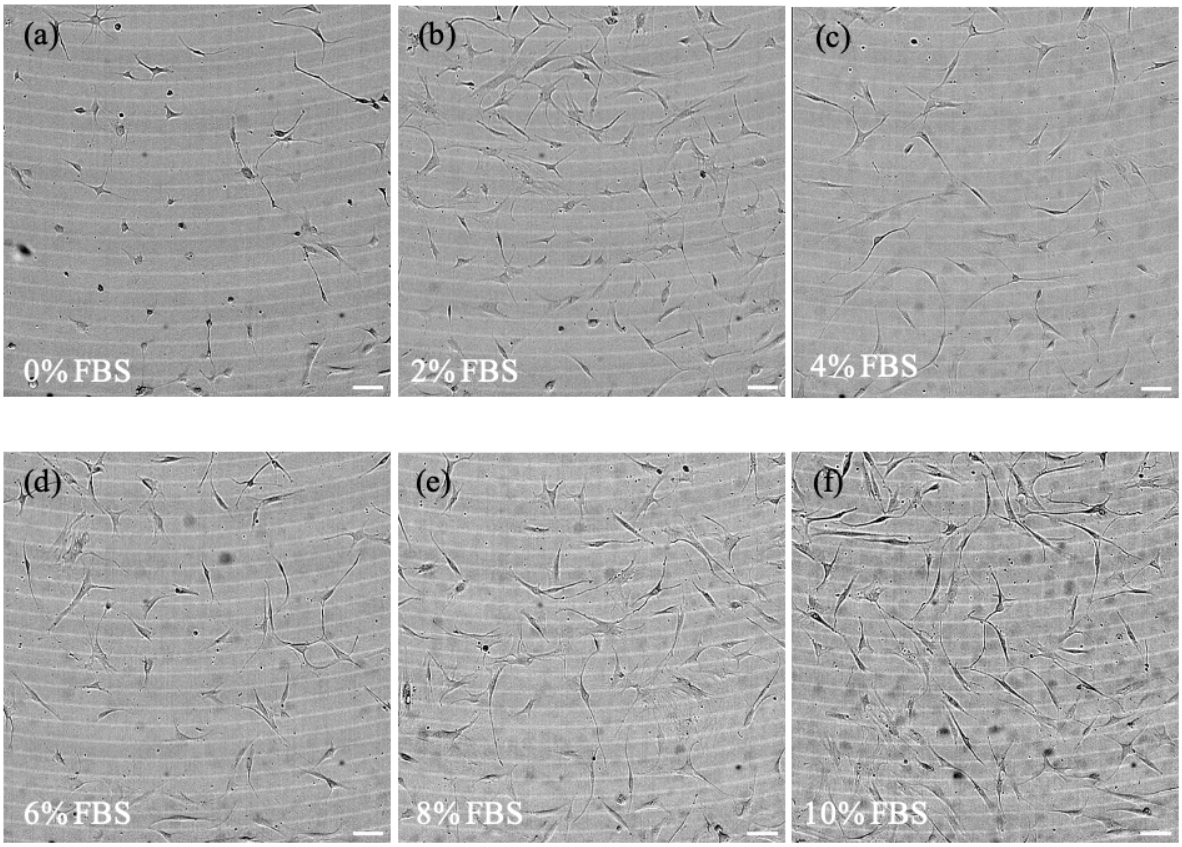

Figure 4-7 Effect of increasing serum concentration on fibroblast morphology and spreading.
Representative brightfield images of 1BR3 human fibroblasts cultured in DMEM with increasing FBS concentrations (0–10% in 2% increments), imaged 24 hours after seeding. Panels: (a) 0%, (b) 2%, (c) 4%, (d) 6%, (e) 8%, and (f) 10% FBS. Acquired on the Opera Phenix at 10×. Scale bar = 100 µm.

Under 0% FBS conditions, cells remained predominantly rounded with minimal spreading. As the FBS concentration increased, progressive enhancement of cell attachment and spreading was observed, with cells cultured in higher serum concentrations exhibiting more typical fibroblast morphology. These observations further indicated that serum-derived factors play a critical role in promoting fibroblast spreading and maintaining typical cell–substrate interactions.

4.1.6 Serum conditioning (10%→0.4% FBS) yields a uniform cell monolayer

After identifying that low-serum conditions were impairing fibroblast attachment and spreading, cells were first allowed to establish a monolayer by culturing in standard

growth medium (10% FBS) for 12 hours. This timeframe is sufficient for fibroblasts to transition from a rounded, suspended state to a stable, well-spread morphology with established focal adhesions, while still being short enough to prevent significant proliferation or overcrowding (275). The cells were then rinsed with PBS and switched to low-serum medium (0.4% FBS) for a further 12 hours to achieve serum starvation prior to compound treatment.

The serum-starvation step was maintained rather than performing the assay entirely in 10% FBS, as the undefined composition of FBS, encompassing growth factors, cytokines, hormones, and serum proteins, can introduce unwanted variability into the assay (276). Such components may interact unpredictably with test compounds, making it difficult to determine whether any observed anti-fibrotic effect is attributable to the compound itself or to an interaction with serum constituents (277). The biochemical composition of FBS also varies between batches, which can alter fibroblast behaviour and affect the reproducibility of fibrosis-related readouts (276). Furthermore, serum proteins such as albumin can bind small-molecule compounds and reduce their effective concentration, thereby modifying the cellular response (278). Serum starvation also serves an important experimental purpose by helping to synchronise cells into a similar cell-cycle state (279). This reduces cell-cycle–dependent variability in experimental responses and allows for more consistent assessment of compound effects once the Scar-in-a-Jar assay components are added.

As shown in Figure 4-8, the transition from 10% FBS (12 hours) to 0.4% FBS (24 hours) produced a uniform monolayer in which fibroblasts displayed robust surface attachment and normal spreading, likely supported by the higher availability of serum-derived adhesion and spreading factors during the initial attachment period (270). No visible clumping or aggregation was observed. This indicated that allowing initial attachment under high-serum conditions can effectively prevent the impaired spreading and clustering previously observed under continuous low-serum culture.

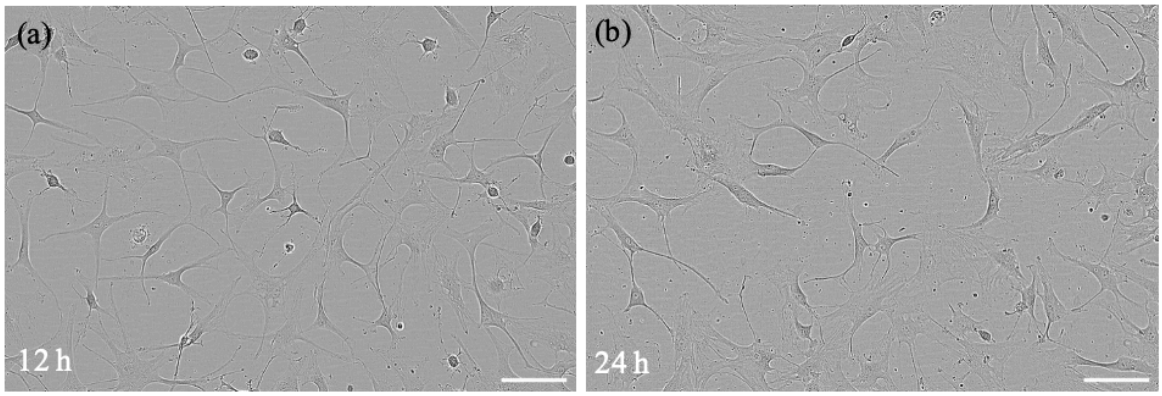

Figure 4-8 Fibroblast morphology during attachment and subsequent serum starvation.
Representative brightfield images of 1BR3 human fibroblasts after (a) 12 hours in 10% FBS and (b) a subsequent 12 hours in 0.4% FBS. Acquired on the Incucyte S3 system at 20×. Scale bar = 100 µm.

The Scar-in-a-Jar assay (v4) was performed using the same seeding density as in the previous serum conditioning experiment (3,000 cells per well). A nuclear stain (Hoechst) was incorporated to enable accurate nuclei quantification, as the nuclei-detection module in the image analysis software is not sufficiently reliable when identifying nuclei from brightfield images alone. As this introduced a blue fluorescence channel, imaging was carried out using the Opera Phenix high-content microscope.

4.1.7 Scar-in-a-Jar v4: Background-level fibrotic marker staining

Analysis of the v4 Scar-in-a-Jar assay revealed that staining specificity was insufficient to enable reliable quantification of either fibrotic marker. For α-SMA, the MFI of the primary and secondary stain (3.869 ± 0.090) was only modestly higher than the secondary-only control (2.818 ± 0.156), with no distinct fibre structures visible in the images (Figure 4-9), indicating that the signal did not rise meaningfully above background. Col-I staining showed the same pattern, with the primary and secondary condition (7.695 ± 0.730) only slightly exceeding the secondary-only control (6.049 ± 0.087).

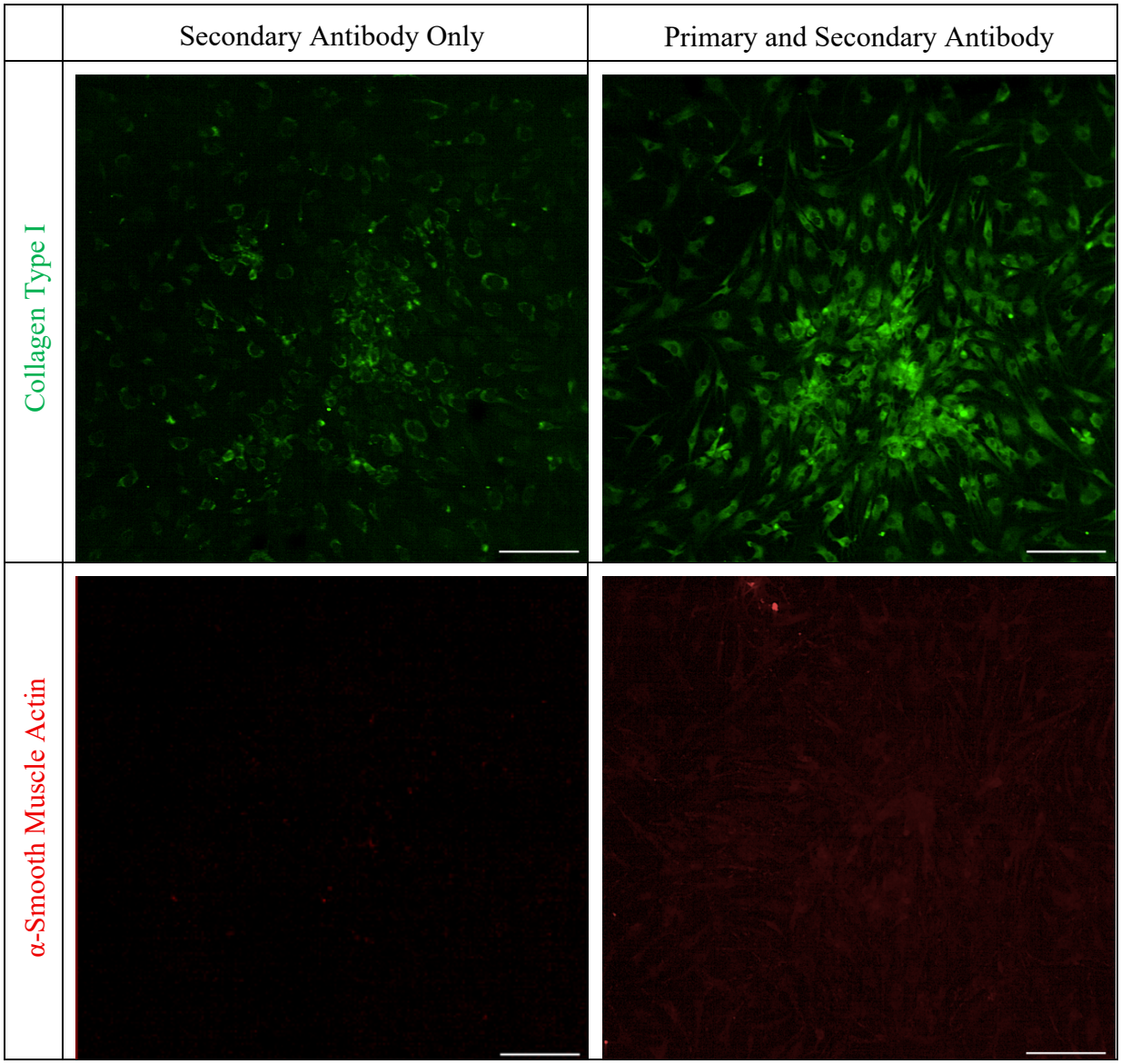

Figure 4-9 Comparison of secondary-only control and full antibody staining for α-smooth muscle actin and collagen type I in the v4 Scar-in-a-Jar assay.
Acquired 72 hours after assay component addition on the Opera Phenix at 10×. Scale bar = 200 µm.

As a consequence of this poor staining specificity, the positive and negative controls were indistinguishable: the TGF-β-free negative control (3.605 ± 0.129) was virtually identical to the positive vehicle control (3.594 ± 0.153) for α-SMA, and similarly negligible differences were observed for Col-I between the TGF-β-free condition (6.616 ± 0.680) and the DMSO vehicle condition (6.671 ± 0.364) (Figure 4-10). Together, these findings confirmed that the assay was not generating a reliable biological signal.

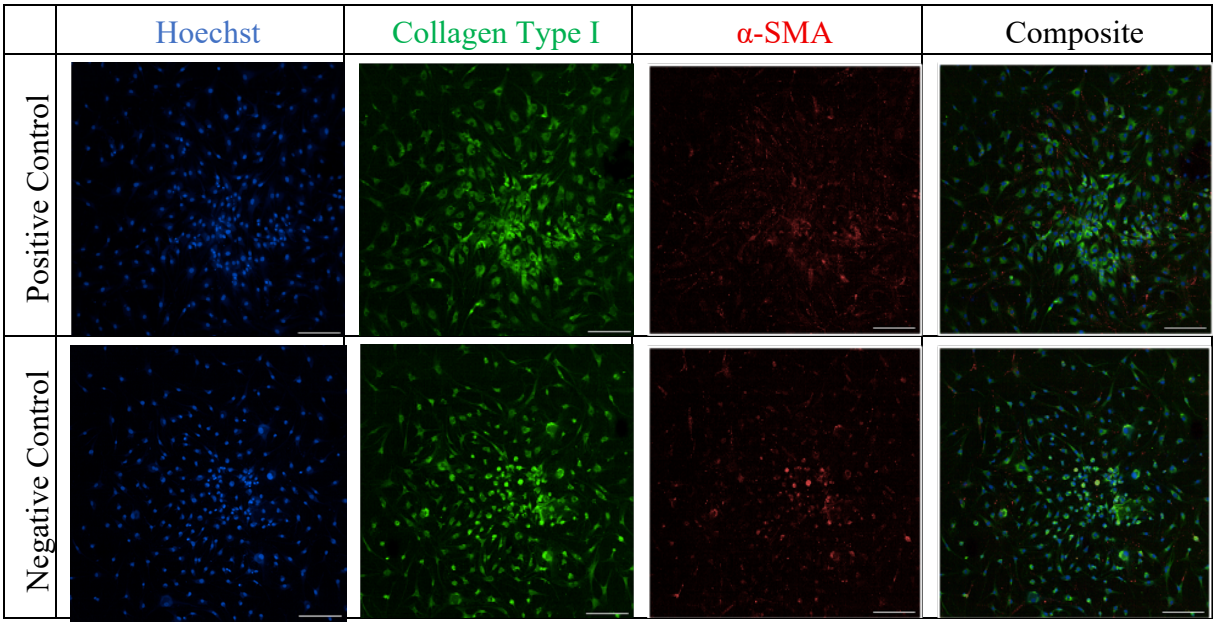

Figure 4-10 Representative images of positive and negative controls in the v4 Scar-in-a-Jar assay.
Images show the positive control (TGF-β1-treated) and negative control (TGF-β1-free) conditions. Within each row, images are presented as: Hoechst (nuclei, blue), Alexa Fluor 488 (collagen type I, green), Alexa Fluor 647 (α-smooth muscle actin [α-SMA], red), and merged composite. Acquired 72 hours after assay component addition on the Opera Phenix at 10×. Scale bar = 200 µm.

To address these limitations, several refinements were implemented in subsequent assays. First, permeabilisation conditions were strengthened by using 0.1% Triton X-100 for 10 minutes, improving intracellular antibody penetration and enhancing detection of α-SMA fibres. Second, fluorophore assignments were optimised by detecting α-SMA with the brighter Alexa Fluor 488 secondary antibody, while Col-I was assigned to Alexa Fluor 647, thereby increasing sensitivity for the lower-abundance α-SMA signal. Third, a plasma membrane stain was incorporated to enable accurate ROI definition by clearly delineating individual cell boundaries. Together, these methodological adjustments were expected to improve staining specificity, increase signal-to-background ratios, and enable more robust and reliable quantitative image analysis in future Scar-in-a-Jar experiments.

4.1.8 Scar-in-a-Jar v5: Permeabilisation and fluorophore refinements insufficient to resolve background-level staining

In the v5 Scar-in-a-Jar assay, both Col-I and α-SMA staining remained at background levels, with α-SMA in particular showing no convincing evidence of induction above secondary-only controls (Figure 4-11). The fluorescence signal in both channels appeared diffuse and lacked the characteristic structural patterns expected of true staining, namely, fibrillar collagen bundles or intracellular α-SMA stress fibres. This strongly suggested that the fluorescence observed did not represent specific protein expression.

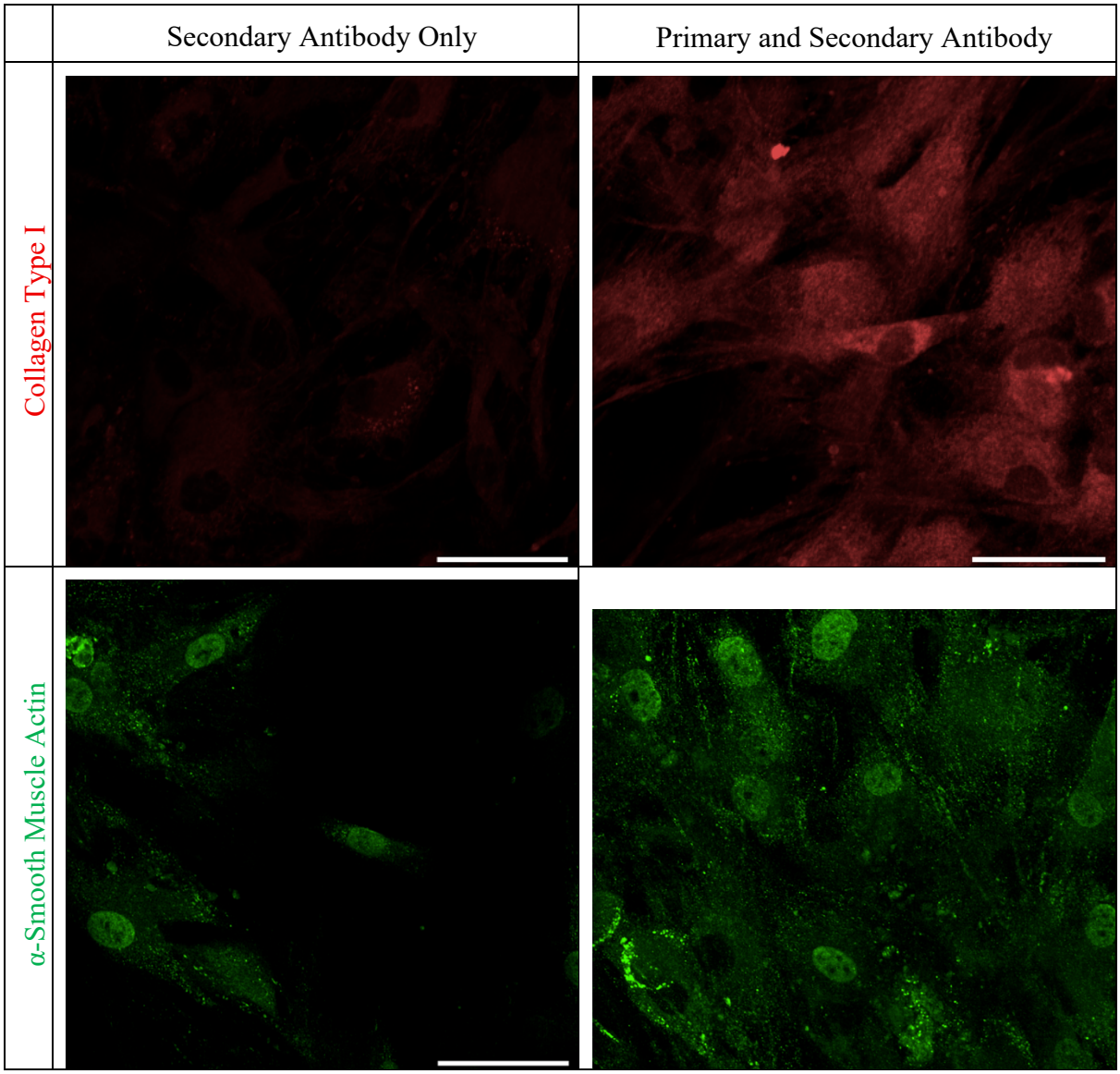

Figure 4-11 Comparison of secondary-only and full antibody staining for α-smooth muscle actin and collagen type I in the v5 Scar-in-a-Jar assay.
Acquired 72 hours after assay component addition on the Opera Phenix at 63x. Scale bar = 50 µm.

On further investigation, Rønnow et al. (251) reported significant α-SMA induction in fibroblasts under Scar-in-a-Jar conditions only at 8 and 12 days, but not at 4 days, relative to untreated controls, suggesting that the original 4-day assay duration was likely insufficient to allow robust myofibroblast differentiation. Based on these findings, the experimental duration was extended from 4 to 7 days in Scar-in-a-Jar v6, with medium exchanged for freshly prepared assay medium and compounds at 72 hours after initial treatment to maintain stimulation throughout the extended culture period.

A technical issue with the antibody staining procedure was also identified. During co-incubation of the primary antibodies for Col-I and α-SMA, adding 100 µL of each antibody at the intended working dilution into a single 200 µL volume inadvertently introduced an additional 1:2 dilution step, resulting in final working concentrations of approximately 1:800 for Col-I and 1:600 for α-SMA, substantially lower than intended. In subsequent experiments, the antibody mixture was prepared at twice the desired working concentration to ensure that the final on-cell dilution matched the optimised values.

4.1.9 Scar-in-a-Jar v6: Identification of poor antibody quality as the primary barrier to signal detection

In v6 of the Scar-in-a-Jar assay, extending the culture period from 4 to 7 days and doubling the primary antibody concentrations did not resolve the staining issues observed previously. Background fluorescence remained high, and no fibrillar Col-I bundles or intracellular α-SMA stress fibres were visible in any condition (Figure 4-12). Quantitatively, the MFI of the secondary-only α-SMA control (8.371) was unexpectedly higher than that of the primary and secondary α-SMA stain (4.995), indicating that true α-SMA signal was not being detected above background. This suggested that the α-SMA antibody may require a higher working concentration, may not be performing adequately under these assay conditions, or that α-SMA expression may be too low to detect at the tested time point.

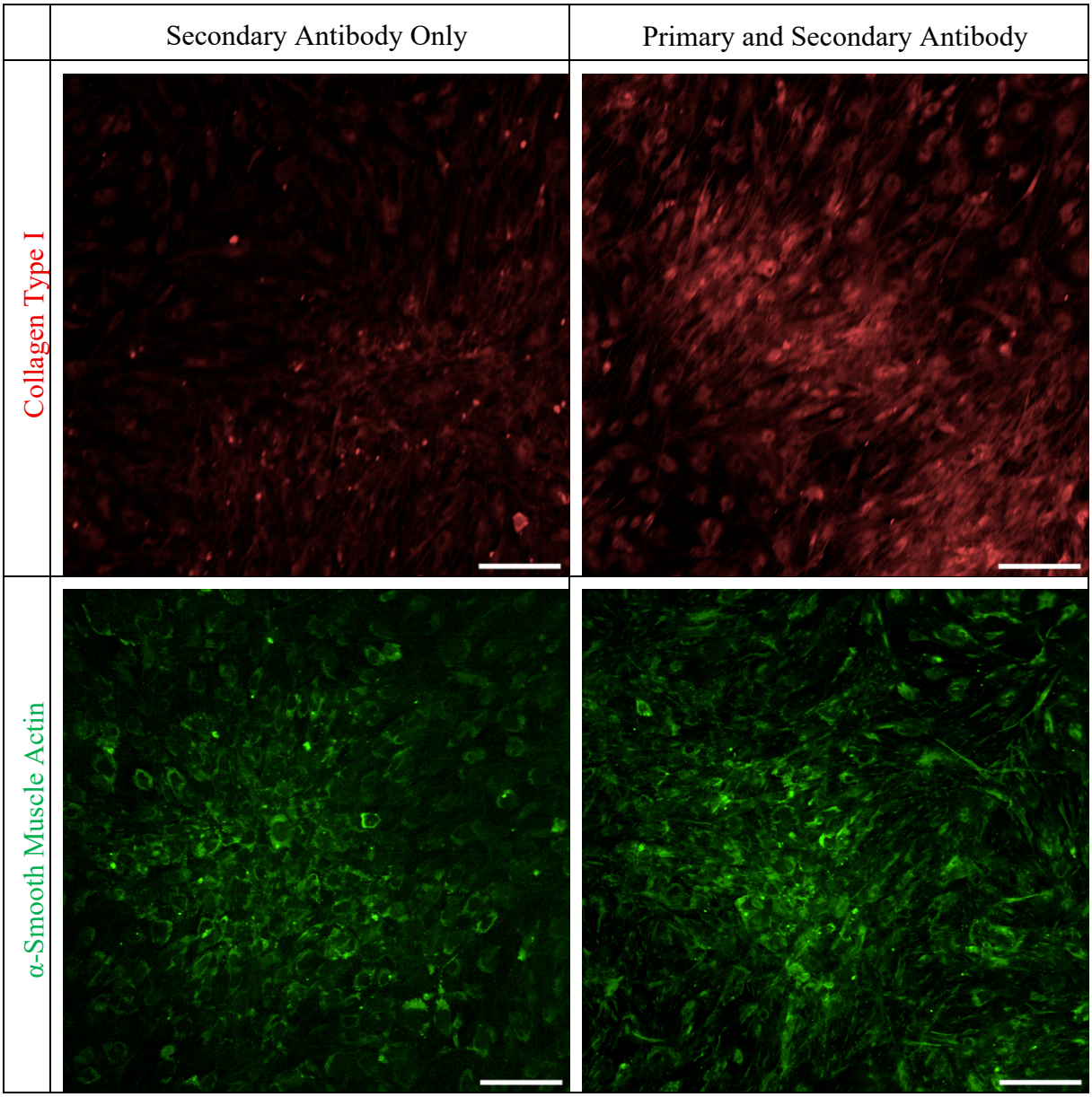

Figure 4-12 Comparison of secondary-only and full antibody staining for α-smooth muscle actin and collagen type I in the v6 Scar-in-a-Jar assay.
Acquired 72 hours after assay component addition on the Opera Phenix at 10×. Scale bar = 200 µm.

To address this possibility, an α-SMA antibody titration series was performed using a dilution range selected based on the manufacturer's recommended working concentrations and, in parallel, an alternative α-SMA antibody from Cell Signaling Technology (CST, Danvers, Massachusetts, USA; Cat. # 19245) was evaluated to determine whether improved sensitivity or specificity could be achieved (Figure 4-13).

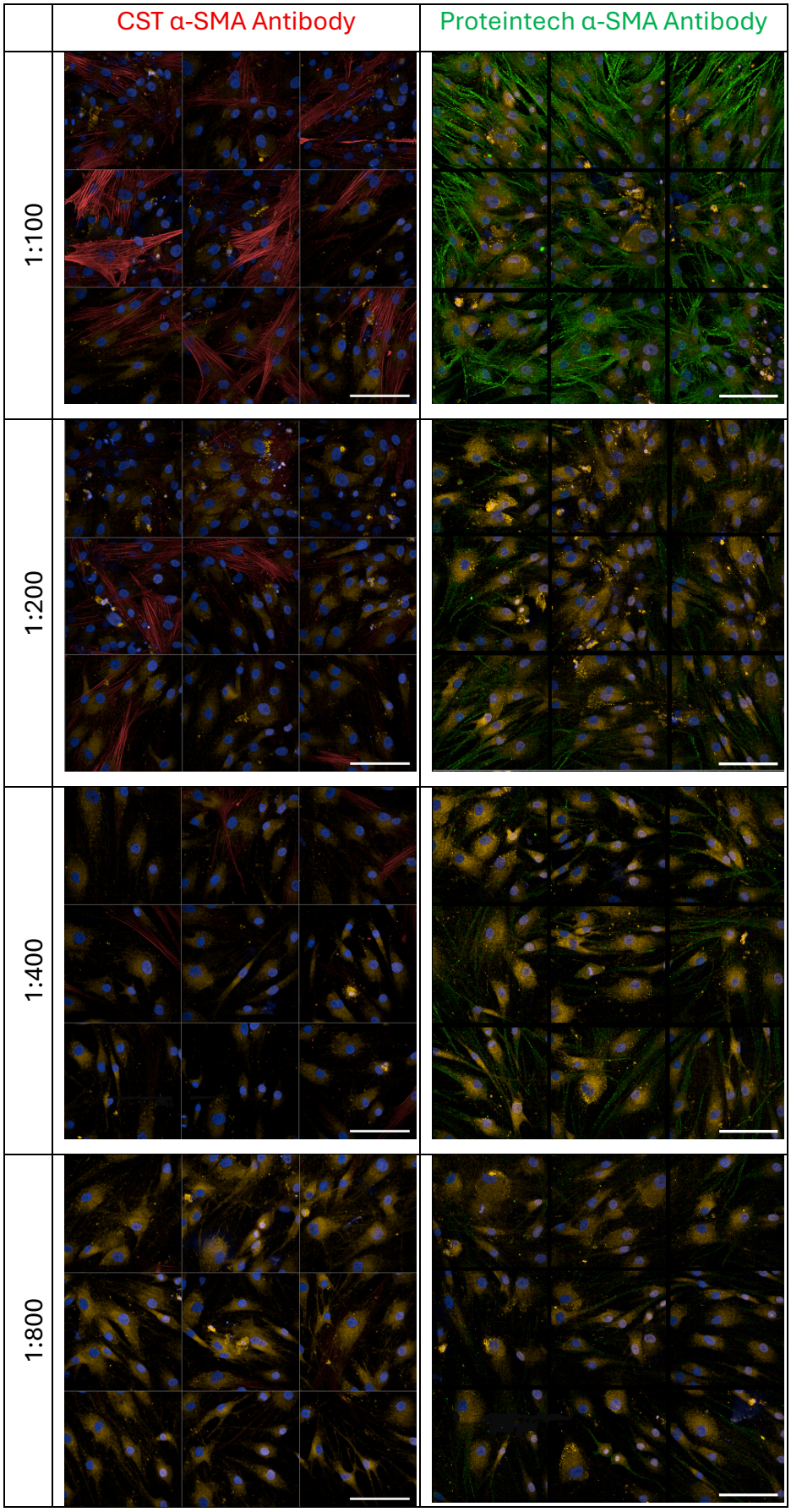
CST α-SMA Antibody
Proteintech α-SMA Antibody
1:100
1:200
1:400
1:800

Figure 4-13 Titration of α-smooth muscle actin (α-SMA) antibodies from Cell Signaling Technology (Cat. #19245) and Proteintech (Cat. #67735-1-Ig).
α-SMA immunostaining across a 1:2 dilution series (1:100–1:800). Each panel includes Hoechst (nuclei, blue), CellMask Orange (plasma membrane, orange), and α-SMA immunofluorescence via Alexa Fluor–conjugated secondary antibody. Acquired on day 7 of the Scar-in-a-Jar assay on the Opera Phenix at 63x. Scale bar = 100 µm.

At a 1:100 dilution, both α-SMA antibodies produced detectable intracellular staining, but with markedly different levels of clarity and structural definition. The original antibody (Proteintech, Illinois, United States, Cat. #67735-1-Ig) generated a green filamentous signal in which some α-SMA–positive structures were visible; however, these fibres appeared faint, discontinuous, and lacked the sharp organisation characteristic of mature α-SMA stress fibres. When this antibody was diluted further (1:200, 1:400, and 1:800), the staining intensity declined sharply, resulting in dim, diffuse fluorescence that was barely distinguishable from background. In contrast, the CST α-SMA antibody produced strong, well-defined red stress fibres at a 1:100 dilution, with clearly aligned, bundled, and structurally coherent actin–myofibroblast fibres throughout the cytoplasm. These fibres exhibited the expected architecture of myofibroblast differentiation, indicating markedly improved specificity, contrast, and fibre resolution compared with the original antibody. When titrated further, the CST antibody showed a predictable dilution-dependent decrease in signal intensity: staining at 1:200 and 1:400 remained detectable but progressively weaker, whereas at 1:800 the α-SMA signal was barely visible above background. Together, these results strongly suggested that the poor α-SMA fibre definition observed in earlier assays was due to suboptimal performance of the Proteintech antibody rather than a biological absence of α-SMA expression.

Moreover, an antibody titration of the Col-I antibody (Proteintech, Illinois, United States; Cat. #83752-5-RR) was performed to assess whether the previously observed weak Col-I staining was due to insufficient antibody concentration (Figure 4-14).

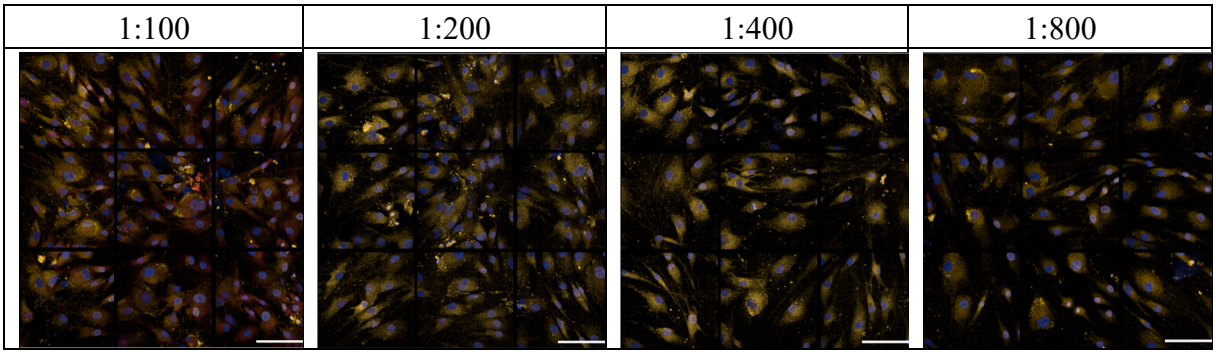

Figure 4-14 Titration of collagen type I antibody from Proteintech (Cat. #83752-5-RR).
Collagen type I immunostaining across a 1:2 dilution series (1:100–1:800). Each panel includes Hoechst (nuclei, blue), CellMask Orange (plasma membrane, orange), and collagen type I immunofluorescence via Alexa Fluor 647–conjugated secondary antibody. Acquired on day 7 of the Scar-in-a-Jar assay on the Opera Phenix at 63x. Scale bar = 100 µm.

Across the Col-I antibody titration series, the red Col-I signal remained dim and diffuse at all dilutions, including the highest concentration tested (1:100). At 1:100, a weak pericellular red signal was detectable, but it lacked brightness, structural definition, and the characteristic fibrillar collagen organisation expected under Scar-in-a-Jar conditions. At 1:200 the Col-I signal was barely detectable, and at 1:400 and 1:800 it was effectively absent, showing no staining above background. Given the consistently poor signal across all dilutions, a different Col-I antibody was required. The anti-Col-I (COL1A1) mouse monoclonal antibody, clone COL-1 (Sigma-Aldrich, NSW, Australia; Cat. #C2456), which has been successfully used in the Scar-in-a-Jar context by Good et al. (51), was selected for subsequent optimisation. A titration series using a dilution range of 1:500, 1:1,000, and 1:2,000, selected in accordance with the manufacturer's recommended working dilutions, was performed to determine the optimal working dilution for achieving robust and specific Col-I detection. Performing the titration upfront helps save time and resources by preventing failed or suboptimal experiments caused by inappropriate antibody concentrations.

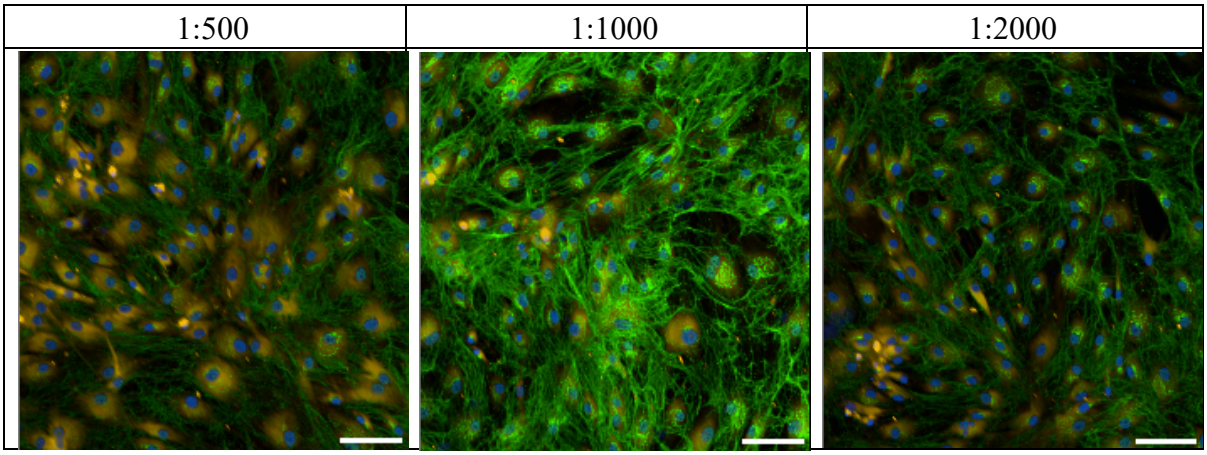

Figure 4-15 Titration of collagen type I antibody from Sigma-Aldrich (Cat. #C2456). Anti-collagen type I (COL1A1, clone COL-1) immunostaining across a 1:2 dilution series (1:500–1:2000). Each panel includes Hoechst (nuclei, blue), CellMask Orange (plasma membrane, orange), and collagen type I immunofluorescence via Alexa Fluor 488–conjugated secondary antibody. Acquired on day 7 of the Scar-in-a-Jar assay on the Opera Phenix at 20×. Scale bar = 100 µm.

Across the titration series (1:500, 1:1,000, 1:2,000), the brightest and most well-defined Col-I signal was observed at the 1:1,000 dilution, indicating strong and specific antibody binding. In comparison, the 1:500 dilution produced a slightly more diffuse and saturated signal, while the 1:2,000 dilution showed noticeably weaker fluorescence with diminished fibre clarity. Together, these results suggested that 1:1,000 is the optimal working dilution for the COL1A1 antibody under these assay conditions.

4.1.10 Scar-in-a-Jar v7: Successful fibrotic marker staining and assay validation

4.1.10.1 Cell seeding density optimisation

Because the assay duration was extended to 7 days in the Scar-in-a-Jar v6, fibroblasts had substantially more time to proliferate compared with the previous 72-hour protocol. As a result, many wells approached high confluence, making cell boundaries difficult to distinguish and preventing reliable ROI determination. To resolve this issue, a seeding-density optimisation experiment was performed using a 1:2 serial dilution starting from 6,250 cells per well (three dilution steps) to identify a density that would allow cells to form a clear but not overcrowded monolayer. Very low seeding densities are also unsuitable because insufficient cell–cell contact prevents fibroblasts from establishing

essential paracrine signalling networks, leading to slow proliferation, poor attachment, prolonged lag phases, and increased cell death (264).

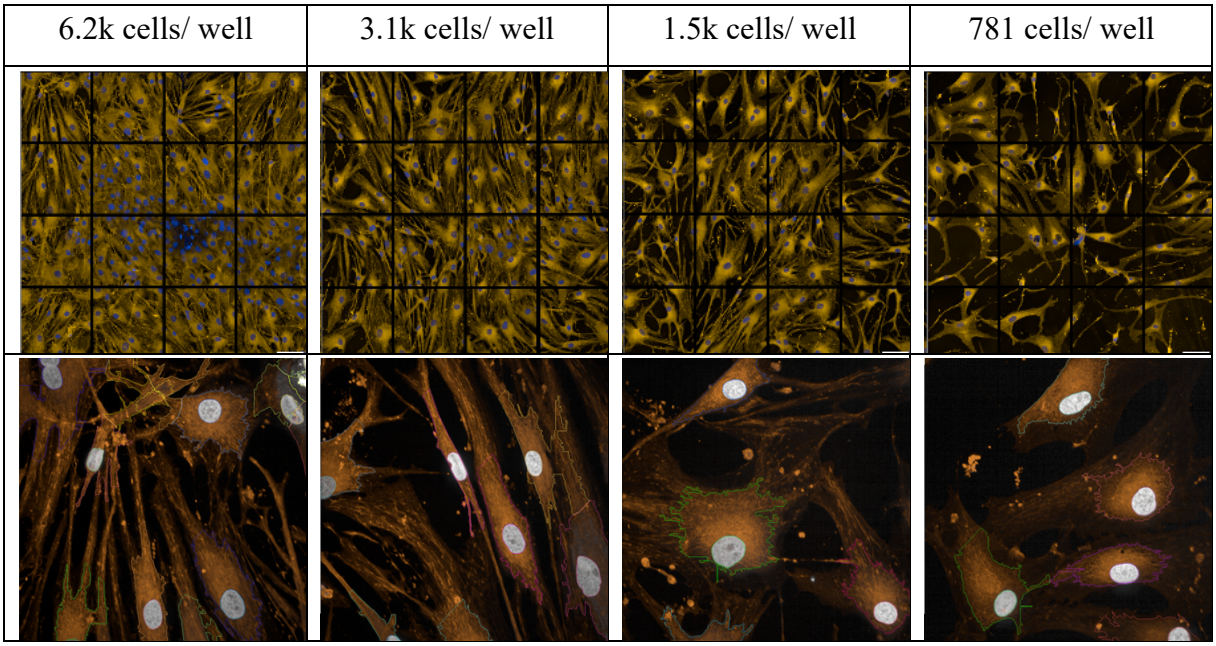

Figure 4-16 Cell seeding density optimisation for the v7 Scar-in-a-Jar assay. Representative images of 1BR3 human fibroblasts seeded at decreasing densities (6,250; 3,125; 1,563; 781 cells per well) via 1:2 serial dilution. Upper panels: CellMask Orange (plasma membrane, orange) and Hoechst (nuclei, blue) staining. Lower panels: representative plasma membrane segmentation masks generated in Harmony Image Analysis Software 5.2, illustrating mask application to a single field of view from the corresponding images above (each comprising 16 fields of view). Acquired on the Opera Phenix at 63x. Scale bars = 100 µm (upper) and 50 µm (lower).

Across the dilutions tested, the most appropriate seeding density was observed at approximately 1,500 cells per well, where fibroblasts formed a uniform monolayer with clearly defined cell boundaries that could be reliably detected by the image analysis software. Based on these findings, a seeding density of 1,350 cells per well was selected for subsequent experiments.

4.1.10.2 Validation of fibrotic marker staining

Secondary-only controls in the v7 Scar-in-a-Jar assay exhibited only faint, diffuse background fluorescence without discernible fibrillar or structural features in either channel (Figure 4-17). In contrast, primary and secondary stained samples displayed

strong, target-specific fluorescence, with Col-I staining producing bright extracellular fibres with clear pericellular organisation and extensive ECM deposition, and α-SMA staining generating robust, sharply defined intracellular stress fibres extensively bundled throughout the cytoplasm. This confirmed that the staining observed in experimental conditions was antigen-specific and not attributable to non-specific background fluorescence, validating the protocol for subsequent immunofluorescence-based compound screening.

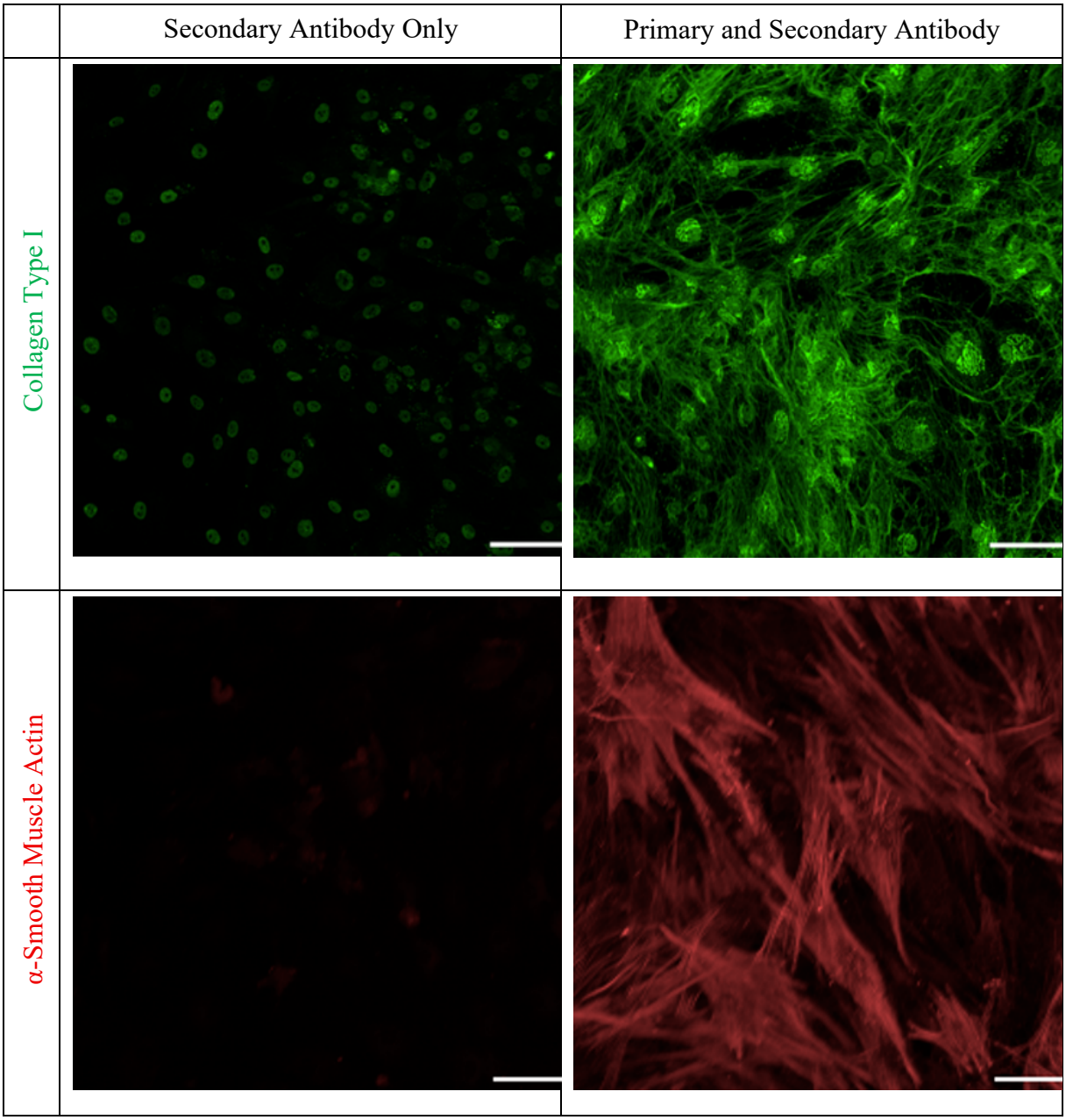

Figure 4-17 Comparison of secondary-only and full antibody staining for α-smooth muscle actin and collagen type I in the v7 Scar-in-a-Jar assay.
Acquired on day 7 on the Opera Phenix at 20×. Scale bar = 50 µm.

Furthermore, α-SMA staining revealed clear and well-defined stress fibres in both the positive control (TGF-β1–treated) and the 0.1% DMSO vehicle control, indicating robust induction of myofibroblast differentiation under these conditions (Figure 4-18). In contrast, the TGF-β1-free negative control showed no visible α-SMA fibres, displaying only minimal background signal. Col-I staining followed a similar pattern: the positive and vehicle controls exhibited bright, abundant pericellular Col-I fibres of comparable

intensity, whereas the negative control showed markedly weaker and sparser collagen deposition, indicating low basal Col-I production in the absence of TGF-β1. Together, these results demonstrated strong TGF-β1-dependent activation of both ECM deposition and cytoskeletal remodelling, validating the assay's responsiveness and the creation of an in vitro fibrosis model.

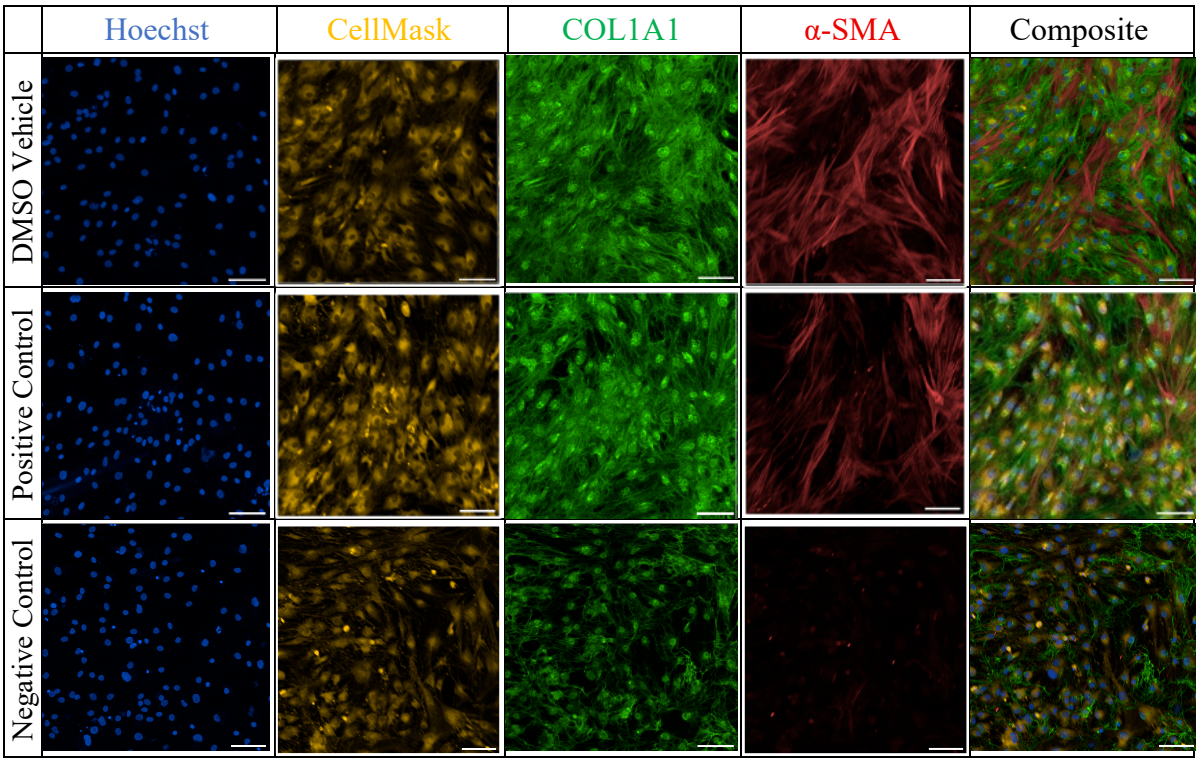

Figure 4-18 Representative images from the v7 Scar-in-a-Jar assay.
Images show the vehicle control (0.1% DMSO), positive control (TGF-β1–treated), and negative control (TGF-β1–free) conditions. Channels presented left to right: Hoechst (nuclei, blue), CellMask Orange (plasma membrane, orange), Alexa Fluor 488 (collagen type I, green), Alexa Fluor 647 (α-smooth muscle actin [α-SMA], red), and merged composite. Acquired on day 7 on the Opera Phenix at 20×. Scale bar = 100 µm.

4.2 Pseudolycorine demonstrated the strongest antifibrotic activity among the candidate alkaloids

Following optimisation of the Scar-in-a-Jar assay, the validated protocol was used to evaluate the in vitro antifibrotic activity of the candidate compounds and identify the lead compound for further investigation. Figure 4-19a presents representative immunocytochemical images of Col-I deposition and α-SMA expression in wells treated

at 1 μM; the corresponding quantitative analysis, expressed as percentage inhibition relative to the vehicle control, is presented in Figure 4-19b, with statistical significance indicated where applicable. The same evaluation was conducted at 10 μM (Figure 4-20).

(a)

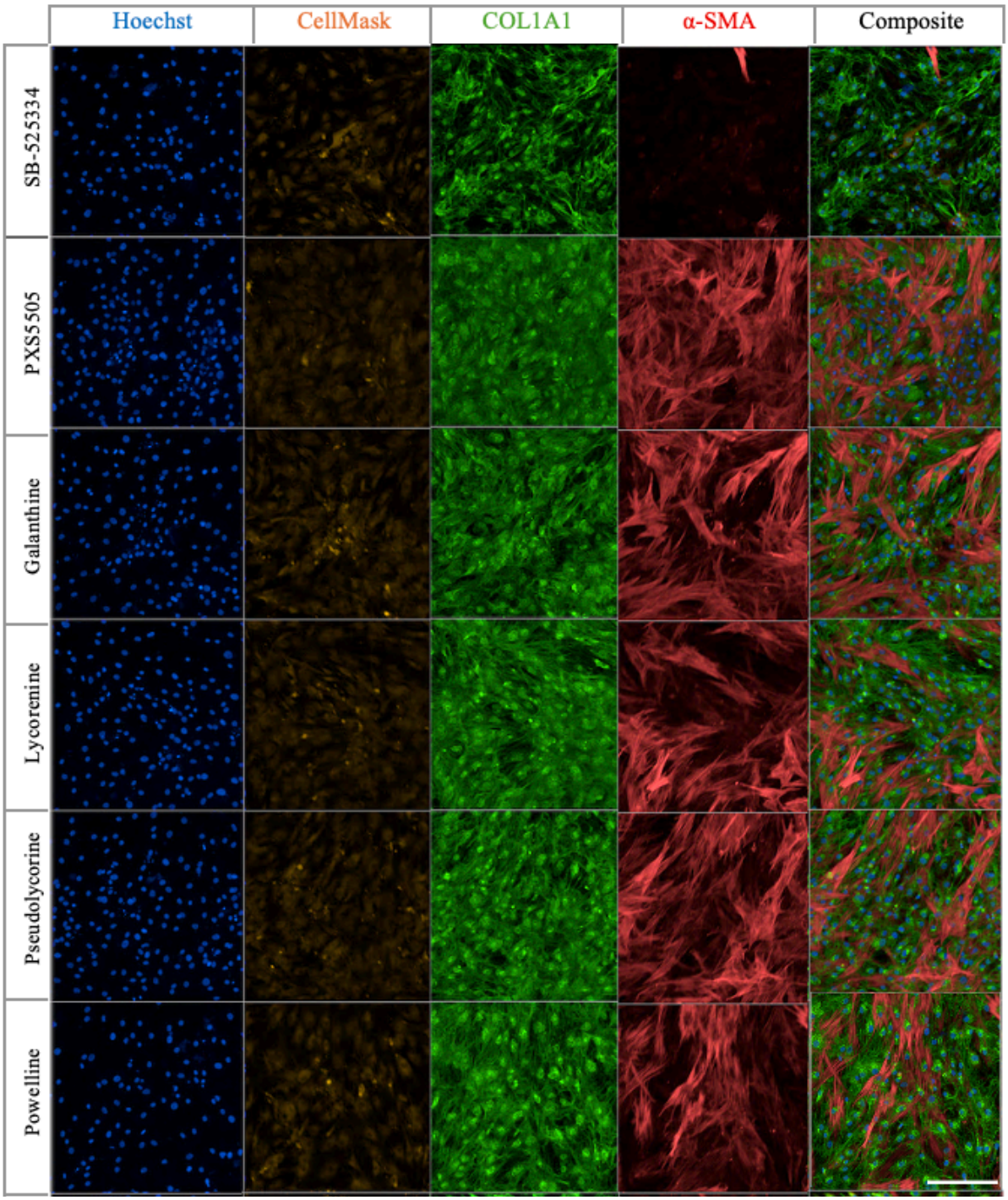
Hoechst
CellMask
COL1A1
α-SMA
Composite
SB-525334
PXS5505
Galanthine
Lycorenine
Pseudolycorine
Powelline

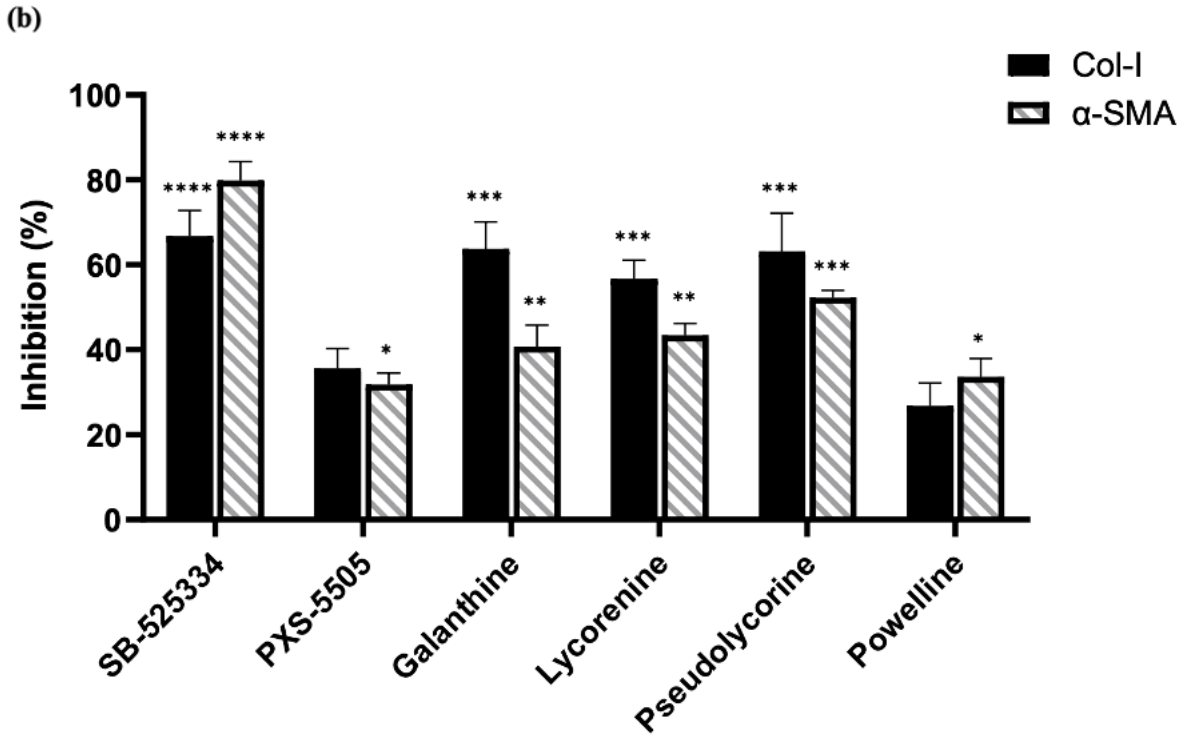

Figure 4-19 Immunocytochemical staining and quantification of fibrotic markers in the Scar-in-a-Jar model following treatment with test compounds at 1 µM.
(a) 1BR3 human fibroblasts treated with SB-525334 (positive control), PXS-5505 (pharmacological reference control), galanthine, lycorenine, pseudolycorine, and powelline at 1 µM (top to bottom). Channels presented left to right: Hoechst (nuclei, blue), CellMask Orange (plasma membrane, orange), Alexa Fluor 488 (collagen type I, green), Alexa Fluor 647 (α-SMA, red), and merged composite. Representative of three independent experiments; acquired on the Opera Phenix at 20× (14 fields of view per well). Scale bar = 50 µm. (b) Percentage inhibition of collagen type I (Col-I) deposition and α-SMA expression, normalised to vehicle control (0% inhibition). Data represent mean ± SEM of n = 3 independent experiments. One-way ANOVA with Sidak's multiple comparisons test: *$p \leq 0.05$, **$p \leq 0.01$, ***$p \leq 0.001$, ****$p \leq 0.0001$.

Figure 4-19 demonstrates that at 1 µM, the TGF-β receptor inhibitor SB-525334 (positive control) produced the strongest inhibitory effect on both Col-I deposition and α-SMA expression, consistent with expectations. The reference compound PXS-5505 demonstrated significant inhibition of α-SMA expression but not Col-I deposition. Of the four test compounds, galanthine and pseudolycorine demonstrated significant inhibitory activity on Col-I deposition, with effects broadly comparable to each other and to SB-525334. Lycorenine also produced a significant inhibitory effect on Col-I deposition, albeit of lesser magnitude, while powelline had no significant effect. With respect to α-SMA expression, all four alkaloids demonstrated significant inhibitory activity, with

pseudolycorine producing the greatest effect, followed by lycorenine, galanthine, and powelline in descending order of effect size.

(a)

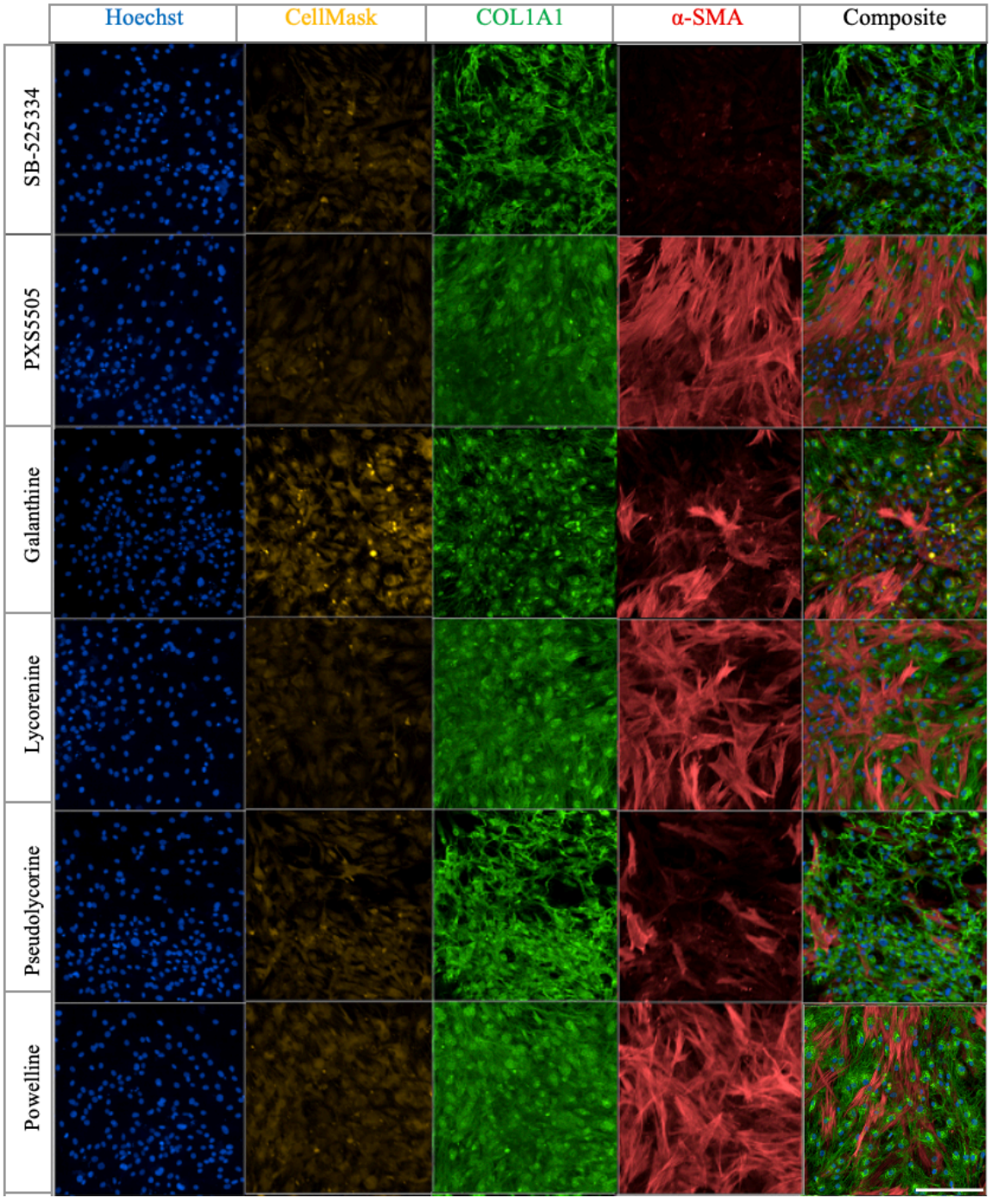

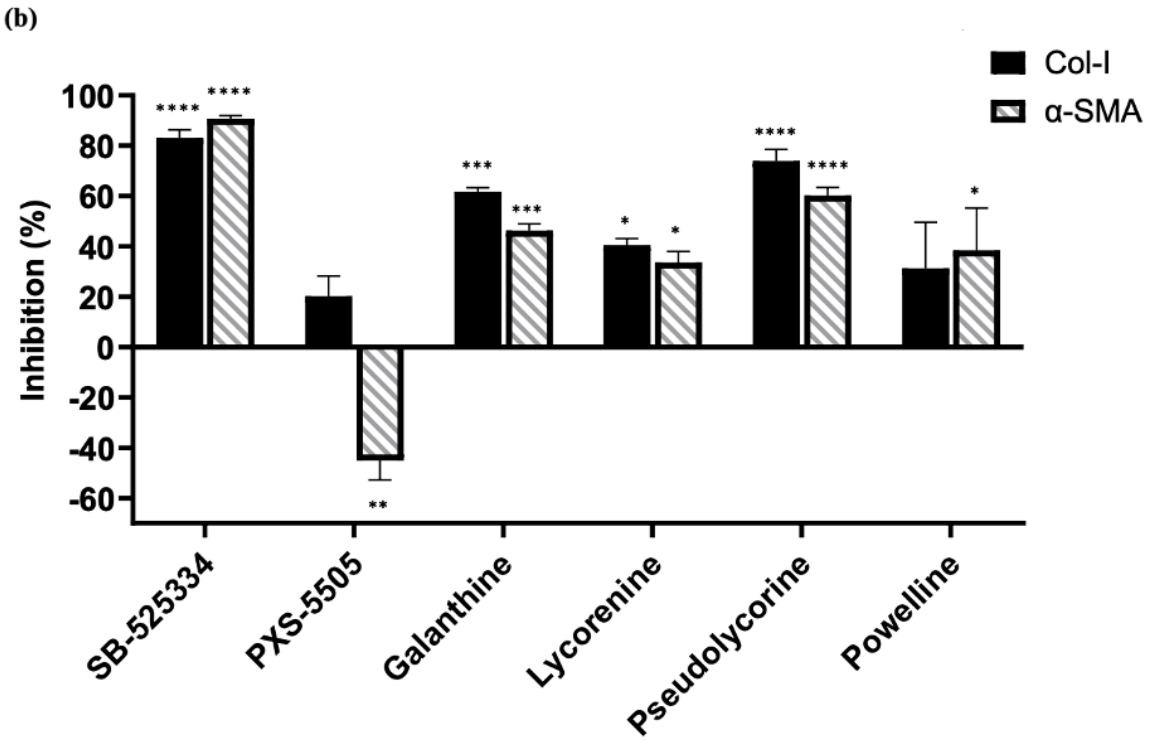

Figure 4-20 Immunocytochemical staining and quantification of fibrotic markers in the Scar-in-a-Jar model following treatment with test compounds at 10 µM.
(a) 1BR3 human fibroblasts treated with SB-525334 (positive control), PXS-5505 (pharmacological reference control), galanthine, lycorenine, pseudolycorine, and powelline at 10 µM (top to bottom). Channels presented left to right: Hoechst (nuclei, blue), CellMask Orange (plasma membrane, orange), Alexa Fluor 488 (collagen type I, green), Alexa Fluor 647 (α-SMA, red), and merged composite. Representative of three independent experiments; acquired on the Opera Phenix at 20× (14 fields of view per well). Scale bar = 100 µm. (b) Percentage inhibition of collagen type I (Col-I) deposition and α-SMA expression, normalised to vehicle control (0% inhibition). Data represent mean ± SEM of n = 3 independent experiments. One-way ANOVA with Sidak's multiple comparisons test: *$p \leq 0.05$, **$p \leq 0.01$, ***$p \leq 0.001$, ****$p \leq 0.0001$.

Figure 4-20 illustrates that at 10 µM, SB-525334 remained the most potent inhibitor, significantly suppressing both Col-I deposition and α-SMA expression. In contrast, PXS-5505 demonstrated no significant inhibition of Col-I deposition and, notably, exhibited a significant pro-fibrotic effect on α-SMA expression at this concentration. Among the alkaloids, pseudolycorine demonstrated the most robust inhibitory effect on Col-I deposition, followed by galanthine, lycorenine, and powelline, with statistically significant effects observed for all compounds except powelline. With respect to α-SMA expression, all four alkaloids demonstrated significant inhibitory activity, with

pseudolycorine producing the greatest effect, followed by galanthine, lycorenine, and powelline in descending order of effect size. Taken together, pseudolycorine demonstrated the most consistent and potent inhibitory activity across both fibrotic markers and both concentrations tested, and was therefore selected as the lead compound for IC_{50} determination and subsequent mechanistic investigation.

4.3 Pseudolycorine exhibited an IC_{50} of 1.84 μM against α-SMA expression

Following the identification of pseudolycorine as the most potent antifibrotic candidate among the screened alkaloids, a dose-response analysis was conducted to determine its IC_{50} (Figure 4-21). Utilising a 3.16-fold serial dilution range (1 nM to 10 μM), the IC_{50} was specifically calculated based on the inhibition of α-SMA expression. This concentration was established as the benchmark for subsequent RT-qPCR experiment to ensure that transcriptomic changes were evaluated at a pharmacologically effective dose.

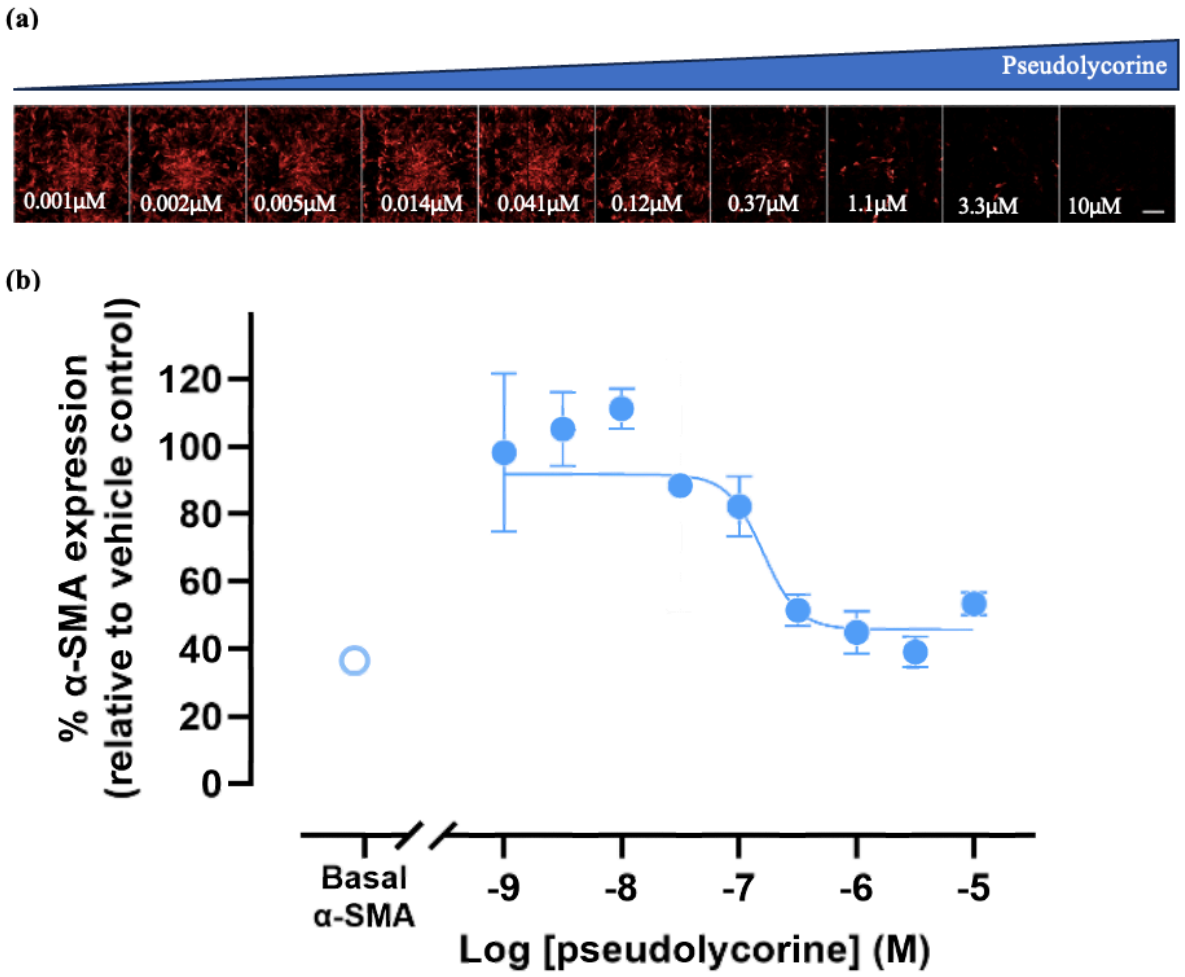

Figure 4-21 Dose-response analysis of pseudolycorine in the Scar-in-a-Jar model. (a) Representative immunocytochemical images of α-smooth muscle actin (α-SMA) staining across ten concentrations of pseudolycorine (3.16-fold serial dilutions, 1 nM–10 µM) acquired on the Opera Phenix at 20× (14 fields of view per well). Scale bar = 1 mm. (b) α-SMA mean fluorescence intensity (MFI), normalised to vehicle control, plotted against log concentration of pseudolycorine. The basal control represents α-SMA expression in the absence of TGF-β1. Data presented as mean ± SD; n = 3 per concentration.

Pseudolycorine demonstrated an IC_{50} for α-SMA of 1.84 µM.

4.4 RT-qPCR array analysis of 84 fibrosis-related genes to elucidate pseudolycorine's mechanism of action

4.4.1 Validation of RNA integrity and quality

Prior to gene expression analysis via RT-qPCR, the integrity of total RNA extracted from 1BR3 fibroblasts was assessed using the Agilent 4200 TapeStation system. High-quality RNA is a prerequisite for accurate quantification, as degradation can significantly bias C_t values. As shown in Figure 4-22, all samples exhibited distinct 18S and 28S ribosomal RNA bands with no evidence of genomic DNA contamination or significant degradation. The RNA Integrity Number equivalent for all samples exceeded 9.3, confirming that the RNA was of sufficient quality for downstream transcriptomic analysis.

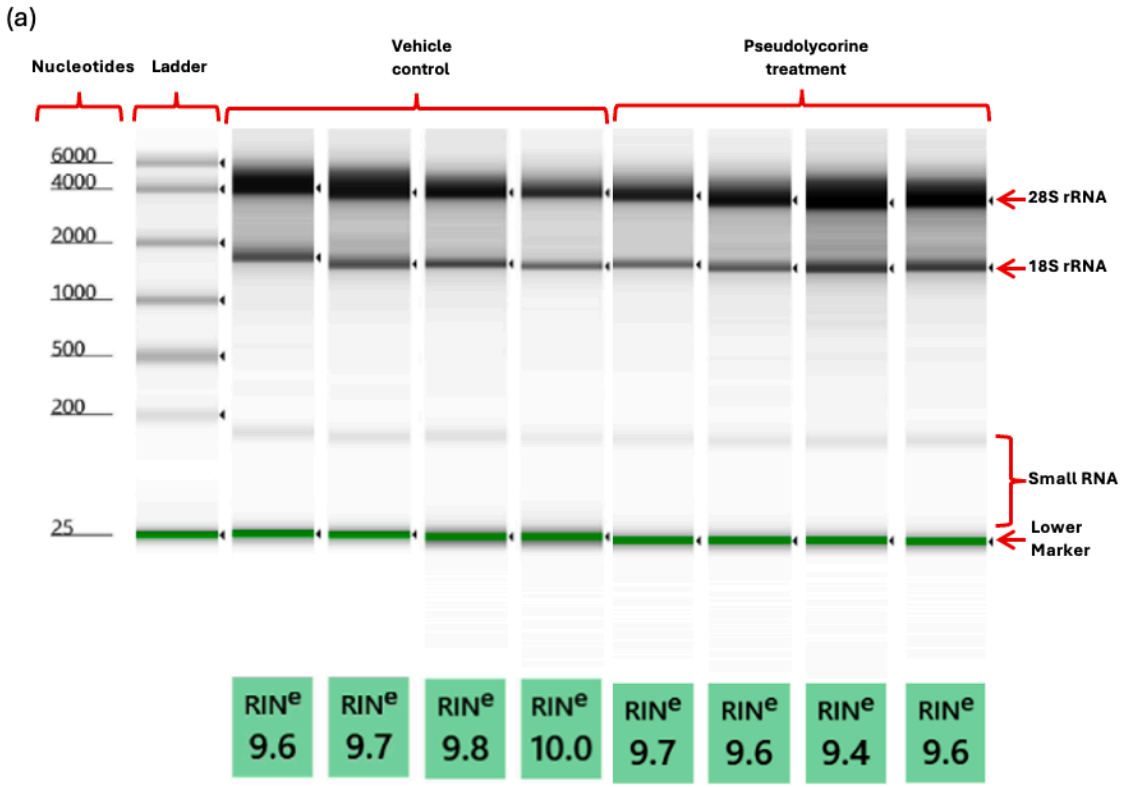

(b)

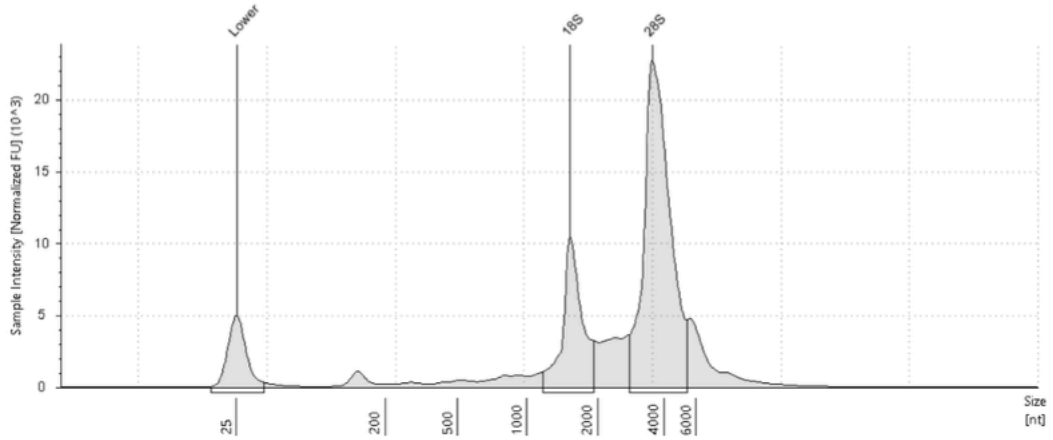

Figure 4-22 RNA quality analysis using the Agilent 4200 TapeStation system.
(a) Digital gel image of total RNA separation profiles from 1BR3 fibroblasts treated with pseudolycorine (1.84 µM) or vehicle (0.1% DMSO) under Scar-in-a-Jar conditions (n = 4 biological replicates per group). (b) Representative electropherogram from a pseudolycorine-treated replicate, showing distinct 18S and 28S ribosomal RNA peaks and the lower marker.

4.4.2 Categorisation of the 84 fibrosis-related genes evaluated by RT-qPCR array

To investigate the molecular mechanism of action of pseudolycorine, an 84-gene fibrosis-focused RT-qPCR array was performed on 1BR3 fibroblasts treated with pseudolycorine at its established IC_{50} for α-SMA inhibition (1.84 µM) under Scar-in-a-Jar assay conditions. The genes targeted by the RT^2 Profiler Human Fibrosis PCR Array were organised into functional categories as defined by the manufacturer, representing the diverse biological processes involved in the initiation and progression of fibrosis. This categorical approach facilitated a comprehensive pathway-level analysis of the transcriptomic response to pseudolycorine treatment.

Table 5 Functional classification of genes in the RT^2 Profiler PCR Array Human Fibrosis panel, as defined by the manufacturer (QIAGEN)

Functional Category	Gene Symbols
Pro-Fibrotic Signalling	*ACTA2, AGT, CCL11, CCL2, CCL3, CCN2, GREM1, IL13, IL13RA2, IL4, IL5, SNAI1*
Anti-Fibrotic Factors	*BMP7, HGF, IFNG, IL10, IL13RA2*
ECM Structural Constituents	*COL1A2, COL3A1*
ECM Remodelling Enzymes	*LOX, MMP1, MMP2, MMP3, MMP8, MMP9, MMP13, MMP14, PLAT, PLAU, PLG, SERPINA1, SERPINE1, SERPINH1, TIMP1, TIMP2, TIMP3, TIMP4*
Cell Adhesion Molecules	*ITGA1, ITGA2, ITGA3, ITGAV, ITGB1, ITGB3, ITGB5, ITGB6, ITGB8*
Inflammatory Cytokines & Chemokines	*CCL11, CCL2, CCL3, CCR2, CXCR4, IFNG, IL10, IL13, IL13RA2, IL1A, IL1B, IL4, IL5, ILK, TNF*
Growth Factors	*AGT, CCN2, EDN1, EGF, HGF, PDGFA, PDGFB, VEGFA*
TGF- β Superfamily Members	*BMP7, CAV1, DCN, ENG, GREM1, INHBE, LTBP1, SMAD2, SMAD3, SMAD4, SMAD 6, SMAD7, TGFB1, TGFB2, TGFB3, TGFBR1, TGFBR2, TGIF1, THBS1, THBS2*
Signal Transduction	*AKT1, CEBPB, JUN, MYC, NFKB1, SP1, STAT1, STAT6*
Epithelial-to-Mesenchymal Transition	*AKT1, BMP7, COL1A2, COL3A1, ILK, ITGAV, ITGB1, MMP2, MMP3, MMP9, SERPIN E1, SMAD2, SNAI1, TGFB1, TGFB2, TGFB3, TIMP1*
Apoptosis Regulation	*BCL2, FASLG*

4.4.3 Pseudolycorine significantly reduced the expression of the pro-fibrotic gene CCL11

RT-qPCR array analysis revealed that pseudolycorine significantly suppressed the transcript levels of Chemokine (C-C motif) ligand 11 (*CCL11*; Figure 4-23a). Interestingly, this treatment had no significant effect on the expression of the anti-fibrotic genes within the array (Figure 4-23b).

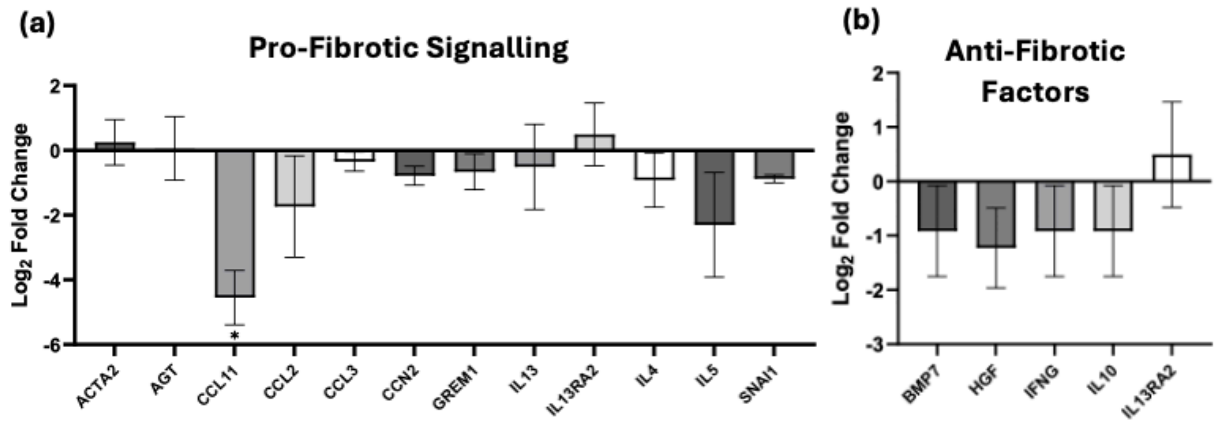

Figure 4-23 Relative expression of pro-fibrotic and anti-fibrotic genes in pseudolycorine-treated 1BR3 fibroblasts in the Scar-in-a-Jar model.
RT-qPCR array data expressed as $\log_2$ fold change relative to vehicle control (0.1% DMSO) calculated using the $2^{-\Delta\Delta CT}$ method (n = 4 biological replicates per group). Target gene expression normalised to GAPDH. Data presented as mean ± SD. Statistical significance determined by two-tailed t-tests via Qiagen GeneGlobe data analysis software. *$p \leq 0.05$.

4.4.4 Pseudolycorine significantly reduced the expression of ECM remodelling genes: MMP14, PLAU, and TIMP4

While pseudolycorine did not have a significant effect on the expression of ECM structural constituents (Figure 4-24a) or cell adhesion molecules (Figure 4-24b), it significantly reduced the transcript levels of specific ECM remodelling enzymes (Figure 4-24c). Specifically, treatment resulted in the downregulation of matrix metallopeptidase 14 (*MMP14*), plasminogen activator, urokinase (*PLAU*), and TIMP metallopeptidase inhibitor 4 (*TIMP4*).

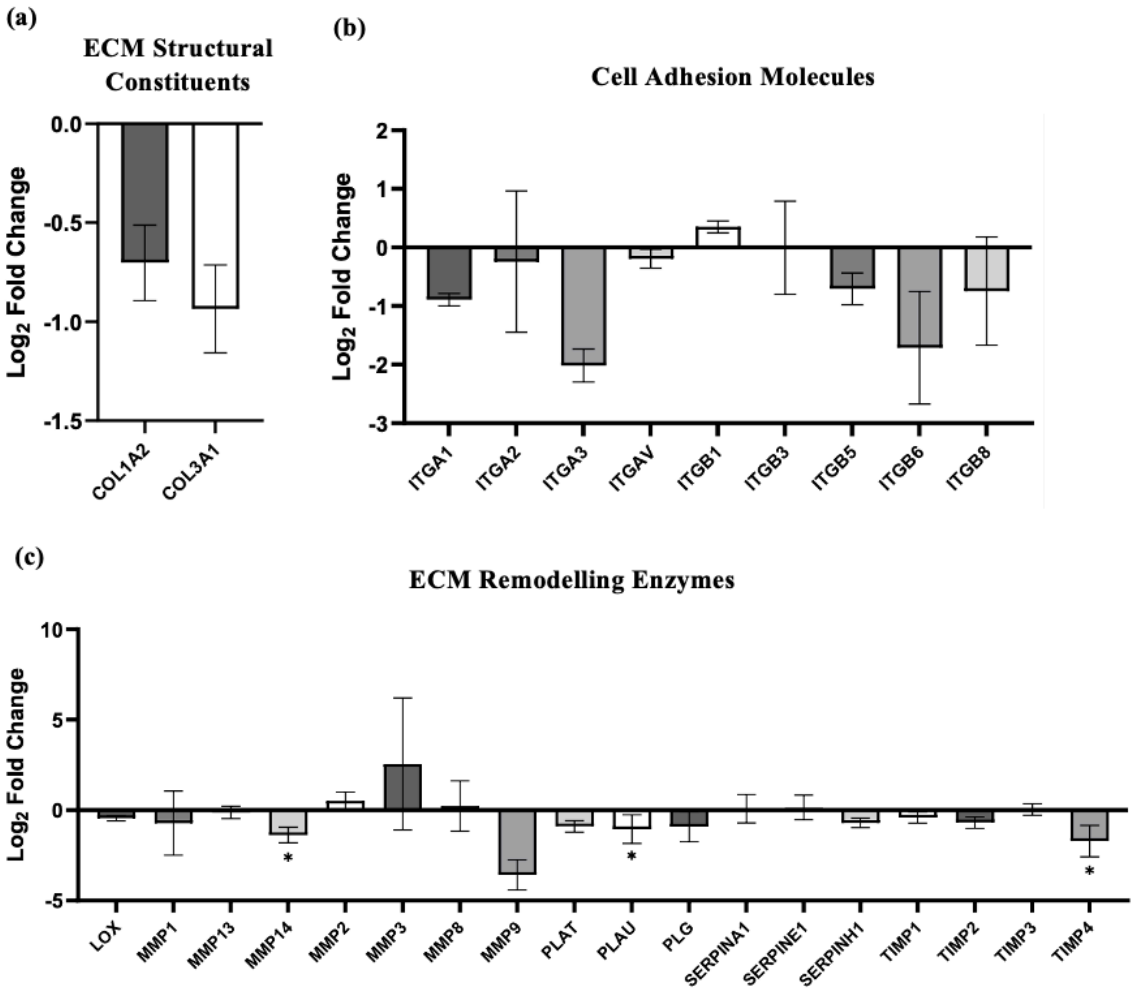

Figure 4-24 Relative expression of extracellular matrix (ECM) and cell adhesion molecule genes in pseudolycorine-treated fibroblasts in the Scar-in-a-Jar model. RT-qPCR array data presented for (a) ECM structural constituents, (b) cell adhesion molecules, and (c) ECM remodelling enzymes. Results expressed as $\log_2$ fold change relative to vehicle control (0.1% DMSO), calculated using the $2^{-\Delta\Delta CT}$ method (n = 4 biological replicates per group). Target gene expression normalised to GAPDH. Data presented as mean ± SD. Statistical significance determined by two-tailed t-tests via Qiagen GeneGlobe data analysis software. *$p \leq 0.05$.

4.4.5 Pseudolycorine significantly reduced the expression of inflammatory cytokine and chemokine genes: CCR2 and CCL11

In terms of the inflammatory cytokine and chemokine genes analysed, pseudolycorine significantly suppressed the expression of both *CCL11* and C-C motif chemokine receptor 2 (*CCR2*; Figure 4-25).

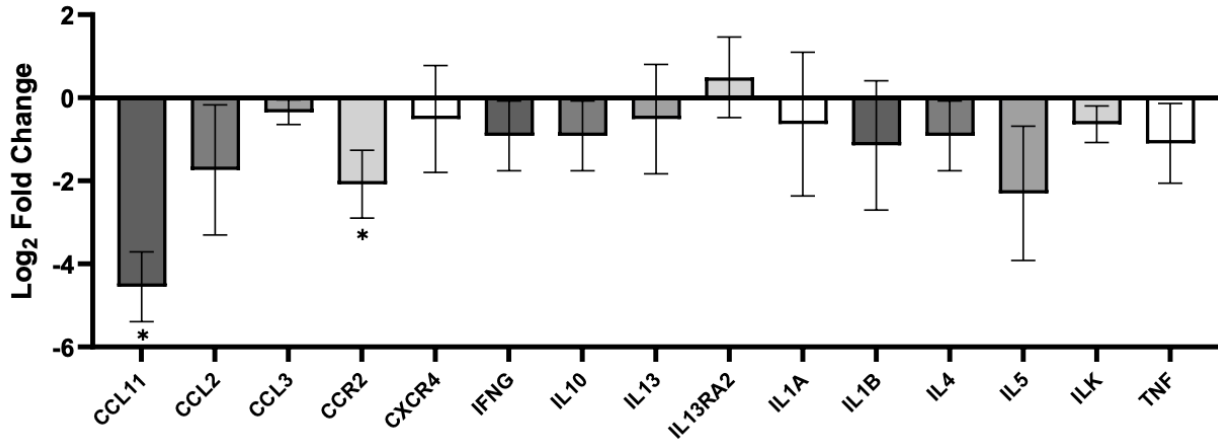

Figure 4-25 Relative expression of inflammatory cytokine and chemokine genes in pseudolycorine-treated fibroblasts in the Scar-in-a-Jar model.
RT-qPCR array data expressed as $\log_2$ fold change relative to vehicle control (0.1% DMSO), calculated using the $2^{-\Delta\Delta CT}$ method (n = 4 biological replicates per group). Target gene expression normalised to GAPDH. Data presented as mean ± SD. Statistical significance determined by two-tailed unpaired Student's t-test via QIAGEN GeneGlobe Data Analysis Center. *$p \leq 0.05$.

4.4.6 Pseudolycorine did not significantly alter the expression of growth factor genes

As shown in Figure 4-26, pseudolycorine did not significantly alter the expression of the growth factor genes tested in the array.

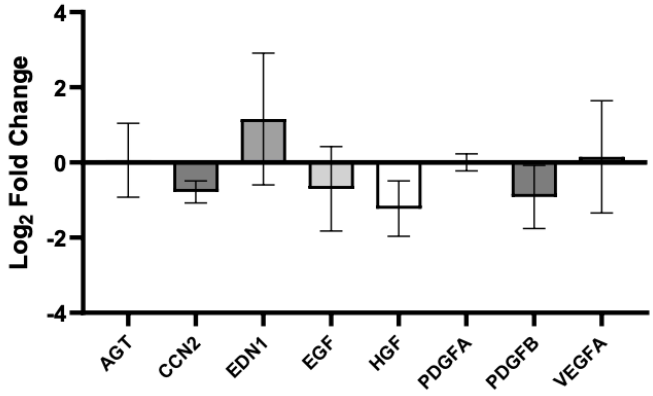

Figure 4-26 Relative expression of growth factor genes in pseudolycorine-treated fibroblasts in the Scar-in-a-Jar model.
RT-qPCR array data expressed as $\log_2$ fold change relative to vehicle control (0.1% DMSO), calculated using the $2^{-\Delta\Delta CT}$ method (n = 4 biological replicates per group). Target gene expression normalised to GAPDH. Data presented as mean ± SD. Statistical significance determined by two-tailed unpaired Student's t-test via QIAGEN GeneGlobe Data Analysis Center.

4.4.7 Pseudolycorine significantly increased the expression of the transcription factor CEBPB

The only gene significantly upregulated by pseudolycorine was the transcription factor CCAAT/enhancer-binding protein beta (*CEBPB*; Figure 4-27a). Notably, the compound did not significantly alter the expression of the 20 TGF-β superfamily members tested in the array (Figure 4-27b).

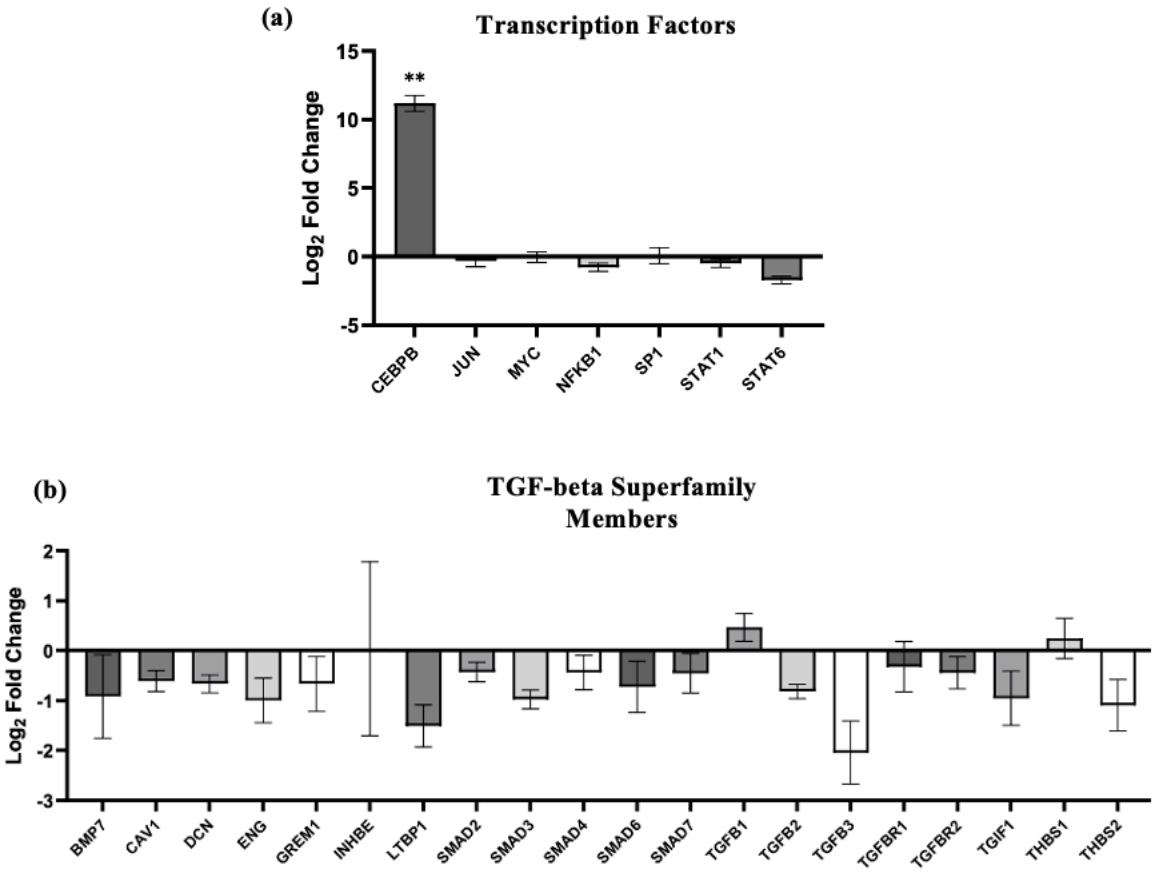

Figure 4-27 Relative expression of signal transduction genes in pseudolycorine-treated fibroblasts in the Scar-in-a-Jar model.
RT-qPCR array data are presented for (a) transcription factors, and (b) TGF-beta superfamily members. Results are expressed as $\log_2$ fold change relative to vehicle control (0.1% DMSO), calculated using the $2^{-\Delta\Delta CT}$ method (n = 4 biological replicates per group). Target gene expression normalised to GAPDH. Data presented as mean ± SD. Statistical significance determined by two-tailed unpaired Student's t-test via QIAGEN GeneGlobe Data Analysis Center.

4.4.8 Pseudolycorine did not significantly affect the expression of epithelial-to-mesenchymal transition genes

Pseudolycorine had no significant effect on the expression of epithelial-to-mesenchymal transition genes (Figure 4-28).

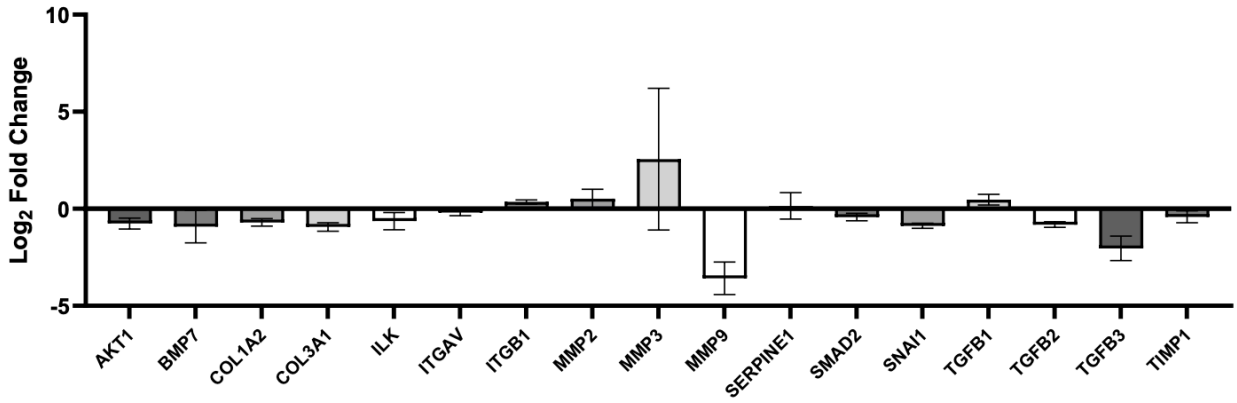

Figure 4-28 Relative expression of epithelial-to-mesenchymal transition genes in pseudolycorine-treated fibroblasts in the Scar-in-a-Jar model.
RT-qPCR array data expressed as $\log_2$ fold change relative to vehicle control (0.1% DMSO), calculated using the $2^{-\Delta\Delta CT}$ method (n = 4 biological replicates per group). Target gene expression normalised to GAPDH. Data presented as mean ± SD. Statistical significance determined by two-tailed t-tests via Qiagen GeneGlobe data analysis software.

4.4.9 Pseudolycorine did not significantly alter the expression of apoptosis-regulatory genes

RT-qPCR analysis further demonstrated that pseudolycorine had no significant effect on the expression of key apoptosis-regulatory genes, namely B-cell CLL/lymphoma 2 (*BCL2*) and Fas ligand (*FASLG*; Figure 4-29).

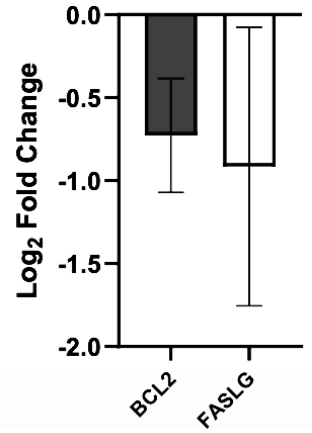

Figure 4-29 Relative expression of other fibrosis-associated genes in pseudolycorine-treated fibroblasts in the Scar-in-a-Jar model.
RT-qPCR array data expressed as $\log_2$ fold change relative to vehicle control (0.1% DMSO) calculated using the $2^{-\Delta\Delta CT}$ method (n = 4 biological replicates per group). Target gene expression normalised to GAPDH. Data presented as mean ± SD. Statistical significance determined by two-tailed t-tests via Qiagen GeneGlobe data analysis software.

4.5 Summary

This chapter began with the results of Scar-in-a-Jar assay optimisation, a prerequisite step to compound screening to ensure a robust platform for high-content imaging. Initial attempts yielded insufficient viable cell numbers, prompting optimisation of seeding density and transition from primary cells to a cell line. Although this resolved the cell number issue, cells were observed to form clumps rather than a uniform monolayer, which would have compromised the accuracy of fluorescence quantification. The primary driver of clumping was identified as the low-serum culture medium; this was addressed by implementing a serum-conditioning step, transitioning cells from high-serum to low-serum medium, which successfully yielded a uniform monolayer. Subsequent challenges arose with immunocytochemical staining, where signal levels were indistinguishable from background. Modifications to permeabilisation conditions, assay duration, and antibody concentration did not resolve this issue; however, substituting antibodies from an alternative supplier produced satisfactory staining. The optimised assay was then validated using a positive control containing TGF-β1 and a negative control without TGF-β1, confirming assay sensitivity.

Following validation, the chapter presented the results of immunofluorescence-based screening of the test compounds at two concentrations, followed by dose-response analysis of the lead compound, pseudolycorine, identifying an IC_{50} of 1.84 μM for α-SMA. Finally, RT-qPCR array analysis revealed treatment-induced changes in fibrosis-associated gene expression following pseudolycorine treatment, with significant differential expression identified in *MMP14, PLAU, TIMP4, CCR2, CCL11,* and *CEBPB*.

Chapter 5 Discussion

This study investigated the in vitro antifibrotic activity of four Amaryllidaceae alkaloids (galanthine, lycorenine, pseudolycorine, and powelline) isolated from Amazonian bulbs to identify candidates capable of modulating signalling pathways relevant to arthrofibrosis post-TKA. Utilising the Scar-in-a-Jar assay, pseudolycorine was identified as the most potent anti-fibrotic candidate. This discussion chapter presents a systematic analysis of pseudolycorine's antifibrotic mechanism by contextualising the RT-qPCR findings within the broader research landscape. It begins with an examination of pseudolycorine's established pharmacological profile, before analysing its selective effects on pericellular matrix remodelling, specifically the coordinated downregulation of the *MMP14/TIMP4* axis and *PLAU*-mediated plasminogen activation pathways, both critical regulators of latent TGF-β1 activation. The stability of SMAD transcripts despite this upstream disruption is then addressed, followed by an exploration of pseudolycorine's immunomodulatory effects through the downregulation of *CCL11* and *CCR2*, and an examination of the upregulation of *CEBPB*. Subsequently, the apparent discrepancy between stable collagen mRNA levels and reduced protein deposition is reconciled, before the collective findings are synthesised into a mechanistic framework to guide the future preclinical evaluation of pseudolycorine as a targeted therapy for arthrofibrosis. Finally, study limitations and prospective research directions are outlined.

5.1 Established pharmacological profile of pseudolycorine

The identification of pseudolycorine as the most potent antifibrotic candidate among the four tested alkaloids aligns with the broader pharmacological profile of the Amaryllidaceae family, which has long been recognised for its diverse biological activities, including anti-inflammatory, antitumour, antidiabetic, antiparasitic, cardioprotective, antibacterial, and neuroprotective effects (280,281). Pseudolycorine itself has demonstrated antiviral activity against both RNA- and DNA-containing viruses, including Japanese encephalitis virus, vaccinia virus, and lentivirus (282), as well as anti-leukemic effects (281). More critically for the present study, pseudolycorine has been

shown to inhibit the dose-dependent expression of the pro-inflammatory cytokines TNF-α and IL-1β in human peripheral blood mononuclear cells (236). The authors of that study suggested its clinical utility in chronic inflammatory conditions such as rheumatoid arthritis and inflammatory bowel disease, a profile that aligns closely with the inflammatory signalling pathways that drive fibrotic progression. However, despite this established anti-inflammatory background, the specific antifibrotic potential of pseudolycorine had not been investigated prior to this study.

5.2 Targeted disruption of the pericellular matrix-remodelling axis

Treatment with pseudolycorine produced a strikingly selective transcriptional response within the matrix-remodelling network. The stability of six major secreted MMPs (MMP1, 2, 3, 8, 9, 13) and three of the four TIMPs (TIMP1, 2, 3) argues against a generalised effect on matrix-remodelling transcription, pointing instead to a defined response targeting a specific pericellular axis involving *MMP14* and *PLAU*. MMP14 (MT1-MMP) functions as a master regulator of pericellular matrix remodelling, directly degrading interstitial collagens and driving fibroblast invasion through dense collagenous matrices (283). Beyond physical remodelling, it is proposed to drive fibrotic phenotypes through proteolytic regulation of the latent TGF-β1 complex tethered by integrin αvβ8, releasing active TGF-β1 into the local microenvironment and thereby licensing downstream SMAD signalling, myofibroblast persistence, and sustained collagen deposition (284). Indeed, MMP14 has been directly implicated as an instigator of fibrotic disease in human tissue: for instance, in human pterygium, an ocular surface fibroproliferative disorder, MMP14 is over-expressed up to 70-fold, and its selective inhibition attenuates human conjunctival fibroblast migration and mitigates collagen gel contraction (285). Interestingly, pseudolycorine also downregulated *TIMP4*, a principal endogenous regulator of MMP14 (286). Given that *TIMP4*-deficient mice exhibit enhanced MMP14 activity and exaggerated fibrosis (287), the concurrent downregulation of both partners likely reflects a coordinated co-regulation aimed at dampening a central driver of the fibrotic phenotype.

This proteolytic blockade is further bolstered by the downregulation of *PLAU*, the gene encoding urokinase-type plasminogen activator (uPA) (288). As a primary mediator of the conversion of plasminogen into plasmin, uPA plays a critical role in the proteolytic environment of the fibrotic niche (289). Similarly to MMP14, uPA-generated plasmin has been implicated in the activation of latent TGF-β1 and the release of ECM-bound growth factors, thereby sustaining pro-fibrotic signalling (290). Additionally, uPA-dependent plasminogen activation can evoke fibroblast proliferation via the G protein-coupled receptor PAR-1 (288). Consistent with a pro-fibrotic role, increased uPA expression and activity in both the serum and tissue of IPF patients correlate with regions of active fibrogenesis (288). Moreover, inhibition of uPA has been shown to be protective against cardiac fibrosis in animal models (291). The suppression of both *MMP14* and *PLAU* suggests that pseudolycorine targets the proteases required to activate the master fibrotic switch, TGF-β1.

5.3 Reconciling SMAD transcript stability with pathway inhibition

Although both uPA and MMP14 have been implicated in TGF-β1 activation, *SMAD* transcript levels, which lie downstream of TGF-β1 signalling, were not significantly altered in the present dataset. However, this is unlikely to reflect an absence of pathway engagement, as SMAD signalling is regulated predominantly at the post-translational level through receptor-mediated phosphorylation, nuclear translocation, and complex formation, rather than through transcriptional changes in *SMAD* gene expression (43). Indeed, TGF-β1 signalling characteristically induces rapid phosphorylation of SMAD2 and SMAD3 without necessarily altering their transcript levels (56), meaning that mRNA-based profiling alone is insufficient to assess pathway activation.

5.4 Immunomodulatory effects

In addition to its effects on the ECM remodelling network, pseudolycorine produced a concurrent downregulation of inflammatory chemokine signalling, specifically *CCL11* and *CCR2*. CCL11 (eotaxin-1) selectively modulates fibroblast activities by increasing

their proliferation to an extent comparable with that induced by TGF-β, enhancing MMP-2 activity, and inducing collagen protein production independently of TGF-β (292). Notably, CCL11 does not induce myofibroblast differentiation, suggesting it acts primarily in the early phases of tissue remodelling (292). CCL11 is also a potent chemoattractant for eosinophils and mast cells, which are important sources of profibrogenic and proangiogenic mediators, to sites of inflammation (293); these cells are in turn able to enhance CCL11 release from fibroblasts, creating an amplification loop of remodelling (294). CCL11 has been implicated in liver (295), cardiac (296), and pulmonary fibrosis (292), and its depletion has been shown to prevent pulmonary fibrosis in mice (297). Downregulation of *CCL11* by pseudolycorine may therefore attenuate fibroblast proliferation and collagen synthesis through a TGF-β-independent pathway, complementing its effects on the MMP14/uPA proteolytic axis.

The immunomodulatory effect of pseudolycorine is further bolstered by the downregulation of *CCR2*, the cognate receptor for the pivotal pro-fibrotic cytokine CCL2 (298). This receptor is essential for the recruitment and migration of fibroblast precursor cells to sites of injury (299). Beyond its role in trafficking, CCR2 expression identifies a distinct pro-fibrotic fibroblast phenotype characterised by the overexpression of α-SMA, Col-I, connective tissue growth factor, and CCL2 itself, suggesting an autocrine regulatory loop that sustains the fibrotic response (298). Consequently, the absence or pharmacological inhibition of this receptor consistently correlates with reduced fibrotic susceptibility in various models (299). Downregulation of CCR2 by pseudolycorine may therefore limit the recruitment of fibroblast precursors while simultaneously attenuating the autocrine pro-fibrotic signalling loops.

Taken together, the concurrent downregulation of *CCL11* and *CCR2* suggests that pseudolycorine can suppress both the direct stimulation of fibroblast activity and the inflammatory recruitment of fibrogenic cell populations, representing a complementary mechanism to its effects on pericellular proteolysis.

5.5 The context-dependent role of *CEBPB* upregulation

The most striking transcriptomic change observed following pseudolycorine treatment was the marked upregulation of *CEBPB*, which encodes the bZIP transcription factor CCAAT/enhancer-binding protein beta (C/EBPβ). C/EBPβ is a critical regulator of immune and inflammatory responses, binding to regulatory regions of several acute-phase cytokines, including IL-6 (300). It also modulates the expression of fibrosis-associated genes such as *COL1A1* and *ACTA2*, thereby influencing ECM remodelling and myofibroblast differentiation (301). The functional outcome of C/EBPβ signalling depends on the relative abundance of its three isoforms, all translated from a single *CEBPB* mRNA (302). For example, the liver-enriched activator protein (LAP) isoform typically activates *ACTA2* transcription, while the truncated liver-enriched inhibitory protein (LIP) isoform lacks the activation domain of LAP and suppresses *ACTA2* expression, possibly through competitive binding at the same promoter element (303,304). Because the balance between these isoforms varies by cell type and stimulus, C/EBPβ's role in fibrosis is highly context-dependent (300,305). In the lung and liver, it appears predominantly pro-fibrotic; *CEBPB* knockout attenuates pulmonary fibrosis (302), while its phosphorylation in the liver promotes the survival of activated hepatic stellate cells, the primary drivers of fibrogenesis, by inhibiting apoptosis (306). Similarly, its knockdown reduces inflammation and collagen deposition in models of autoimmune myocarditis (301). Conversely, C/EBPβ serves an anti-fibrotic function in other cardiac settings. It is downregulated in fibrotic heart tissue during diabetic cardiomyopathy and hypertensive heart disease, where its overexpression significantly attenuates fibrotic progression (307,308). This complexity suggests that the upregulation of *CEBPB* observed in this study need not indicate a pro-fibrotic response. Instead, it may reflect preferential induction of the inhibitory LIP isoform, potentially accounting for the observed reduction in protein deposition and paralleling the protective role of C/EBPβ described in diabetic and hypertensive cardiac fibrosis (307,308).

5.6 Post-translational regulation of collagen deposition

A key observation in this study was that while the PCR array indicated no significant reduction in *COL1A2* or *COL3A1* transcript levels, a marked reduction in Col-I protein deposition was observed in the Scar-in-a-Jar assay. This discrepancy highlights the importance of the post-translational environment. Collagens undergo extensive maturation, including post-translational modifications (PTMs) and cross-linking, which determine the final assembly of the ECM (309). Pseudolycorine may therefore act downstream of collagen gene expression by modulating the proteolytic, secretory, or cross-linking machinery rather than by suppressing collagen transcription directly.

5.7 A mechanistic framework for preclinical evaluation

In summary, pseudolycorine produced a selective transcriptional response, with upregulation of *CEBPB* and downregulation of *MMP14, TIMP4, PLAU, CCL11*, and *CCR2*, while most ECM remodelling genes and all TGF-β/SMAD pathway transcripts remained unchanged. The downregulation of *MMP14*, a master regulator of pericellular matrix remodelling and a key driver of latent TGF-β1 activation, alongside its principal endogenous regulator *TIMP4*, likely reflects coordinated co-regulation aimed at dampening a central driver of the fibrotic phenotype. This proteolytic blockade is further reinforced by the downregulation of *PLAU*, encoding uPA, which similarly activates latent TGF-β1, releases ECM-bound growth factors, and promotes fibroblast proliferation. The concurrent downregulation of *CCL11* and *CCR2* points to suppression of both direct fibroblast stimulation and inflammatory recruitment of fibrogenic cell populations, representing a complementary immunomodulatory mechanism. The marked upregulation of *CEBPB* may reflect a protective regulatory mechanism given its established anti-fibrotic role in certain contexts. The selectivity of this response argues against a non-specific mechanism and suggests a pharmacologically defined mode of action, providing preliminary evidence to support the further preclinical evaluation of pseudolycorine as a candidate therapy for post-TKA arthrofibrosis.

5.8 Study limitations

While this study provides compelling evidence for the anti-fibrotic potential of pseudolycorine, several limitations inherent to the experimental design must be acknowledged. First, all experiments were conducted using a single human fibroblast cell line under Scar-in-a-Jar conditions, which, while providing a relevant and reproducible in vitro model of fibrosis, does not fully recapitulate the complexity of the in vivo articular fibrotic environment. Arthrofibrosis following TKA involves a heterogeneous population of cell types, including synovial fibroblasts, macrophages, T lymphocytes, and mast cells, as well as dynamic mechanical and paracrine interactions that cannot be modelled in a monolayer cell culture system (5). The translational relevance of findings therefore requires careful consideration.

Second, the Scar-in-a-Jar assay is unable to detect antifibrotic effects mediated through inhibition of collagen cross-linking. This was evidenced in the present study by the pharmacological reference control PXS-5505, a pan-LOX inhibitor that acts primarily by preventing collagen cross-linking, which did not produce a significant reduction in Col-I deposition despite its established antifibrotic activity. This observation is consistent with findings from other studies investigating compounds that act through interference with cross-linking in the Scar-in-a-Jar model, which have similarly reported no detectable decrease in Col-I deposition (248,310), highlighting that the assay is unable to differentiate or quantify cross-linked from non-cross-linked collagen. Evidence from heritable connective tissue disorders (311) suggests that disrupting collagen cross-linking does not reduce collagen synthesis but may instead render scar tissue more susceptible to degradation (312,313). Within the timeframe of this assay, however, any increase in collagen turnover resulting from reduced cross-linking may not be readily detectable, as ongoing enhanced collagen deposition can mask this effect. Therefore, a reduction in collagen cross-linking by PXS-5505 does not necessarily translate into a measurable reduction in the pericellular collagen being assessed by the assay. These considerations suggest that the antifibrotic potential of compounds acting through this mechanism may be systematically underestimated by the Scar-in-a-Jar model.

Third, the transcriptomic analysis was limited to 84 fibrosis-associated genes as defined by the RT^2 Profiler Human Fibrosis PCR Array. While this targeted approach provides a focused pathway-level analysis, it precludes the detection of antifibrotic effects operating through genes not represented on the array.

Fourth, the discordance observed between *COL1A2* and *COL3A1* transcript levels, which were not significantly altered, and the significant reduction in Col-I protein deposition observed in the Scar-in-a-Jar assay highlights the limitation of mRNA-based profiling as a sole readout of fibrotic activity because gene expression does not always correlate linearly with protein abundance or enzymatic activity (314). Similarly, the absence of significant changes in *SMAD* transcript levels cannot be interpreted as evidence of TGF-β1/SMAD pathway disengagement.

5.9 Future research directions

The findings of the present study provide a foundation for several avenues of future investigation. First, the antifibrotic activity of pseudolycorine should be validated in a more disease-relevant cellular model to strengthen the clinical relevance of the present findings. Synovial fibroblasts isolated from patients undergoing rTKA for arthrofibrosis would represent a physiologically appropriate cell type, as these cells are likely to be key effectors of periarticular and intraarticular scar tissue formation in the post-TKA joint.

Second, the mechanistic hypotheses generated by the RT-qPCR array require protein-level validation. Protein quantification of MMP14, TIMP4, uPA, CCL11, and CCR2 would determine whether the observed transcriptomic changes translate into functionally relevant differences in protein expression. Zymography could also be employed to assess MMP14 and uPA enzymatic activity, thereby providing functional validation of pathways implicated by the gene expression data. Moreover, Western blotting for phosphorylated SMAD2/3 would clarify whether pseudolycorine modulates TGF-β1/SMAD pathway engagement, as SMAD signalling is regulated post-translationally and cannot be inferred from transcript levels alone (315).

Third, an unbiased whole-transcriptome approach, such as RNA sequencing, would provide a more comprehensive characterisation of pseudolycorine's mechanism of action. This would enable detection of antifibrotic effects operating through pathways not represented on the 84-gene array and may reveal additional regulatory networks involved in pseudolycorine-mediated suppression of fibrosis.

Fourth, the effect of pseudolycorine on collagen cross-linking should be investigated using techniques capable of quantifying cross-link density, such as high-performance liquid chromatography or liquid chromatography–tandem mass spectrometry (310). This would address a limitation of the Scar-in-a-Jar assay, which may not fully capture cross-link-mediated changes in ECM organisation, and provide a more complete understanding of pseudolycorine's impact on ECM maturation and stability.

Finally, and most critically, the in vitro findings of the present study should be validated in vivo. An established animal model of post-surgical arthrofibrosis, would enable assessment of pseudolycorine's antifibrotic efficacy, bioavailability, joint penetration, and systemic tolerability within a physiologically intact system. Successful in vivo validation would represent a critical step towards establishing pseudolycorine as a viable pharmacological candidate for the treatment of arthrofibrosis following TKA.

Chapter 6 Conclusion

Current mechanical and surgical interventions for post-TKA arthrofibrosis are associated with unpredictable outcomes and considerable procedural risk. Moreover, the projected rise in arthrofibrosis prevalence, in parallel with increasing TKA rates, is expected to place a growing clinical and socioeconomic burden on patients and healthcare systems. In this context, this research aimed to evaluate the in vitro antifibrotic activity of four Amaryllidaceae alkaloids (galanthine, lycorenine, pseudolycorine, and powelline) isolated from Amazonian bulbs, using the Scar-in-a-Jar phenotypic assay, with the goal of identifying a lead compound for further mechanistic investigation.

Pseudolycorine emerged as the most potent antifibrotic candidate, demonstrating consistent and significant inhibitory activity across both hallmark markers of the fibrotic phenotype, Col-I deposition and α-SMA expression, at both concentrations tested. This finding is meaningful for several reasons. First, it demonstrates that naturally derived Amaryllidaceae alkaloids can modulate fibrotic pathways in a clinically relevant in vitro model, providing proof-of-concept for this compound class as a source of antifibrotic leads. Second, the IC_{50} of 1.84 μM established by dose-response analysis under Scar-in-a-Jar conditions falls within a pharmacologically achievable range, suggesting that pseudolycorine may be suitable for further development as a therapeutic candidate. Third, the transcriptomic profiling revealed that the antifibrotic activity of pseudolycorine likely operates through the concurrent downregulation of multiple pro-fibrotic axes, rather than through a single molecular target. This is supported by the finding that pseudolycorine modulated pericellular matrix remodelling enzymes, including *MMP14, TIMP4*, and *PLAU*, alongside inflammatory chemokine signalling, such as *CCL11* and *CCR2*, and markedly upregulated *CEBPB*, encoding the transcription factor C/EBPβ, a critical and context-dependent regulator of both inflammatory and fibrosis-associated gene networks. This multi-target profile is particularly significant in the context of fibrosis, where redundant signalling pathways have historically confounded single-target therapeutic approaches. The convergence of some these downregulated genes on TGF-β1 activation further suggests that pseudolycorine may

attenuate the central fibrotic driver without directly targeting TGF-β1 itself, potentially offering a more nuanced and better-tolerated therapeutic strategy.

The findings of this study are of direct relevance to patients who develop arthrofibrosis following TKA and currently face a treatment landscape dominated by painful physiotherapy, repeated surgical procedures, and unpredictable outcomes. Should the antifibrotic activity of pseudolycorine be validated in synovial fibroblasts and subsequently confirmed in vivo, it would represent a promising candidate for pharmacological intervention in post-TKA arthrofibrosis. Intra-articular delivery in particular would offer a clinically attractive route of administration, enabling localised suppression of fibrotic scar formation in the post-operative joint while minimising systemic exposure, an important consideration given the tolerability requirements of a peri-operative therapeutic context. More broadly, given that the fibrotic pathways targeted by pseudolycorine are conserved across fibrotic conditions affecting multiple organs, the findings may have relevance beyond arthrofibrosis to other fibroproliferative disorders. The identification of pseudolycorine as a bioactive alkaloid with antifibrotic potential also contributes to the growing body of evidence supporting natural product-derived compounds as a valuable source of pharmacological leads for fibrosis, a disease area where therapeutic options remain severely limited.

Bibliography

1. Abdul N, Dixon D, Walker A, Horabin J, Smith N, Weir DJ, et al. Fibrosis is a common outcome following total knee arthroplasty. Sci Rep. 2015 Nov 10;5(1):16469. doi:10.1038/srep16469

2. Hegazy AM, Elsoufy MA. Arthroscopic Arthrolysis for Arthrofibrosis of the Knee after Total Knee Replacement. HSS Journal®: The Musculoskeletal Journal of Hospital for Special Surgery. 2011 Jul;7(2):130–3. doi:10.1007/s11420-011-9202-7

3. Christensen CP, Crawford JJ, Olin MD, Vail TP. Revision of the stiff total knee arthroplasty. The Journal of Arthroplasty. 2002 Jun;17(4):409–15. doi:10.1054/arth.2002.32105

4. D'Urso M, Kurniawan NA. Mechanical and Physical Regulation of Fibroblast–Myofibroblast Transition: From Cellular Mechanoresponse to Tissue Pathology. Front Bioeng Biotechnol. 2020 Dec 22;8. doi:10.3389/fbioe.2020.609653

5. Usher KM, Zhu S, Mavropalias G, Carrino JA, Zhao J, Xu J. Pathological mechanisms and therapeutic outlooks for arthrofibrosis. Bone Res. 2019 Mar 26;7(1):9. doi:10.1038/s41413-019-0047-x

6. Wakolbinger-Habel R, Gaudernak J, Scheffold BE, Fiala R, Breuer R, Bittner-Frank M, et al. Conservative treatment of knee arthrofibrosis according to a cellular cytokine-based model: A retrospective pilot evaluation. Wien Klin Wochenschr. 2025 Feb 3. doi:10.1007/s00508-024-02497-0

7. Moffatt F, Narayanasamy M, Smith B, Stocks J, Sheehan K, Sackley C, et al. "My bloody leg" – The lived experience of arthrofibrosis after total knee arthroplasty. Physiotherapy. 2026 Mar;130:101862. doi:10.1016/j.physio.2025.101862

8. Magit D, Wolff A, Sutton K, Medvecky MJ. Arthrofibrosis of the Knee: Journal of the American Academy of Orthopaedic Surgeons. 2007 Nov;15(11):682–94. doi:10.5435/00124635-200711000-00007

9. Haklar U, Ayhan E, Ulku TK, Karaoğlu S. Arthrofibrosis of the Knee. In: Doral MN, Karlsson J, editors. Sports Injuries [Internet]. Berlin, Heidelberg: Springer Berlin Heidelberg; 2015 [cited 2025 Jun 21]. p. 915–31. Available from: https://link.springer.com/10.1007/978-3-642-36569-0_100 doi:10.1007/978-3-642-36569-0_100

10. Bonutti PM, McGrath MS, Ulrich SD, McKenzie SA, Seyler TM, Mont MA. Static progressive stretch for the treatment of knee stiffness. The Knee. 2008 Aug;15(4):272–6. doi:10.1016/j.knee.2008.04.002

11. Bhave A, Mont M, Tennis S, Nickey M, Starr R, Etienne G. Functional Problems and Treatment Solutions After Total Hip and Knee Joint Arthroplasty. Journal of Bone and Joint Surgery. 2005 Dec;87(suppl_2):9–21. doi:10.2106/JBJS.E.00628

12. Kylies J, Fahlbusch H, Brauneck E, Bannier D, Berninger MT, Frings J, et al. Arthroscopic Arthrolysis, a Minimally Invasive Approach to Treat Arthrofibrosis of the Knee. Arthroscopy Techniques. 2025 Jan;103446. doi:10.1016/j.eats.2025.103446

13. Cheuy VA, Foran JRH, Paxton RJ, Bade MJ, Zeni JA, Stevens-Lapsley JE. Arthrofibrosis Associated With Total Knee Arthroplasty. The Journal of Arthroplasty. 2017 Aug;32(8):2604–11. doi:10.1016/j.arth.2017.02.005

14. Schiavone Panni A, Cerciello S, Vasso M, Tartarone M. Stiffness in total knee arthroplasty. J Orthopaed Traumatol. 2009 Sep;10(3):111–8. doi:10.1007/s10195-009-0054-6

15. Enad JG. Arthroscopic Lysis of Adhesions for the Stiff Total Knee Arthroplasty. Arthroscopy Techniques. 2014 Oct;3(5):e611–4. doi:10.1016/j.eats.2014.07.001

16. Walocha A, Rutowicz B, Przybycień W, Zarzecki M, Kłosiński M, Depukat P, et al. Arthrofibrosis - a myth or true joint disorder? Folia Med Cracov. 2022 Jun 29;62(1):55–70. doi:10.24425/fmc.2022.141691 PubMed PMID: 36088593.

17. Kalson NS, Borthwick LA, Mann DA, Deehan DJ, Lewis P, Mann C, et al. International consensus on the definition and classification of fibrosis of the knee joint. The Bone & Joint Journal. 2016 Nov;98-B(11):1479–88. doi:10.1302/0301-620X.98B10.37957

18. Mamarelis G, Sunil-Kumar KH, Khanduja V. Timing of manipulation under anaesthesia for stiffness after total knee arthroplasty. Ann Transl Med. 2015 Nov;3(20):316. doi:10.3978/j.issn.2305-5839.2015.10.09 PubMed PMID: 26697476; PubMed Central PMCID: PMC4669325.

19. Ramos MS, Pasqualini I, Surace PA, Molloy RM, Deren ME, Piuzzi NS. Arthrofibrosis After Total Knee Arthroplasty: A Critical Analysis Review. JBJS Reviews. 2023 Dec;11(12). doi:10.2106/jbjs.rvw.23.00140

20. De Carlo MS, Sell KE. Normative Data for Range of Motion and Single-Leg Hop in High School Athletes. Journal of Sport Rehabilitation. 1997 Aug;6(3):246–55. doi:10.1123/jsr.6.3.246

21. Kittelson AJ, Elings J, Colborn K, Hoogeboom TJ, Christensen JC, Van Meeteren NLU, et al. Reference chart for knee flexion following total knee arthroplasty: a novel tool for monitoring postoperative recovery. BMC Musculoskelet Disord. 2020 Dec;21(1):482. doi:10.1186/s12891-020-03493-x

22. Lee BC, Moon CW, Choi WS, Kim YM, Joo YB, Lee DG, et al. Clinical evaluation of usefulness and effectiveness of sitting-type continuous passive motion machines in patients with total knee arthroplasty: a dual-center randomized controlled trial. BMC Musculoskelet Disord. 2024 Dec 19;25(1):1039. doi:10.1186/s12891-024-08062-0

23. Pitta M, Esposito CI, Li Z, Lee Y yu, Wright TM, Padgett DE. Failure After Modern Total Knee Arthroplasty: A Prospective Study of 18,065 Knees. The Journal of Arthroplasty. 2018 Feb;33(2):407–14. doi:10.1016/j.arth.2017.09.041

24. Tjoumakaris FP, Tucker BC, Post Z, Pepe MD, Rozco F, Ong AC. Arthroscopic Lysis of Adhesions for the Stiff Total Knee: Results After Failed Manipulation. Orthopedics. 2014 May;37(5). doi:10.3928/01477447-20140430-60

25. Daluga D, Lombardi AV, Mallory TH, Vaughn BK. Knee manipulation following total knee arthroplasty. The Journal of Arthroplasty. 1991 Jun;6(2):119–28. doi:10.1016/S0883-5403(11)80006-9

26. Namba RS, Cafri G, Khatod M, Inacio MCS, Brox TW, Paxton EW. Risk Factors for Total Knee Arthroplasty Aseptic Revision. The Journal of Arthroplasty. 2013 Sep;28(8):122–7. doi:10.1016/j.arth.2013.04.050

27. Mont MA, Seyler TM, Marulanda GA, Delanois RE, Bhave A. Surgical Treatment and Customized Rehabilitation for Stiff Knee Arthroplasties: Clinical Orthopaedics and Related Research. 2006 May;446:193–200. doi:10.1097/01.blo.0000214419.36959.8c

28. Fitzsimmons SE, Vazquez EA, Bronson MJ. How to Treat the Stiff Total Knee Arthroplasty?: A Systematic Review. Clinical Orthopaedics & Related Research. 2010 Apr;468(4):1096–106. doi:10.1007/s11999-010-1230-y

29. Sanders TL, Kremers HM, Bryan AJ, Kremers WK, Stuart MJ, Krych AJ. Procedural intervention for arthrofibrosis after ACL reconstruction: trends over two decades. Knee Surg Sports Traumatol Arthrosc. 2017 Feb;25(2):532–7. doi:10.1007/s00167-015-3799-x

30. Traut P. Klinische Diagnostik, Differenzialdiagnostik, Pathogenese- und Stadienmodell der Arthrofibrose. Unfallchirurgie. 2022 Nov;125(11):839–48. doi:10.1007/s00113-022-01237-1

31. Dubin JA, Bains SS, Hameed D, Gottlich C, Turpin R, Nace J, et al. Projected volume of primary total joint arthroplasty in the USA from 2019 to 2060. Eur J Orthop Surg Traumatol. 2024 May 15;34(5):2663–70. doi:10.1007/s00590-024-03953-3

32. Rullán PJ, Deren ME, Zhou G, Emara AK, Klika AK, Schiltz NK, et al. The Arthroplasty Surgeon Growth Indicator: A Tool for Monitoring Supply and Demand Trends in

the Orthopaedic Surgeon Workforce from 2020 to 2050. Journal of Bone and Joint Surgery. 2023 Jul 5;105(13):1038–45. doi:10.2106/JBJS.22.00874

33. Shichman I, Roof M, Askew N, Nherera L, Rozell JC, Seyler TM, et al. Projections and Epidemiology of Primary Hip and Knee Arthroplasty in Medicare Patients to 2040-2060. JB JS Open Access. 2023;8(1):e22.00112. doi:10.2106/JBJS.OA.22.00112 PubMed PMID: 36864906; PubMed Central PMCID: PMC9974080.

34. Mamun AA, Shao C, Geng P, Wang S, Xiao J. Recent advances in molecular mechanisms of skin wound healing and its treatments. Front Immunol. 2024 May 21;15:1395479. doi:10.3389/fimmu.2024.1395479

35. Freeman TA, Parvizi J, Dela Valle CJ, Steinbeck MJ. Mast cells and hypoxia drive tissue metaplasia and heterotopic ossification in idiopathic arthrofibrosis after total knee arthroplasty. Fibrogenesis Tissue Repair. 2010 Dec;3(1):17. doi:10.1186/1755-1536-3-17

36. Bogadi S, Uddin ME, Rahman MdH, Satyanarayana Reddy Karri VV, Begum R, Udeabor SE. Wound healing in the modern era: Emerging research, biomedical advances, and transformative clinical approaches. Journal of Drug Delivery Science and Technology. 2025 Aug;110:107058. doi:10.1016/j.jddst.2025.107058

37. Tai Y, Woods EL, Dally J, Kong D, Steadman R, Moseley R, et al. Myofibroblasts: Function, Formation, and Scope of Molecular Therapies for Skin Fibrosis. Biomolecules. 2021 Jul 23;11(8):1095. doi:10.3390/biom11081095 PubMed PMID: 34439762; PubMed Central PMCID: PMC8391320.

38. Wallace HA, Basehore BM, Zito PM. Wound Healing Phases. In: StatPearls [Internet]. Treasure Island (FL): StatPearls Publishing; 2025 [cited 2025 Jul 8]. Available from: http://www.ncbi.nlm.nih.gov/books/NBK470443/ PubMed PMID: 29262065.

39. Lee DR, Therrien E, Song BM, Camp CL, Krych AJ, Stuart MJ, et al. Arthrofibrosis Nightmares: Prevention and Management Strategies. Sports Med Arthrosc Rev. 2022 Mar 1;30(1):29–41. doi:10.1097/JSA.0000000000000324 PubMed PMID: 35113841; PubMed Central PMCID: PMC8830598.

40. Ly TD, Sambale M, Klösener L, Traut P, Fischer B, Hendig D, et al. Understanding of arthrofibrosis: New explorative insights into extracellular matrix remodeling of synovial fibroblasts. Xu L, editor. PLoS ONE. 2023 May 26;18(5):e0286334. doi:10.1371/journal.pone.0286334

41. Rybinski B, Franco-Barraza J, Cukierman E. The wound healing, chronic fibrosis, and cancer progression triad. Physiological Genomics. 2014 Apr 1;46(7):223–44. doi:10.1152/physiolgenomics.00158.2013

42. Duffield JS, Lupher M, Thannickal VJ, Wynn TA. Host responses in tissue repair and fibrosis. Annu Rev Pathol. 2013 Jan 24;8:241–76. doi:10.1146/annurev-pathol-020712-163930 PubMed PMID: 23092186; PubMed Central PMCID: PMC3789589.

43. Bonniaud P, Margetts PJ, Ask K, Flanders K, Gauldie J, Kolb M. TGF-beta and Smad3 signaling link inflammation to chronic fibrogenesis. J Immunol. 2005 Oct 15;175(8):5390–5. doi:10.4049/jimmunol.175.8.5390 PubMed PMID: 16210645.

44. Györfi AH, Matei AE, Distler JHW. Targeting TGF-β signaling for the treatment of fibrosis. Matrix Biology. 2018 Aug;68–69:8–27. doi:10.1016/j.matbio.2017.12.016

45. Dees C, Pötter S, Zhang Y, Bergmann C, Zhou X, Luber M, et al. TGF-β-induced epigenetic deregulation of SOCS3 facilitates STAT3 signaling to promote fibrosis. J Clin Invest. 2020 May 1;130(5):2347–63. doi:10.1172/JCI122462 PubMed PMID: 31990678; PubMed Central PMCID: PMC7190914.

46. Watson RS, Gouze E, Levings PP, Bush ML, Kay JD, Jorgensen MS, et al. Gene delivery of TGF-β1 induces arthrofibrosis and chondrometaplasia of synovium in vivo. Laboratory Investigation. 2010 Nov;90(11):1615–27. doi:10.1038/labinvest.2010.145

47. Chen X, Wang Z, Huang Y, Deng W, Zhou Y, Chu M. Identification of novel biomarkers for arthrofibrosis after total knee arthroplasty in animal models and clinical patients. EBioMedicine. 2021 Aug;70:103486. doi:10.1016/j.ebiom.2021.103486 PubMed PMID: 34311327; PubMed Central PMCID: PMC8325099.

48. Wyatt PB, Satalich J, Cyrus J, O'Neill C, O'Connell R. Biochemical markers of postsurgical knee arthrofibrosis: A systematic review. J Orthop. 2023 Jan;35:1–6. doi:10.1016/j.jor.2022.10.008 PubMed PMID: 36325249; PubMed Central PMCID: PMC9619298.

49. Chen CZ, Raghunath M. Focus on collagen: in vitro systems to study fibrogenesis and antifibrosis state of the art. Fibrogenesis Tissue Repair. 2009 Dec 15;2:7. doi:10.1186/1755-1536-2-7 PubMed PMID: 20003476; PubMed Central PMCID: PMC2805599.

50. Stebler S, Raghunath M. The Scar-in-a-Jar: In Vitro Fibrosis Model for Anti-Fibrotic Drug Testing. Methods Mol Biol. 2021;2299:147–56. doi:10.1007/978-1-0716-1382-5_11 PubMed PMID: 34028741.

51. Good RB, Eley JD, Gower E, Butt G, Blanchard AD, Fisher AJ, et al. A high content, phenotypic 'scar-in-a-jar' assay for rapid quantification of collagen fibrillogenesis using disease-derived pulmonary fibroblasts. BMC biomed eng. 2019 Dec;1(1). doi:10.1186/s42490-019-0014-z

52. Ayers NB, Sun CM, Chen SY. Transforming growth factor-β signaling in systemic sclerosis. J Biomed Res. 2018 Jan 18;32(1):3–12. doi:10.7555/JBR.31.20170034 PubMed PMID: 29353817; PubMed Central PMCID: PMC5956255.

53. Robertson IB, Horiguchi M, Zilberberg L, Dabovic B, Hadjiolova K, Rifkin DB. Latent TGF-β-binding proteins. Matrix Biol. 2015 Sep;47:44–53. doi:10.1016/j.matbio.2015.05.005 PubMed PMID: 25960419; PubMed Central PMCID: PMC4844006.

54. Oezel L, Wohltmann M, Gondorf N, Wille J, Güven I, Windolf J, et al. Dupuytren's Disease Is Mediated by Insufficient TGF-β1 Release and Degradation. IJMS. 2023 Oct 11;24(20):15097. doi:10.3390/ijms242015097

55. Lichtman MK, Otero-Vinas M, Falanga V. Transforming growth factor beta (TGF-β) isoforms in wound healing and fibrosis. Wound Repair Regen. 2016 Mar;24(2):215–22. doi:10.1111/wrr.12398 PubMed PMID: 26704519.

56. Meng X ming, Nikolic-Paterson DJ, Lan HY. TGF-β: the master regulator of fibrosis. Nat Rev Nephrol. 2016 Jun;12(6):325–38. doi:10.1038/nrneph.2016.48

57. Berry CE, Downer M, Morgan AG, Griffin M, Liang NE, Kameni L, et al. The effects of mechanical force on fibroblast behavior in cutaneous injury. Front Surg. 2023;10:1167067. doi:10.3389/fsurg.2023.1167067 PubMed PMID: 37143767; PubMed Central PMCID: PMC10151708.

58. Chen W, Ten Dijke P. Immunoregulation by members of the TGFβ superfamily. Nat Rev Immunol. 2016 Nov 25;16(12):723–40. doi:10.1038/nri.2016.112 PubMed PMID: 27885276.

59. Sanjabi S, Oh SA, Li MO. Regulation of the Immune Response by TGF-β: From Conception to Autoimmunity and Infection. Cold Spring Harb Perspect Biol. 2017 Jun 1;9(6):a022236. doi:10.1101/cshperspect.a022236 PubMed PMID: 28108486; PubMed Central PMCID: PMC5453394.

60. Bracey NA, Gershkovich B, Chun J, Vilaysane A, Meijndert HC, Wright JR, et al. Mitochondrial NLRP3 protein induces reactive oxygen species to promote Smad protein signaling and fibrosis independent from the inflammasome. J Biol Chem. 2014 Jul 11;289(28):19571–84. doi:10.1074/jbc.M114.550624 PubMed PMID: 24841199; PubMed Central PMCID: PMC4094069.

61. Liu RM, Gaston Pravia KA. Oxidative stress and glutathione in TGF-beta-mediated fibrogenesis. Free Radic Biol Med. 2010 Jan 1;48(1):1–15. doi:10.1016/j.freeradbiomed.2009.09.026 PubMed PMID: 19800967; PubMed Central PMCID: PMC2818240.

62. Koli K, Myllärniemi M, Keski-Oja J, Kinnula VL. Transforming growth factor-beta activation in the lung: focus on fibrosis and reactive oxygen species. Antioxid

Redox Signal. 2008 Feb;10(2):333–42. doi:10.1089/ars.2007.1914 PubMed PMID: 17961070.

63. Xu X, Zheng L, Yuan Q, Zhen G, Crane JL, Zhou X, et al. Transforming growth factor-β in stem cells and tissue homeostasis. Bone Res. 2018;6:2. doi:10.1038/s41413-017-0005-4 PubMed PMID: 29423331; PubMed Central PMCID: PMC5802812.

64. Deng YQ, Zhao H, Ma AL, Zhou JY, Xie SB, Zhang XQ, et al. Selected Cytokines Serve as Potential Biomarkers for Predicting Liver Inflammation and Fibrosis in Chronic Hepatitis B Patients With Normal to Mildly Elevated Aminotransferases. Medicine (Baltimore). 2015 Nov;94(45):e2003. doi:10.1097/MD.0000000000002003 PubMed PMID: 26559292; PubMed Central PMCID: PMC4912286.

65. Milosavljevic N, Gazdic M, Simovic Markovic B, Arsenijevic A, Nurkovic J, Dolicanin Z, et al. Mesenchymal stem cells attenuate liver fibrosis by suppressing Th17 cells - an experimental study. Transpl Int. 2018 Jan;31(1):102–15. doi:10.1111/tri.13023 PubMed PMID: 28805262.

66. Ruthenborg RJ, Ban JJ, Wazir A, Takeda N, Kim JW. Regulation of wound healing and fibrosis by hypoxia and hypoxia-inducible factor-1. Mol Cells. 2014 Sep;37(9):637–43. doi:10.14348/molcells.2014.0150 PubMed PMID: 24957212; PubMed Central PMCID: PMC4179131.

67. Basu RK, Hubchak S, Hayashida T, Runyan CE, Schumacker PT, Schnaper HW. Interdependence of HIF-1α and TGF-β/Smad3 signaling in normoxic and hypoxic renal epithelial cell collagen expression. Am J Physiol Renal Physiol. 2011 Apr;300(4):F898-905. doi:10.1152/ajprenal.00335.2010 PubMed PMID: 21209004; PubMed Central PMCID: PMC3075002.

68. Zhang H, Akman HO, Smith ELP, Zhao J, Murphy-Ullrich JE, Batuman OA. Cellular response to hypoxia involves signaling via Smad proteins. Blood. 2003 Mar 15;101(6):2253–60. doi:10.1182/blood-2002-02-0629 PubMed PMID: 12411310.

69. Wynn TA, Ramalingam TR. Mechanisms of fibrosis: therapeutic translation for fibrotic disease. Nat Med. 2012 Jul 6;18(7):1028–40. doi:10.1038/nm.2807 PubMed PMID: 22772564; PubMed Central PMCID: PMC3405917.

70. Monument MJ, Hart DA, Salo PT, Befus AD, Hildebrand KA. Neuroinflammatory Mechanisms of Connective Tissue Fibrosis: Targeting Neurogenic and Mast Cell Contributions. Adv Wound Care (New Rochelle). 2015 Mar 1;4(3):137–51. doi:10.1089/wound.2013.0509 PubMed PMID: 25785237; PubMed Central PMCID: PMC4352697.

71. Ao M, Brewer BM, Yang L, Franco Coronel OE, Hayward SW, Webb DJ, et al. Stretching Fibroblasts Remodels Fibronectin and Alters Cancer Cell Migration. Sci Rep. 2015 Feb 9;5(1). doi:10.1038/srep08334

72. Kolahian S, Fernandez IE, Eickelberg O, Hartl D. Immune Mechanisms in Pulmonary Fibrosis. Am J Respir Cell Mol Biol. 2016 Sep;55(3):309–22. doi:10.1165/rcmb.2016-0121TR PubMed PMID: 27149613.

73. Lathan R. Exploring unconventional targets in myofibroblast transdifferentiation outside classical TGF-β signaling in renal fibrosis. Front Physiol. 2024 May 14;15:1296504. doi:10.3389/fphys.2024.1296504

74. Wynn TA, Barron L. Macrophages: master regulators of inflammation and fibrosis. Semin Liver Dis. 2010 Aug;30(3):245–57. doi:10.1055/s-0030-1255354 PubMed PMID: 20665377; PubMed Central PMCID: PMC2924662.

75. Hold GL, Untiveros P, Saunders KA, El-Omar EM. Role of host genetics in fibrosis. Fibrogenesis Tissue Repair. 2009 Dec;2(1):6. doi:10.1186/1755-1536-2-6

76. Campbell TM, Trudel G, Wong KK, Laneuville O. Genome wide Gene Expression Analysis of the Posterior Capsule in Patients with Osteoarthritis and Knee Flexion Contracture. J Rheumatol. 2014 Nov;41(11):2232–9. doi:10.3899/jrheum.140079

77. Skutek M, Elsner HA, Slateva K, Mayr HO, Weig TG, Van Griensven M, et al. Screening for arthrofibrosis after anterior cruciate ligament reconstruction: Analysis of association with human leukocyte antigen. Arthroscopy: The Journal of Arthroscopic & Related Surgery. 2004 May;20(5):469–73. doi:10.1016/j.arthro.2004.03.003

78. Felitti VJ, Anda RF, Nordenberg D, Williamson DF, Spitz AM, Edwards V, et al. Relationship of Childhood Abuse and Household Dysfunction to Many of the Leading Causes of Death in Adults. American Journal of Preventive Medicine. 1998 May;14(4):245–58. doi:10.1016/S0749-3797(98)00017-8

79. Elwenspoek MMC, Hengesch X, Leenen FAD, Schritz A, Sias K, Schaan VK, et al. Proinflammatory T Cell Status Associated with Early Life Adversity. The Journal of Immunology. 2017 Dec 15;199(12):4046–55. doi:10.4049/jimmunol.1701082

80. Ayers DC, Franklin PD, Ploutz-Snyder R, Boisvert CB. Total Knee Replacement Outcome and Coexisting Physical and Emotional Illness: Clinical Orthopaedics and Related Research. 2005 Nov;440(NA;):157–61. doi:10.1097/01.blo.0000185447.43622.93

81. Fisher DA, Dierckman B, Watts MR, Davis K. Looks Good But Feels Bad: Factors That Contribute to Poor Results After Total Knee Arthroplasty. The Journal of Arthroplasty. 2007 Sep;22(6):39–42. doi:10.1016/j.arth.2007.04.011

82. Bufalino C, Hepgul N, Aguglia E, Pariante CM. The role of immune genes in the association between depression and inflammation: A review of recent clinical studies. Brain, Behavior, and Immunity. 2013 Jul;31:31–47. doi:10.1016/j.bbi.2012.04.009

83. Raison CL, Capuron L, Miller AH. Cytokines sing the blues: inflammation and the pathogenesis of depression. Trends in Immunology. 2006 Jan;27(1):24–31. doi:10.1016/j.it.2005.11.006

84. Alad M, Yousef F, Epure LM, Lui A, Grant MP, Merle G, et al. Unraveling Osteoarthritis: Mechanistic Insights and Emerging Therapies Targeting Pain and Inflammation. Biomolecules. 2025 Jun 16;15(6):874. doi:10.3390/biom15060874

85. Scanzello CR, Umoh E, Pessler F, Diaz-Torne C, Miles T, DiCarlo E, et al. Local cytokine profiles in knee osteoarthritis: elevated synovial fluid interleukin-15 differentiates early from end-stage disease. Osteoarthritis and Cartilage. 2009 Aug;17(8):1040–8. doi:10.1016/j.joca.2009.02.011

86. Oehler S, Neureiter D, Meyer-Scholten C, Aigner T. Subtyping of osteoarthritic synoviopathy. Clin Exp Rheumatol. 2002;20(5):633–40. PubMed PMID: 12412193.

87. Remst DFG, Blaney Davidson EN, Van Der Kraan PM. Unravelling osteoarthritis-related synovial fibrosis: a step closer to solving joint stiffness. Rheumatology. 2015 Nov;54(11):1954–63. doi:10.1093/rheumatology/kev228

88. Zhang W, Ouyang H, Dass CR, Xu J. Current research on pharmacologic and regenerative therapies for osteoarthritis. Bone Res. 2016 Mar 1;4(1):15040. doi:10.1038/boneres.2015.40

89. Snelling SJB, Bas S, Puskas GJ, Dakin SG, Suva D, Finckh A, et al. Presence of IL-17 in synovial fluid identifies a potential inflammatory osteoarthritic phenotype. PLoS One. 2017;12(4):e0175109. doi:10.1371/journal.pone.0175109 PubMed PMID: 28399156; PubMed Central PMCID: PMC5388337.

90. Zhen G, Wen C, Jia X, Li Y, Crane JL, Mears SC, et al. Inhibition of TGF-β signaling in mesenchymal stem cells of subchondral bone attenuates osteoarthritis. Nat Med. 2013 Jun;19(6):704–12. doi:10.1038/nm.3143

91. Ioan-Facsinay A, Kloppenburg M. An emerging player in knee osteoarthritis: the infrapatellar fat pad. Arthritis Res Ther. 2013;15(6):225. doi:10.1186/ar4422

92. Turhan E, Doral MN, Atay AÖ, Demirel M. A giant extrasynovial osteochondroma in the infrapatellar fat pad: end stage Hoffa's disease. Arch Orthop Trauma Surg. 2008 May;128(5):515–9. doi:10.1007/s00402-007-0397-5

93. Chalmers BP, Suleiman LI, Sculco PK, Abdel MP. A Comprehensive Approach to Stiffness in Total Knee Arthroplasty. The Journal of Arthroplasty. 2025 Sep;40(9):S59–65. doi:10.1016/j.arth.2025.04.054

94. Marks PH, Donaldson MLC. Inflammatory Cytokine Profiles Associated With Chondral Damage in the Anterior Cruciate Ligament–Deficient Knee. Arthroscopy: The Journal of Arthroscopic & Related Surgery. 2005 Nov;21(11):1342–7. doi:10.1016/j.arthro.2005.08.034

95. Ipach I, Mittag F, Lahrmann J, Kunze B, Kluba T. Arthrofibrosis after TKA - Influence factors on the absolute flexion and gain in flexion after manipulation under anaesthesia. BMC Musculoskelet Disord. 2011 Dec;12(1):184. doi:10.1186/1471-2474-12-184

96. Kisseleva T, Cong M, Paik Y, Scholten D, Jiang C, Benner C, et al. Myofibroblasts revert to an inactive phenotype during regression of liver fibrosis. Proc Natl Acad Sci U S A. 2012 Jun 12;109(24):9448–53. doi:10.1073/pnas.1201840109 PubMed PMID: 22566629; PubMed Central PMCID: PMC3386114.

97. Trautwein C, Friedman SL, Schuppan D, Pinzani M. Hepatic fibrosis: Concept to treatment. J Hepatol. 2015 Apr;62(1 Suppl):S15-24. doi:10.1016/j.jhep.2015.02.039 PubMed PMID: 25920084.

98. Gandhi R, De Beer J, Leone J, Petruccelli D, Winemaker M, Adili A. Predictive Risk Factors for Stiff Knees in Total Knee Arthroplasty. The Journal of Arthroplasty. 2006 Jan;21(1):46–52. doi:10.1016/j.arth.2005.06.004

99. Schwarzkopf R, William A, Deering RM, Fitz W. Arthroscopic Lysis of Adhesions for Stiff Total Knee Arthroplasty. Orthopedics. 2013 Dec;36(12). doi:10.3928/01477447-20131120-20

100. Pfefferle KJ, Shemory ST, Dilisio MF, Fening SD, Gradisar IM. Risk factors for manipulation after total knee arthroplasty: a pooled electronic health record database study. J Arthroplasty. 2014 Oct;29(10):2036–8. doi:10.1016/j.arth.2014.05.001 PubMed PMID: 24927868.

101. Moon HK, Han CD, Yang IH, Cha BS. Factors Affecting Outcome after Total Knee Arthroplasty in Patients with Diabetes Mellitus. Yonsei Med J. 2008;49(1):129. doi:10.3349/ymj.2008.49.1.129

102. Yercan HS, Sugun TS, Bussiere C, Ait Si Selmi T, Davies A, Neyret P. Stiffness after total knee arthroplasty: Prevalence, management and outcomes. The Knee. 2006 Mar;13(2):111–7. doi:10.1016/j.knee.2005.10.001

103. Van de Ven MPF, Bongers J, Spekenbrink-Spooren A, Koëter S. Factors associated with arthrofibrosis-related revision following 14,325 total or unicompartmental knee arthro-plasties: an analysis from the Dutch Arthroplasty Registry. Acta

Orthop. 2024 Oct 15;95:607–11. doi:10.2340/17453674.2024.41988 PubMed PMID: 39404490; PubMed Central PMCID: PMC11475797.

104. Bade MJ, Kittelson JM, Kohrt WM, Stevens-Lapsley JE. Predicting functional performance and range of motion outcomes after total knee arthroplasty. Am J Phys Med Rehabil. 2014 Jul;93(7):579–85. doi:10.1097/PHM.0000000000000065 PubMed PMID: 24508937; PubMed Central PMCID: PMC4350663.

105. Koshino T, Ejima M, Okamoto R, Morii T. Gradual low riding of the patella during postoperative course after total knee arthroplasty in osteoarthritis and rheumatoid arthritis. The Journal of Arthroplasty. 1990 Dec;5(4):323–7. doi:10.1016/S0883-5403(08)80091-5

106. Ritter MA, Harty LD, Davis KE, Meding JB, Berend ME. PREDICTING RANGE OF MOTION AFTER TOTAL KNEE ARTHROPLASTY: CLUSTERING, LOG-LINEAR REGRESSION, AND REGRESSION TREE ANALYSIS. The Journal of Bone and Joint Surgery-American Volume. 2003 Jul;85(7):1278–85. doi:10.2106/00004623-200307000-00014

107. Beaupre LA, Lier D, Davies DM, Johnston DBC. The effect of a preoperative exercise and education program on functional recovery, health related quality of life, and health service utilization following primary total knee arthroplasty. J Rheumatol. 2004 Jun;31(6):1166–73. PubMed PMID: 15170931.

108. Bong MR, Di Cesare PE. Stiffness After Total Knee Arthroplasty: Journal of the American Academy of Orthopaedic Surgeons. 2004 May;12(3):164–71. doi:10.5435/00124635-200405000-00004

109. Ali M, Ferguson C, Singh I, Phillips D, Sadhwani S, Kahan M, et al. Arthrofibrosis in Robotic Total Knee Arthroplasty: An Investigation Into How Robotic Assistance May Contribute to a Tight Knee. JAAOS Glob Res Rev. 2023 May;7(5). doi:10.5435/JAAOSGlobal-D-23-00025

110. Kim JH. Effect of Posterior Femoral Condylar Offset and Posterior Tibial Slope on Maximal Flexion Angle of the Knee in Posterior Cruciate Ligament Sacrificing Total Knee Arthroplasty. Knee Surg Relat Res. 2013 Jun 30;25(2):54–9. doi:10.5792/ksrr.2013.25.2.54

111. Malviya A, Lingard EA, Weir DJ, Deehan DJ. Predicting range of movement after knee replacement: the importance of posterior condylar offset and tibial slope. Knee Surg Sports Traumatol Arthrosc. 2009 May;17(5):491–8. doi:10.1007/s00167-008-0712-x

112. Massin P, Gournay A. Optimization of the Posterior Condylar Offset, Tibial Slope, and Condylar Roll-back in Total Knee Arthroplasty. The Journal of Arthroplasty. 2006 Sep;21(6):889–96. doi:10.1016/j.arth.2005.10.019

113. Thompson R, Novikov D, Cizmic Z, Feng JE, Fideler K, Sayeed Z, et al. Arthrofibrosis After Total Knee Arthroplasty. Orthopedic Clinics of North America. 2019 Jul;50(3):269–79. doi:10.1016/j.ocl.2019.02.005

114. Lizaur A, Marco L, Cebrian R. PREOPERATIVE FACTORS INFLUENCING THE RANGE OF MOVEMENT AFTER TOTAL KNEE ARTHROPLASTY FOR SEVERE OSTEOARTHRITIS. The Journal of Bone and Joint Surgery British volume. 1997 Jul;79-B(4):626–9. doi:10.1302/0301-620X.79B4.0790626

115. Witvrouw E, Bellemans J, Victor J. Manipulation under anaesthesia versus low stretch device in poor range of motion after TKA. Knee Surg Sports Traumatol Arthrosc. 2013 Dec;21(12):2751–8. doi:10.1007/s00167-012-2152-x

116. Scheidt M, Ellman MB, Bhatia S. Knee Arthrofibrosis. In: Evidence-Based Management of Complex Knee Injuries [Internet]. Elsevier; 2022 [cited 2025 Mar 11]. p. 385–95. Available from: https://linkinghub.elsevier.com/retrieve/pii/B9780323713108000359 doi:10.1016/B978-0-323-71310-8.00035-9

117. Vun SH, Shields DW, Sen A, Shareef S, Sinha S, Campbell AC. A national questionnaire survey on knee manipulation following total knee arthroplasty. Journal of Orthopaedics. 2015 Dec;12(4):193–6. doi:10.1016/j.jor.2015.05.016

118. Li JW, Ma YS, Xiao LK. Postoperative Pain Management in Total Knee Arthroplasty. Orthop Surg. 2019 Oct;11(5):755–61. doi:10.1111/os.12535 PubMed PMID: 31663286; PubMed Central PMCID: PMC6819170.

119. Kieslich K, Rückert U. Prävention, physiotherapeutische prä- und postoperative Behandlung sowie Rehabilitation der Arthrofibrose. Unfallchirurgie. 2022 Nov;125(11):849–55. doi:10.1007/s00113-022-01247-z

120. Haffar A, Goh GS, Fillingham YA, Torchia MT, Lonner JH. Treatment of arthrofibrosis and stiffness after total knee arthroplasty: an updated review of the literature. International Orthopaedics (SICOT). 2022 Jun;46(6):1253–79. doi:10.1007/s00264-022-05344-x

121. Mauerhan DR, Mokris JG, Ly A, Kiebzak GM. Relationship between length of stay and manipulation rate after total knee arthroplasty. The Journal of Arthroplasty. 1998 Dec;13(8):896–900. doi:10.1016/S0883-5403(98)90196-6

122. Rauzi MR, Foran JRH, Bade MJ. Multimodal conservative management of arthrofibrosis after total knee arthroplasty compared to manipulation under anesthesia: a feasibility study with retrospective cohort comparison. Pilot Feasibility Stud. 2022 Dec;8(1):71. doi:10.1186/s40814-022-01026-y

123. Jerosch J, Aldawoudy AM. Arthroscopic treatment of patients with moderate arthrofibrosis after total knee replacement. Knee Surg Sports Traumatol Arthr. 2007 Jan 17;15(1):71–7. doi:10.1007/s00167-006-0099-5

124. Stephenson JJ, Quimbo RA, Gu T. Knee-attributable medical costs and risk of re-surgery among patients utilizing non-surgical treatment options for knee arthrofibrosis in a managed care population. Current Medical Research and Opinion. 2010 May;26(5):1109–18. doi:10.1185/03007991003676479

125. Millett PJ, Johnson B, Carlson J, Krishnan S, Steadman JR. Rehabilitation of the arthrofibrotic knee. Am J Orthop (Belle Mead NJ). 2003 Nov;32(11):531–8. PubMed PMID: 14653482.

126. Sebastian AS, Sathikumar AS, Thomas AB, Varghese J. Arthroscopic Arthrolysis of Knee: Timing, Technique and Results. JOIO. 2024 Feb;58(2):210–6. doi:10.1007/s43465-023-01081-4

127. Dávila Castrodad IM, Recai TM, Abraham MM, Etcheson JI, Mohamed NS, Edalatpour A, et al. Rehabilitation protocols following total knee arthroplasty: a review of study designs and outcome measures. Ann Transl Med. 2019 Oct;7(Suppl 7):S255. doi:10.21037/atm.2019.08.15 PubMed PMID: 31728379; PubMed Central PMCID: PMC6829007.

128. Mackey AL, Brandstetter S, Schjerling P, Bojsen-Moller J, Qvortrup K, Pedersen MM, et al. Sequenced response of extracellular matrix deadhesion and fibrotic regulators after muscle damage is involved in protection against future injury in human skeletal muscle. FASEB j. 2011 Jun;25(6):1943–59. doi:10.1096/fj.10-176487

129. Kukreja M, Kang J, Curry EJ, Li X. Arthroscopic Lysis of Adhesions and Anterior Interval Release With Manipulation Under Anesthesia for Severe Post-traumatic Knee Stiffness: A Simple and Reproducible Step-by-Step Guide. Arthroscopy Techniques. 2019 May;8(5):e429–35. doi:10.1016/j.eats.2019.01.005

130. McDonald S, Page MJ, Beringer K, Wasiak J, Sprowson A. Preoperative education for hip or knee replacement. Cochrane Musculoskeletal Group, editor. Cochrane Database of Systematic Reviews. 2014 May 13;2015(9). doi:10.1002/14651858.CD003526.pub3

131. Livbjerg AE, Froekjaer S, Simonsen O, Rathleff MS. Pre-Operative Patient Education is Associated With Decreased Risk of Arthrofibrosis After Total Knee Arthroplasty. The Journal of Arthroplasty. 2013 Sep;28(8):1282–5. doi:10.1016/j.arth.2013.01.016

132. Huten D, Chalès G. Conduite à tenir devant une raideur après prothèse totale du genou. Revue du Rhumatisme Monographies. 2016 Jun;83(3):188–93. doi:10.1016/j.monrhu.2016.02.002

133. Topcu H, Alıç T, Yalvaç M, Akdağli Ekici A. The effect of the COVID-19 pandemic on anesthesia techniques in tertiary hospital: general anesthesia or regional anesthesia - a retrospective cohort study. Eur Rev Med Pharmacol Sci. 2023 Mar;27(5):2104–16. doi:10.26355/eurrev_202303_31582 PubMed PMID: 36930510.

134. Zhao C, Liao Q, Yang D, Yang M, Xu P. Advances in perioperative pain management for total knee arthroplasty: a review of multimodal analgesic approaches. J Orthop Surg Res. 2024 Dec 19;19(1):843. doi:10.1186/s13018-024-05324-4

135. Ranawat CS, Ranawat AS, Mehta A. Total knee arthroplasty rehabilitation protocol: Whatmakes the difference? The Journal of Arthroplasty. 2003 Apr;18(3):27–30. doi:10.1054/arth.2003.50080

136. Lavernia C, Cardona D, Rossi MD, Lee D. Multimodal Pain Management and Arthrofibrosis. The Journal of Arthroplasty. 2008 Sep;23(6):74–9. doi:10.1016/j.arth.2008.03.012

137. Premkumar A, Anatone A, Illescas A, Memtsoudis S, Cross MB, Sculco PK, et al. Perioperative Use of Antifibrotic Medications Associated With Lower Rate of Manipulation After Primary TKA: An Analysis of 101,366 Patients. The Journal of Arthroplasty. 2022 Aug;37(8):S1010-S1015.e1. doi:10.1016/j.arth.2022.03.026

138. Hall RP, Verhey JT, Deckey DG, Lebens R, Clarke HD, Spangehl MJ, et al. Which Medications Are Effective in Reducing the Risk of Arthrofibrosis After Total Knee Arthroplasty? The Journal of Arthroplasty. 2025 Jul;S0883540325008800. doi:10.1016/j.arth.2025.07.017

139. Salmons HI, Payne AN, Taunton MJ, Owen AR, Fruth KM, Berry DJ, et al. Nonsteroidal Anti-Inflammatory Drugs and Oral Corticosteroids Mitigated the Risk of Arthrofibrosis After Total Knee Arthroplasty. The Journal of Arthroplasty. 2023 Jun;38(6):S350–4. doi:10.1016/j.arth.2023.03.076

140. Kim DH, Gill TJ, Millett PJ. Arthroscopic treatment of the arthrofibrotic knee. Arthroscopy: The Journal of Arthroscopic & Related Surgery. 2004 Jul;20:187–94. doi:10.1016/j.arthro.2004.04.036

141. Esler CN, Lock K, Harper WM, Gregg PJ. Manipulation of total knee replacements. Is the flexion gained retained? J Bone Joint Surg Br. 1999 Jan;81(1):27–9. doi:10.1302/0301-620x.81b1.8848 PubMed PMID: 10067996.

142. Aspinall SK, Bamber ZA, Hignett SM, Godsiff SP, Wheeler PC, Fong DTP. Medical stretching devices are effective in the treatment of knee arthrofibrosis: A systematic review. Journal of Orthopaedic Translation. 2021 Mar;27:119–31. doi:10.1016/j.jot.2020.11.005

143. Stinton SK, Beckley SJ, Branch TP. Efficacy of non-operative treatment of patients with knee arthrofibrosis using high-intensity home mechanical therapy: a retrospective review of 11,000+ patients. J Orthop Surg Res. 2022 Dec;17(1):337. doi:10.1186/s13018-022-03227-w

144. McElroy MJ, Johnson AJ, Zywiel MG, Mont MA. Devices for the prevention and treatment of knee stiffness after total knee arthroplasty. Expert Review of Medical Devices. 2011 Jan;8(1):57–65. doi:10.1586/erd.10.71

145. Finger E, Willis FB. Dynamic splinting for knee flexion contracture following total knee arthroplasty: a case report. Cases Journal. 2008 Dec;1(1):421. doi:10.1186/1757-1626-1-421

146. McGrath MS, Mont MA, Siddiqui JA, Baker E, Bhave A. Evaluation of a Custom Device for the Treatment of Flexion Contractures after Total Knee Arthroplasty. Clin Orthop Relat Res. 2009 Jun;467(6):1485–92. doi:10.1007/s11999-009-0804-z

147. Seyler TM, Marker DR, Bhave A, Plate JF, Marulanda GA, Bonutti PM, et al. Functional Problems and Arthrofibrosis Following Total Knee Arthroplasty. Journal of Bone and Joint Surgery. 2007 Oct;89(suppl_3):59–69. doi:10.2106/JBJS.G.00457

148. Jansen CM, Windau JE, Bonutti PM, Brillhart MV. Treatment of a Knee Contracture Using a Knee Orthosis Incorporating Stress-Relaxation Techniques. Physical Therapy. 1996 Feb 1;76(2):182–6. doi:10.1093/ptj/76.2.182

149. Stiefel EC, McIntyre L. Arthroscopic Lysis of Adhesions for Treatment of Post-traumatic Arthrofibrosis of the Knee Joint. Arthroscopy Techniques. 2017 Aug;6(4):e939–44. doi:10.1016/j.eats.2017.03.001

150. Wu J, Lv M, Zhou Y. Association of knee range of motion and continuous passive motion following total knee arthroplasty: a meta-analysis. Ann Joint. 2016 May 20;1:5–5. doi:10.21037/aoj.2016.04.02

151. Harvey LA, Brosseau L, Robert D Herbert. Continuous passive motion following total knee arthroplasty in people with arthritis. Cochrane Musculoskeletal Group, editor. Cochrane Database of Systematic Reviews. 2014 Feb 6;2014(3). doi:10.1002/14651858.CD004260.pub3

152. Brosseau L, Milne S, Wells G, Tugwell P, Robinson V, Casimiro L, et al. Efficacy of continuous passive motion following total knee arthroplasty: a metaanalysis. J Rheumatol. 2004 Nov;31(11):2251–64. PubMed PMID: 15517640.

153. Boese CK, Weis M, Phillips T, Lawton-Peters S, Gallo T, Centeno L. The Efficacy of Continuous Passive Motion After Total Knee Arthroplasty: A Comparison of Three

Protocols. The Journal of Arthroplasty. 2014 Jun;29(6):1158–62. doi:10.1016/j.arth.2013.12.005

154. Joshi RN, White PB, Murray-Weir M, Alexiades MM, Sculco TP, Ranawat AS. Prospective Randomized Trial of the Efficacy of Continuous Passive Motion Post Total Knee Arthroplasty: Experience of the Hospital for Special Surgery. The Journal of Arthroplasty. 2015 Dec;30(12):2364–9. doi:10.1016/j.arth.2015.06.006

155. Maniar RN, Baviskar JV, Singhi T, Rathi SS. To Use or Not to Use Continuous Passive Motion Post–Total Knee Arthroplasty. The Journal of Arthroplasty. 2012 Feb;27(2):193-200.e1. doi:10.1016/j.arth.2011.04.009

156. Issa K, Banerjee S, Kester MA, Khanuja HS, Delanois RE, Mont MA. The effect of timing of manipulation under anesthesia to improve range of motion and functional outcomes following total knee arthroplasty. J Bone Joint Surg Am. 2014 Aug 20;96(16):1349–57. doi:10.2106/JBJS.M.00899 PubMed PMID: 25143495.

157. Brigati DP, Huddleston J, Lewallen D, Illgen R, Jaffri H, Ziegenhorn D, et al. Manipulation Under Anesthesia After Total Knee: Who Still Requires a Revision Arthroplasty? The Journal of Arthroplasty. 2020 Jun;35(6):S348–51. doi:10.1016/j.arth.2020.03.009

158. Newman ET, Herschmiller TA, Attarian DE, Vail TP, Bolognesi MP, Wellman SS. Risk Factors, Outcomes, and Timing of Manipulation Under Anesthesia After Total Knee Arthroplasty. The Journal of Arthroplasty. 2018 Jan;33(1):245–9. doi:10.1016/j.arth.2017.08.002

159. Thorsteinsson H, Hedström M, Robertsson O, Lundin N, W-Dahl A. Manipulation under anesthesia after primary knee arthroplasty in Sweden: incidence, patient characteristics and risk of revision. Acta Orthop. 2019 Oct;90(5):484–8. doi:10.1080/17453674.2019.1637177 PubMed PMID: 31269851; PubMed Central PMCID: PMC6746267.

160. Werner BC, Carr JB, Wiggins JC, Gwathmey FW, Browne JA. Manipulation Under Anesthesia After Total Knee Arthroplasty is Associated with An Increased Incidence of Subsequent Revision Surgery. The Journal of Arthroplasty. 2015 Sep;30(9):72–5. doi:10.1016/j.arth.2015.01.061

161. Sala J, Jaroma A, Sund R, Huopio J, Kröger H, Sirola J. Manipulation under anesthesia after total knee arthroplasty: a retrospective study of 145 patients. Acta Orthop. 2022 Jun 21;93:583–7. doi:10.2340/17453674.2022.3167 PubMed PMID: 35727106; PubMed Central PMCID: PMC9214639.

162. Ofa SA, Ross BJ, Flick TR, Patel AH, Sherman WF. Robotic Total Knee Arthroplasty vs Conventional Total Knee Arthroplasty: A Nationwide Database Study. Arthroplasty Today. 2020 Dec;6(4):1001-1008.e3. doi:10.1016/j.artd.2020.09.014

163. Rullán PJ, Zhou G, Emara AK, Klika AK, Koroukian S, Piuzzi NS. Understanding rates, risk factors, and complications associated with manipulation under anesthesia after total knee arthroplasty (TKA): An analysis of 100,613 TKAs. The Knee. 2022 Oct;38:170–7. doi:10.1016/j.knee.2022.08.009

164. Chandi SK, Hawes JD, Kolin DA, Debbi EM, Ast MP, Haas SB, et al. Nearly 14-Fold Increased Risk of Manipulation Under Anesthesia After Total Knee Arthroplasty When Previous Contralateral Total Knee Arthroplasty Required Manipulation Under Anesthesia. The Journal of Arthroplasty. 2024 Sep;39(9):S449–53. doi:10.1016/j.arth.2024.05.073

165. Areti A, Ratcliff T, Perake V, Sambandam SN. Factors predicting manipulation under anaesthesia after total knee replacement. Arch Orthop Trauma Surg. 2025 Jan 23;145(1):138. doi:10.1007/s00402-025-05758-3 PubMed PMID: 39849219.

166. Patel S, Tran S, Overbey J, Ksajikian A, Gupta R, Kenter K, et al. Risk Factors for the Need for Manipulation Under Anesthesia Following total Knee Arthroplasty: A Systematic Review and Meta-Analysis. The Journal of Arthroplasty. 2025 Apr;S0883540325003018. doi:10.1016/j.arth.2025.03.064

167. Crawford DA, Adams JB, Morris MJ, Berend KR, Lombardi AV. Manipulation under Anesthesia after Knee Arthroplasty Is Associated with Worse Long-Term Clinical Outcomes and Survivorship. J Knee Surg. 2021 Jun;34(7):739–44. doi:10.1055/s-0039-1700569 PubMed PMID: 31645072.

168. Desai AS, Karmegam A, Dramis A, Board TN, Raut V. Manipulation for stiffness following total knee arthroplasty: when and how often to do it? Eur J Orthop Surg Traumatol. 2014 Oct;24(7):1291–5. doi:10.1007/s00590-013-1387-7

169. Brassard M, Insall J, Scuderi G, Faris P. Complications of total knee arthroplasty. Surgery of the Knee, ed. 2001;3:1814–6.

170. Walsh JM, Sullivan TC, Varghese B, Incavo SJ, Brown TS, Park KJ. Manipulation Under Anesthesia After Primary Total Knee Arthroplasty. The Journal of Arthroplasty. 2025 May;S0883540325005273. doi:10.1016/j.arth.2025.05.032

171. Scranton PE. Management of knee pain and stiffness after total knee arthroplasty. The Journal of Arthroplasty. 2001 Jun;16(4):428–35. doi:10.1054/arth.2001.22250

172. Yoo JH, Oh JC, Oh HC, Park SH. Manipulation under Anesthesia for Stiffness after Total Knee Arthroplasty. Knee Surg Relat Res. 2015 Dec;27(4):233–9. doi:10.5792/ksrr.2015.27.4.233 PubMed PMID: 26676186; PubMed Central PMCID: PMC4678244.

173. Choi HR, Siliski J, Malchau H, Freiberg A, Rubash H, Kwon YM. How often is functional range of motion obtained by manipulation for stiff total knee

arthroplasty? Int Orthop. 2014 Aug;38(8):1641–5. doi:10.1007/s00264-014-2421-z PubMed PMID: 24993649; PubMed Central PMCID: PMC4115126.

174. Colacchio ND, Abela D, Bono JV, Shah VM, Bono OJ, Scott RD. Efficacy of manipulation under anesthesia beyond three months following total knee arthroplasty. Arthroplast Today. 2019 Dec;5(4):515–20. doi:10.1016/j.artd.2019.08.002 PubMed PMID: 31886400; PubMed Central PMCID: PMC6920722.

175. Gu A, Michalak AJ, Cohen JS, Almeida ND, McLawhorn AS, Sculco PK. Efficacy of Manipulation Under Anesthesia for Stiffness Following Total Knee Arthroplasty: A Systematic Review. The Journal of Arthroplasty. 2018 May;33(5):1598–605. doi:10.1016/j.arth.2017.11.054

176. Abram SGF, Yusuf B, Alvand A, Sabah SA, Beard DJ, Price AJ. Manipulation Under Anesthetic After Primary Knee Arthroplasty Is Associated With a Higher Rate of Subsequent Revision Surgery. The Journal of Arthroplasty. 2020 Sep;35(9):2640-2645.e2. doi:10.1016/j.arth.2020.04.015

177. Fox JL, Poss R. The role of manipulation following total knee replacement. J Bone Joint Surg Am. 1981 Mar;63(3):357–62. PubMed PMID: 7204431.

178. Sharma V, Maheshwari AV, Tsailas PG, Ranawat AS, Ranawat CS. The results of knee manipulation for stiffness after total knee arthroplasty with or without an intra-articular steroid injection. Indian J Orthop. 2008 Jul;42(3):314–8. doi:10.4103/0019-5413.41855 PubMed PMID: 19753158; PubMed Central PMCID: PMC2739471.

179. Yeoh D, Nicolaou N, Goddard R, Willmott H, Miles K, East D, et al. Manipulation under anaesthesia post total knee replacement: Long term follow up. The Knee. 2012 Aug;19(4):329–31. doi:10.1016/j.knee.2011.05.009

180. Lindenfeld TN, Wojtys EM, Husain A. Instructional Course Lectures, The American Academy of Orthopaedic Surgeons - Operative Treatment of Arthrofibrosis of the Knee*†: The Journal of Bone & Joint Surgery. 1999 Dec;81(12):1772–84. doi:10.2106/00004623-199912000-00015

181. Moscony AMB. Common Wrist and Hand Fractures. In: Fundamentals of Hand Therapy [Internet]. Elsevier; 2007 [cited 2025 Jun 19]. p. 251–85. Available from: https://linkinghub.elsevier.com/retrieve/pii/B0323033865500163 doi:10.1016/B0-32-303386-5/50016-3

182. Chitnavis J. Silent burn: the hidden danger and effects of bright light from fibre-optic cables in arthroscopic knee surgery. J Surg Case Rep. 2020 Apr;2020(4):rjaa068. doi:10.1093/jscr/rjaa068 PubMed PMID: 32280444; PubMed Central PMCID: PMC7136709.

183. Leggett AR, Schneider GJ, Kissin YD, Cheng EY, Rossman SR. Arthroscopic Lysis of Adhesions for the Stiff Total Knee Arthroplasty. JBJS Essent Surg Tech. 2023;13(1):e22.00001. doi:10.2106/JBJS.ST.22.00001 PubMed PMID: 38274277; PubMed Central PMCID: PMC10807902.

184. Bodendorfer BM, Kotler JA, Zelenty WD, Termanini K, Sanchez R, Argintar EH. Outcomes and Predictors of Success for Arthroscopic Lysis of Adhesions for the Stiff Total Knee Arthroplasty. Orthopedics. 2017 Nov 1;40(6):e1062–8. doi:10.3928/01477447-20171012-06 PubMed PMID: 29058757.

185. Yayac MF, Albana MF, Braithwaite HC, Post ZD, Ponzio DY, Tjoumakaris FP, et al. A Decade of Experience With Arthroscopic Lysis of Adhesions for Arthrofibrosis After Total Knee Arthroplasty. The Journal of Arthroplasty. 2025 May;S0883540325005121. doi:10.1016/j.arth.2025.05.017

186. Court C, Gauliard C, Nordin JY. [Technical aspects of arthroscopic arthrolysis after total knee replacement]. Rev Chir Orthop Reparatrice Appar Mot. 1999 Jul;85(4):404–10. PubMed PMID: 10457561.

187. Arbuthnot JE, Brink RB. Arthroscopic arthrolysis for the treatment of stiffness after total knee replacement gives moderate improvements in range of motion and functional knee scores. Knee Surg Sports Traumatol Arthrosc. 2010 Mar;18(3):346–51. doi:10.1007/s00167-009-0878-x PubMed PMID: 19649615.

188. Chen MR, Dragoo JL. Arthroscopic Releases for Arthrofibrosis of the Knee: American Academy of Orthopaedic Surgeon. 2011 Nov;19(11):709–16. doi:10.5435/00124635-201111000-00007

189. Allum R. COMPLICATIONS OF ARTHROSCOPY OF THE KNEE. The Journal of Bone and Joint Surgery British volume. 2002 Sep;84-B(7):937–45. doi:10.1302/0301-620X.84B7.0840937

190. Diduch DR, Scuderi GR, Scott WN, Insall JN, Kelly MA. The efficacy of arthroscopy following total knee replacement. Arthroscopy: The Journal of Arthroscopic & Related Surgery. 1997 Apr;13(2):166–71. doi:10.1016/S0749-8063(97)90150-X

191. Keyhani S, Movahedinia M, Sherafat Vaziri A, Soleymanha M, Vosoughi F, Tahami M, et al. Is posterior knee arthroscopy using posterior portals necessary for orthopedic surgeons? The latest evidence on applications and techniques. EFORT Open Rev. 2023 Apr 25;8(4):189–98. doi:10.1530/EOR-22-0133 PubMed PMID: 37097043; PubMed Central PMCID: PMC10155121.

192. Millett PJ, Williams RJ, Wickiewicz TL. Open Debridement and Soft Tissue Release as a Salvage Procedure for the Severely Arthrofibrotic Knee. Am J Sports Med. 1999 Sep;27(5):552–61. doi:10.1177/03635465990270050201

193. Cho BW, Hong HT, Koh YG, Park KK, Kang KT. Comparative Study on Three Different Designs of Locking Mechanisms in Total Knee Arthroplasty. Bioengineering. 2025 Feb 10;12(2):169. doi:10.3390/bioengineering12020169

194. Keeney JA, Clohisy JC, Curry M, Maloney WJ. Revision Total Knee Arthroplasty for Restricted Motion: Clinical Orthopaedics and Related Research. 2005 Nov;440(NA;):135–40. doi:10.1097/01.blo.0000185312.43955.c8

195. Hutchinson JRM, Parish EN, Cross MJ. Results of open arthrolysis for the treatment of stiffness after total knee replacement. The Journal of Bone and Joint Surgery British volume. 2005 Oct;87-B(10):1357–60. doi:10.1302/0301-620X.87B10.16228

196. Pretzsch M, Dippold A. Ergebnisse der operativen Arthrolyse in der Behandlung von Bewegungseinschränkungen des Kniegelenkes. Z Orthop Ihre Grenzgeb. 2008 Mar 18;137(04):334–9. doi:10.1055/s-2008-1039721

197. Babis GC, Trousdale RT, Pagnano MW, Morrey BF. Poor Outcomes of Isolated Tibial Insert Exchange and Arthrolysis for the Management of Stiffness Following Total Knee Arthroplasty: The Journal of Bone and Joint Surgery-American Volume. 2001 Oct;83(10):1534–6. doi:10.2106/00004623-200110000-00012

198. Ghani H, Maffulli N, Khanduja V. Management of stiffness following total knee arthroplasty: A systematic review. The Knee. 2012 Dec;19(6):751–9. doi:10.1016/j.knee.2012.02.010

199. Xing W, Sun L, Sun L, Liu C, Kong Z, Cui J, et al. Comparison of minimally invasive arthrolysis vs. conventional arthrolysis for post-traumatic knee stiffness. Journal of Orthopaedic Science. 2018 Jan;23(1):112–6. doi:10.1016/j.jos.2017.09.021

200. Dalury DF, Pomeroy DL, Gorab RS, Adams MJ. Why are Total Knee Arthroplasties Being Revised? The Journal of Arthroplasty. 2013 Sep;28(8):120–1. doi:10.1016/j.arth.2013.04.051

201. Schroer WC, Berend KR, Lombardi AV, Barnes CL, Bolognesi MP, Berend ME, et al. Why Are Total Knees Failing Today? Etiology of Total Knee Revision in 2010 and 2011. The Journal of Arthroplasty. 2013 Sep;28(8):116–9. doi:10.1016/j.arth.2013.04.056

202. Le DH, Goodman SB, Maloney WJ, Huddleston JI. Current Modes of Failure in TKA: Infection, Instability, and Stiffness Predominate. Clinical Orthopaedics & Related Research. 2014 Jul;472(7):2197–200. doi:10.1007/s11999-014-3540-y

203. Kirwan MJ, Diltz ZR, Dixon DT, Rivera-Peraza CA, Gammage CJ, Mihalko WM, et al. The AAHKS Clinical Research Award: Extended Postoperative Oral Tranexamic Acid in Total Knee Arthroplasty: A Randomized Controlled Pilot Study. J

Arthroplasty. 2024 Sep;39(9S2):S13–7. doi:10.1016/j.arth.2024.02.073 PubMed PMID: 38430972.

204. Rutherford RW, Jennings JM, Levy DL, Parisi TJ, Martin JR, Dennis DA. Revision Total Knee Arthroplasty for Arthrofibrosis. The Journal of Arthroplasty. 2018 Jul;33(7):S177–81. doi:10.1016/j.arth.2018.03.037

205. Donaldson JR, Tudor F, Gollish J. Revision surgery for the stiff total knee arthroplasty. The Bone & Joint Journal. 2016 May;98-B(5):622–7. doi:10.1302/0301-620X.98B5.35969

206. Kim GK, Mortazavi SMJ, Parvizi J, Purtill JJ. Revision for stiffness following TKA: A predictable procedure? The Knee. 2012 Aug;19(4):332–4. doi:10.1016/j.knee.2011.06.016

207. Ackerman IN, Bohensky MA, Zomer E, Tacey M, Gorelik A, Brand CA, et al. The projected burden of primary total knee and hip replacement for osteoarthritis in Australia to the year 2030. BMC Musculoskelet Disord. 2019 Dec;20(1):90. doi:10.1186/s12891-019-2411-9

208. Vincent KR, Vincent HK, Lee LW, Alfano AP. Inpatient Rehabilitation Outcomes in Primary and Revision Total Knee Arthroplasty Patients: Clinical Orthopaedics and Related Research. 2006 May;446:201–7. doi:10.1097/01.blo.0000214435.72398.0e

209. Kremers HM, Visscher SL, Moriarty JP, Reinalda MS, Kremers WK, Naessens JM, et al. Determinants of Direct Medical Costs in Primary and Revision Total Knee Arthroplasty. Clinical Orthopaedics & Related Research. 2013 Jan;471(1):206–14. doi:10.1007/s11999-012-2508-z

210. Greidanus NV, Peterson RC, Masri BA, Garbuz DS. Quality of Life Outcomes in Revision Versus Primary Total Knee Arthroplasty. The Journal of Arthroplasty. 2011 Jun;26(4):615–20. doi:10.1016/j.arth.2010.04.026

211. Haidukewych GJ, Jacofsky DJ, Pagnano MW, Trousdale RT. Functional Results After Revision of Well-Fixed Components for Stiffness After Primary Total Knee Arthroplasty. The Journal of Arthroplasty. 2005 Feb;20(2):133–8. doi:10.1016/j.arth.2004.09.057

212. Nelson CL, Kim J, Lotke PA. Stiffness After Total Knee Arthroplasty. Journal of Bone and Joint Surgery. 2005 Sep;87(1):264–70. doi:10.2106/JBJS.E-00345

213. Van Kempen RWTM, Schimmel JJP, Van Hellemondt GG, Vandenneucker H, Wymenga AB. Reason for Revision TKA Predicts Clinical Outcome: Prospective Evaluation of 150 Consecutive Patients With 2-years Followup. Clinical Orthopaedics & Related Research. 2013 Jul;471(7):2296–302. doi:10.1007/s11999-013-2940-8

214. Van Rensch PJH, Hannink G, Heesterbeek PJC, Wymenga AB, Van Hellemondt GG. Long-Term Outcome Following Revision Total Knee Arthroplasty is Associated With Indication for Revision. The Journal of Arthroplasty. 2020 Jun;35(6):1671–7. doi:10.1016/j.arth.2020.01.053

215. Liow MHL, Flevas DA, Braun S, Nocon A, Lee GC, Sculco PK, et al. Rotating Hinge Revision Total Knee Arthroplasty Provides Greater Arc of Motion Gains for Patients Who Have Severe Arthrofibrosis. The Journal of Arthroplasty. 2025 Jan;40(1):198–202. doi:10.1016/j.arth.2024.06.056

216. Schneider AM, Rice SJ, Lancaster N, McGraw M, Farid Y, Finn HA. Low-Dose Irradiation and Rotating-Hinge Revision for the Treatment of Severe Idiopathic Arthrofibrosis Following Total Knee Arthroplasty: A Review of 60 Patients With a Mean 6-Year Follow-Up. The Journal of Arthroplasty. 2024 Apr;39(4):1075–82. doi:10.1016/j.arth.2023.10.021

217. Kim GK, Mortazavi SMJ, Purtill JJ, Sharkey PF, Hozack WJ, Parvizi J. Stiffness After Revision Total Knee Arthroplasty. The Journal of Arthroplasty. 2010 Sep;25(6):844–50. doi:10.1016/j.arth.2010.04.001

218. Ries MD, Badalamente M. Arthrofibrosis After Total Knee Arthroplasty: Clinical Orthopaedics and Related Research. 2000 Nov;380:177–83. doi:10.1097/00003086-200011000-00024

219. Bingham JS, Bukowski BR, Wyles CC, Pareek A, Berry DJ, Abdel MP. Rotating-Hinge Revision Total Knee Arthroplasty for Treatment of Severe Arthrofibrosis. J Arthroplasty. 2019 Jul;34(7S):S271–6. doi:10.1016/j.arth.2019.01.072 PubMed PMID: 30819621.

220. Hartman CW, Ting NT, Moric M, Berger RA, Rosenberg AG, Della Valle CJ. Revision Total Knee Arthroplasty for Stiffness. The Journal of Arthroplasty. 2010 Sep;25(6):62–6. doi:10.1016/j.arth.2010.04.013

221. Parvizi J, Bloomfield MR. Multimodal pain management in orthopedics: implications for joint arthroplasty surgery. Orthopedics. 2013 Feb;36(2 Suppl):7–14. doi:10.3928/01477447-20130122-51 PubMed PMID: 23379570.

222. Hoveidaei AH, Smitterberg CW, Misch M, Katanbaf R, Nace J, Delanois RE, et al. Management of Arthrofibrosis After Total Knee Arthroplasty: Insights and Future Directions. J Knee Surg. 2025 Nov 12;a-2741-1796. doi:10.1055/a-2741-1796

223. Letchuman S, Madhuranga HDT, Madhurangi BLNK, Premarathna AD, Saravanan M. Alkaloids unveiled: A comprehensive analysis of novel therapeutic properties, mechanisms, and plant-based innovations. Intelligent Pharmacy. 2025 Aug;3(4):268–76. doi:10.1016/j.ipha.2024.09.007

224. Lin GD, Vishwakarma P, Smith PN, Li RW. The Occurrence and Bioactivities of Amaryllidaceae Alkaloids from Plants: A Taxonomy-Guided Genera-Wide Review. Plants. 2025 Jun 24;14(13):1935. doi:10.3390/plants14131935

225. Kilgore MB, Kutchan TM. The Amaryllidaceae alkaloids: biosynthesis and methods for enzyme discovery. Phytochem Rev. 2016 Jun;15(3):317–37. doi:10.1007/s11101-015-9451-z PubMed PMID: 27340382; PubMed Central PMCID: PMC4914137.

226. Takos A, Rook F. Towards a Molecular Understanding of the Biosynthesis of Amaryllidaceae Alkaloids in Support of Their Expanding Medical Use. IJMS. 2013 May 31;14(6):11713–41. doi:10.3390/ijms140611713

227. Li RW, Lin GD, Leach DN, Waterman PG, Myers SP. Inhibition of COXs and 5-LOX and activation of PPARs by Australian Clematis species (Ranunculaceae). Journal of Ethnopharmacology. 2006 Mar;104(1–2):138–43. doi:10.1016/j.jep.2005.08.061

228. Merindol N, Belem Martins LL, Elfayres G, Custeau A, Berthoux L, Evidente A, et al. Amaryllidaceae Alkaloids Screen Unveils Potent Anticoronaviral Compounds and Associated Structural Determinants. ACS Pharmacol Transl Sci. 2024 Nov 8;7(11):3527–39. doi:10.1021/acsptsci.4c00424

229. Girard MP, Karimzadegan V, Héneault M, Cloutier F, Bérubé G, Berthoux L, et al. Chemical Synthesis and Biological Activities of Amaryllidaceae Alkaloid Norbelladine Derivatives and Precursors. Molecules. 2022 Aug 31;27(17):5621. doi:10.3390/molecules27175621 PubMed PMID: 36080382; PubMed Central PMCID: PMC9457815.

230. Tallini LR, Machado Das Neves G, Vendruscolo MH, Rezende-Teixeira P, Borges W, Bastida J, et al. Antitumoral activity of different Amaryllidaceae alkaloids: In vitro and in silico assays. Journal of Ethnopharmacology. 2024 Jul;329:118154. doi:10.1016/j.jep.2024.118154

231. Nair JJ, Van Staden J. Insight to the antifungal properties of Amaryllidaceae constituents. Phytomedicine. 2020 Jul;73:152753. doi:10.1016/j.phymed.2018.11.013

232. Şener B, Orhan I, Satayavivad J. Antimalarial activity screening of some alkaloids and the plant extracts from Amaryllidaceae. Phytotherapy Research. 2003 Dec;17(10):1220–3. doi:10.1002/ptr.1346

233. Boucher R, Germain H, Desgagné-Penix I. Exploring the Lesser-Known Bioactive Natural Products of Plant Species of the Genus Cannabis L.: Alkaloids, Phenolic Compounds, and Their Therapeutic Potential. Plants. 2025 Apr 30;14(9):1372. doi:10.3390/plants14091372

234. Lin GD, Li RW, Myers SP, Leach DN. A Method of Selecting Plants with Anti-inflammatory Potential for Pharmacological Study. Natural Product Communications. 2008 Jan;3(1):1934578X0800300115. doi:10.1177/1934578X0800300115

235. Li RW, Leach DN, Myers SP, Leach GJ, Lin GD, Brushett DJ, et al. Anti-inflammatory activity, cytotoxicity and active compounds of *Tinospora smilacina* Benth. Phytotherapy Research. 2004 Jan;18(1):78–83. doi:10.1002/ptr.1373

236. Xiaoqiang Y, Tao W, Zhiming M. Medicinal uses of pseudolycorine [Internet]. CN100441186C, 2008. Available from: https://patents.google.com/patent/CN100441186C/en

237. Nair JJ, Van Staden J. Anti-inflammatory Principles of the Plant Family Amaryllidaceae. Planta Med. 2024 Oct;90(12):900–37. doi:10.1055/a-2369-8104

238. Castañeda C, Bravo K, Cortés N, Bedoya J, De Borges WS, Bastida J, et al. Amaryllidaceae alkaloids in skin cancer management: Photoprotective effect on human keratinocytes and anti-proliferative activity in melanoma cells. J Appl Biomed. 2023 Apr 1;21(1):36–47. doi:10.32725/jab.2023.004

239. Chen JX, Zheng J, Cai YM, Xu JX, Sun Y, Yang Z, et al. Medicinal compounds and biotechnology of Amaryllidaceae alkaloids in Lycoris radiata. Front Plant Sci. 2025;16:1639654. doi:10.3389/fpls.2025.1639654 PubMed PMID: 41473140; PubMed Central PMCID: PMC12745432.

240. Formby PM, Donohue MA, Cannova CJ, Caulfield JP. Hydraulic distension of the knee: a novel treatment for arthrofibrosis after total knee replacement (case series). ANZ Journal of Surgery. 2016 Jun;86(6):480–2. doi:10.1111/ans.13540

241. Werner BC, Cancienne JM, Miller MD, Gwathmey FW. Incidence of Manipulation Under Anesthesia or Lysis of Adhesions After Arthroscopic Knee Surgery. Am J Sports Med. 2015 Jul;43(7):1656–61. doi:10.1177/0363546515578660

242. Scholtes SA, Khoo-Summers L, Damico KJ. Presentation and management of arthrofibrosis of the knee: A case report. Physiotherapy Theory and Practice. 2017 Oct 3;33(10):815–24. doi:10.1080/09593985.2017.1346027

243. Schairer WW, Vail TP, Bozic KJ. What Are the Rates and Causes of Hospital Readmission After Total Knee Arthroplasty? Clinical Orthopaedics & Related Research. 2014 Jan;472(1):181–7. doi:10.1007/s11999-013-3030-7

244. Alexiadis A, Reynolds P, Al-Mouazzen L, Toms A, Phillips J, Waterson B. Revision total knee replacement finances: a detailed cost-analysis of operative practice at a regional tertiary referral centre. BMC Health Serv Res. 2024 Jan 4;24(1):19. doi:10.1186/s12913-023-10316-x

245. Royal Australasian College of Surgeons. Activities Report 2023. Melbourne, Australia; 2024.

246. American Academy of Orthopaedic Surgeons. Redefining Retirement: Opportunities Abound for Orthopaedic Surgeons. Illinois, United States; 2024.

247. Weiskirchen S, Schröder SK, Buhl EM, Weiskirchen R. A Beginner's Guide to Cell Culture: Practical Advice for Preventing Needless Problems. Cells. 2023 Feb 21;12(5):682. doi:10.3390/cells12050682 PubMed PMID: 36899818; PubMed Central PMCID: PMC10000895.

248. Chen CZC, Peng YX, Wang ZB, Fish PV, Kaar JL, Koepsel RR, et al. The Scar-in-a-Jar: studying potential antifibrotic compounds from the epigenetic to extracellular level in a single well. Br J Pharmacol. 2009 Nov;158(5):1196–209. doi:10.1111/j.1476-5381.2009.00387.x PubMed PMID: 19785660; PubMed Central PMCID: PMC2782330.

249. Chen C, Loe F, Blocki A, Peng Y, Raghunath M. Applying macromolecular crowding to enhance extracellular matrix deposition and its remodeling in vitro for tissue engineering and cell-based therapies. Advanced Drug Delivery Reviews. 2011 Apr;63(4–5):277–90. doi:10.1016/j.addr.2011.03.003

250. Puerta Cavanzo N, Bigaeva E, Boersema M, Olinga P, Bank RA. Macromolecular Crowding as a Tool to Screen Anti-fibrotic Drugs: The Scar-in-a-Jar System Revisited. Front Med. 2021 Jan 14;7. doi:10.3389/fmed.2020.615774

251. Rønnow SR, Dabbagh RQ, Genovese F, Nanthakumar CB, Barrett VJ, Good RB, et al. Prolonged Scar-in-a-Jar: an in vitro screening tool for anti-fibrotic therapies using biomarkers of extracellular matrix synthesis. Respir Res. 2020 Dec;21(1). doi:10.1186/s12931-020-01369-1

252. Edmondson R, Broglie JJ, Adcock AF, Yang L. Three-dimensional cell culture systems and their applications in drug discovery and cell-based biosensors. Assay Drug Dev Technol. 2014 May;12(4):207–18. doi:10.1089/adt.2014.573 PubMed PMID: 24831787; PubMed Central PMCID: PMC4026212.

253. Lareu RR, Zeugolis DI, Abu-Rub M, Pandit A, Raghunath M. Essential modification of the Sircol Collagen Assay for the accurate quantification of collagen content in complex protein solutions. Acta Biomater. 2010 Aug;6(8):3146–51. doi:10.1016/j.actbio.2010.02.004 PubMed PMID: 20144751.

254. Neuman RE, Logan MA. The determination of hydroxyproline. J Biol Chem. 1950 May;184(1):299–306. PubMed PMID: 15421999.

255. Yao Y, Findlay A, Stolp J, Rayner B, Ask K, Jarolimek W. Pan-Lysyl Oxidase Inhibitor PXS-5505 Ameliorates Multiple-Organ Fibrosis by Inhibiting Collagen Crosslinks in Rodent Models of Systemic Sclerosis. Int J Mol Sci. 2022 May 16;23(10):5533.

doi:10.3390/ijms23105533 PubMed PMID: 35628342; PubMed Central PMCID: PMC9146019.

256. Hafner M, Niepel M, Subramanian K, Sorger PK. Designing Drug-Response Experiments and Quantifying their Results. Curr Protoc Chem Biol. 2017 Jun 19;9(2):96–116. doi:10.1002/cpch.19 PubMed PMID: 28628201; PubMed Central PMCID: PMC5729909.

257. Xie F, Xiao P, Chen D, Xu L, Zhang B. miRDeepFinder: a miRNA analysis tool for deep sequencing of plant small RNAs. Plant Mol Biol. 2012 Jan 31. doi:10.1007/s11103-012-9885-2 PubMed PMID: 22290409.

258. Livak KJ, Schmittgen TD. Analysis of relative gene expression data using real-time quantitative PCR and the 2(-Delta Delta C(T)) Method. Methods. 2001 Dec;25(4):402–8. doi:10.1006/meth.2001.1262 PubMed PMID: 11846609.

259. Zhu Z, Gao S, Zhu H, Chen Y, Wu D, Chen Z, et al. Metformin improves fibroblast metabolism and ameliorates arthrofibrosis in rats. J Orthop Translat. 2023 May;40:92–103. doi:10.1016/j.jot.2023.05.011 PubMed PMID: 37457314; PubMed Central PMCID: PMC10338908.

260. Pilchová V, Richter A, Meurer M, Schulz C, Von Köckritz-Blickwede M. The effect of chemical fixation with paraformaldehyde, glutardialdehyde or methanol on immunofluorescence staining of neutrophils and neutrophil extracellular traps. Innate Immun. 2025 Jan;31:17534259241307563. doi:10.1177/17534259241307563

261. Pipiya VV, Gilazieva ZE, Issa SS, Rizvanov AA, Solovyeva VV. Comparison of primary and passaged tumor cell cultures and their application in personalized medicine. Explor Target Antitumor Ther. 2024;5(3):581–99. doi:10.37349/etat.2024.00237 PubMed PMID: 38966179; PubMed Central PMCID: PMC11220317.

262. Kaur G, Dufour JM. Cell lines: Valuable tools or useless artifacts. Spermatogenesis. 2012 Jan 1;2(1):1–5. doi:10.4161/spmg.19885 PubMed PMID: 22553484; PubMed Central PMCID: PMC3341241.

263. Niepel M, Hafner M, Chung M, Sorger PK. Measuring Cancer Drug Sensitivity and Resistance in Cultured Cells. CP Chemical Biology. 2017 Jan;9(2):55–74. doi:10.1002/cpch.21

264. Asiri A, Tasleem M, Al Said M, Asiri A, Al Qarni AA, Bakillah A. Optimizing Cell Density and Unveiling Cytotoxic Profiles of DMSO and Ethanol in Six Cancer Cell Lines: Experimental and In Silico Insights. Methods Protoc. 2025 Aug 10;8(4):93. doi:10.3390/mps8040093 PubMed PMID: 40863743; PubMed Central PMCID: PMC12388702.

265. Lundholt BK, Scudder KM, Pagliaro L. Technical Notes: A Simple Technique for Reducing Edge Effect in Cell-Based Assays. SLAS Discovery. 2003 Oct;8(5):566–70. doi:10.1177/1087057103256465

266. Jager LD, Canda CMA, Hall CA, Heilingoetter CL, Huynh J, Kwok SS, et al. Effect of enzymatic and mechanical methods of dissociation on neural progenitor cells derived from induced pluripotent stem cells. Advances in Medical Sciences. 2016 Mar;61(1):78–84. doi:10.1016/j.advms.2015.09.005

267. Distelhorst CW, Cramer K, Rogers JC. Selective release of excreted DNA sequences from phytohemagglutinin-stimulated human peripheral blood lymphocytes. Effects of trypsin and divalent cations. J Clin Invest. 1978 May;61(5):1204–17. doi:10.1172/JCI109036 PubMed PMID: 207731; PubMed Central PMCID: PMC372641.

268. Cotaus. How to Plate Beautiful Cell Culture Plates? 2025 Aug.

269. Applied Biophysics Inc. 2018 ECIS User Handbook. Vol. 18. 1–17 p.

270. Subbiahanadar Chelladurai K, Selvan Christyraj JD, Rajagopalan K, Yesudhason BV, Venkatachalam S, Mohan M, et al. Alternative to FBS in animal cell culture - An overview and future perspective. Heliyon. 2021 Aug;7(8):e07686. doi:10.1016/j.heliyon.2021.e07686

271. Takahashi S, Leiss M, Moser M, Ohashi T, Kitao T, Heckmann D, et al. The RGD motif in fibronectin is essential for development but dispensable for fibril assembly. J Cell Biol. 2007 Jul 2;178(1):167–78. doi:10.1083/jcb.200703021 PubMed PMID: 17591922; PubMed Central PMCID: PMC2064432.

272. D'Urso M, Jorba I, van der Pol A, Bouten CVC, Kurniawan NA. Spatial regulation of substrate adhesion directs fibroblast morphotype and phenotype. PNAS Nexus. 2024 Aug;3(8):pgae289. doi:10.1093/pnasnexus/pgae289 PubMed PMID: 39131910; PubMed Central PMCID: PMC11316223.

273. Rogala A, Zaytseva-Zotova D, Oreja E, Barrantes A, Tiainen H. Combining QCM-D with live-cell imaging reveals the impact of serum proteins on the dynamics of fibroblast adhesion on tannic acid-functionalised surfaces. Biomater Sci. 2024;12(13):3345–59. doi:10.1039/D4BM00184B

274. Langhe RP, Gudzenko T, Bachmann M, Becker SF, Gonnermann C, Winter C, et al. Cadherin-11 localizes to focal adhesions and promotes cell–substrate adhesion. Nat Commun. 2016 Mar 8;7(1):10909. doi:10.1038/ncomms10909

275. Grinnell F, Feld MK. Initial adhesion of human fibroblasts in serum-free medium: Possible role of secreted fibronectin. Cell. 1979 May;17(1):117–29. doi:10.1016/0092-8674(79)90300-3

276. Weber T, Malakpour-Permlid A, Chary A, D'Alessandro V, Haut L, Seufert S, et al. Fetal bovine serum: how to leave it behind in the pursuit of more reliable science. Front Toxicol. 2025;7:1612903. doi:10.3389/ftox.2025.1612903 PubMed PMID: 40861932; PubMed Central PMCID: PMC12371577.

277. Urzì O, Olofsson Bagge R, Crescitelli R. The dark side of foetal bovine serum in extracellular vesicle studies. J of Extracellular Vesicle. 2022 Oct;11(10):e12271. doi:10.1002/jev2.12271

278. Li Q, Maddox C, Rasmussen L, Hobrath JV, White LE. Assay development and high-throughput antiviral drug screening against Bluetongue virus. Antiviral Res. 2009 Sep;83(3):267–73. doi:10.1016/j.antiviral.2009.06.004 PubMed PMID: 19559054; PubMed Central PMCID: PMC2727572.

279. Chen M, Huang J, Yang X, Liu B, Zhang W, Huang L, et al. Serum starvation induced cell cycle synchronization facilitates human somatic cells reprogramming. PLoS One. 2012;7(4):e28203. doi:10.1371/journal.pone.0028203 PubMed PMID: 22529890; PubMed Central PMCID: PMC3329488.

280. Phukan MM, Sangma SR, Kalita D, Bora P, Das PP, Manoj K, et al. Alkaloids and terpenoids: Synthesis, classification, isolation and purification, reactions, and applications. In: Handbook of Biomolecules [Internet]. Elsevier; 2023 [cited 2026 Apr 29]. p. 177–213. Available from: https://linkinghub.elsevier.com/retrieve/pii/B9780323916844000177 doi:10.1016/B978-0-323-91684-4.00017-7

281. Aniszewski T. Biology of alkaloids. In: Alkaloids [Internet]. Elsevier; 2015 [cited 2026 Apr 29]. p. 195–258. Available from: https://linkinghub.elsevier.com/retrieve/pii/B9780444594334000031 doi:10.1016/B978-0-444-59433-4.00003-1

282. The Amaryllidaceae Alkaloids. In: The Alkaloids: Chemistry and Biology [Internet]. Elsevier; 1998 [cited 2026 Apr 29]. p. 323–424. Available from: https://linkinghub.elsevier.com/retrieve/pii/S0099959808600085 doi:10.1016/S0099-9598(08)60008-5

283. Gifford V, Itoh Y. MT1-MMP-dependent cell migration: proteolytic and non-proteolytic mechanisms. Biochemical Society Transactions. 2019 Jun 28;47(3):811–26. doi:10.1042/BST20180363

284. Mu D, Cambier S, Fjellbirkeland L, Baron JL, Munger JS, Kawakatsu H, et al. The integrin αvβ8 mediates epithelial homeostasis through MT1-MMP–dependent activation of TGF-β1. The Journal of Cell Biology. 2002 Apr 29;157(3):493–507. doi:10.1083/jcb.200109100

285. Masitas C, Peng Z, Wang M, Konai MM, Avila-Cobian LF, Lemieux L, et al. Matrix Metalloproteinase-14 as an Instigator of Fibrosis in Human Pterygium and Its

Pharmacological Intervention. ACS Pharmacol Transl Sci. 2022 Aug 12;5(8):555–61. doi:10.1021/acsptsci.2c00125 PubMed PMID: 35983271; PubMed Central PMCID: PMC9380204.

286. Gresele P, Falcinelli E, Sebastiano M, Momi S. Matrix Metalloproteinases and Platelet Function. In: Progress in Molecular Biology and Translational Science [Internet]. Elsevier; 2017 [cited 2026 Apr 29]. p. 133–65. Available from: https://linkinghub.elsevier.com/retrieve/pii/S1877117317300133 doi:10.1016/bs.pmbts.2017.01.002

287. Sakamuri SSVP, Watts R, Takawale A, Wang X, Hernandez-Anzaldo S, Bahitham W, et al. Absence of Tissue Inhibitor of Metalloproteinase-4 (TIMP4) ameliorates high fat diet-induced obesity in mice due to defective lipid absorption. Sci Rep. 2017 Jul 24;7(1):6210. doi:10.1038/s41598-017-05951-4

288. Schuliga M, Jaffar J, Harris T, Knight DA, Westall G, Stewart AG. The fibrogenic actions of lung fibroblast-derived urokinase: a potential drug target in IPF. Sci Rep. 2017 Jan 31;7:41770. doi:10.1038/srep41770 PubMed PMID: 28139758; PubMed Central PMCID: PMC5282574.

289. Sarno F, Goubert D, Logie E, Rutten MGS, Koncz M, Deben C, et al. Functional Validation of the Putative Oncogenic Activity of PLAU. Biomedicines. 2022 Dec 30;11(1):102. doi:10.3390/biomedicines11010102 PubMed PMID: 36672610; PubMed Central PMCID: PMC9856075.

290. Smeda M, Maleki EH, Jasztal A. A possible role of plasmin-dependent activation of TGF-β in cancer-associated thrombosis: Implications for therapy. Cancer Metastasis Rev. 2024 Nov 22;44(1):2. doi:10.1007/s10555-024-10222-6 PubMed PMID: 39576347; PubMed Central PMCID: PMC11584501.

291. Gupta KK, Donahue DL, Sandoval-Cooper MJ, Castellino FJ, Ploplis VA. Plasminogen Activator Inhibitor-1 Protects Mice Against Cardiac Fibrosis by Inhibiting Urokinase-type Plasminogen Activator-mediated Plasminogen Activation. Sci Rep. 2017 Mar 23;7(1):365. doi:10.1038/s41598-017-00418-y PubMed PMID: 28336948; PubMed Central PMCID: PMC5428408.

292. Puxeddu I, Bader R, Piliponsky AM, Reich R, Levi-Schaffer F, Berkman N. The CC chemokine eotaxin/CCL11 has a selective profibrogenic effect on human lung fibroblasts. J Allergy Clin Immunol. 2006 Jan;117(1):103–10. doi:10.1016/j.jaci.2005.08.057 PubMed PMID: 16387592.

293. Garcia-Zepeda EA, Rothenberg ME, Ownbey RT, Celestin J, Leder P, Luster AD. Human eotaxin is a specific chemoattractant for eosinophil cells and provides a new mechanism to explain tissue eosinophilia. Nat Med. 1996 Apr;2(4):449–56. doi:10.1038/nm0496-449

294. Wenzel SE, Trudeau JB, Barnes S, Zhou X, Cundall M, Westcott JY, et al. TGF-β and IL-13 Synergistically Increase Eotaxin-1 Production in Human Airway Fibroblasts. The Journal of Immunology. 2002 Oct 15;169(8):4613–9. doi:10.4049/jimmunol.169.8.4613

295. Wang J, Man K, Ng KTP. Emerging Roles of C-C Motif Ligand 11 (CCL11) in Cancers and Liver Diseases: Mechanisms and Therapeutic Implications. IJMS. 2025 May 13;26(10):4662. doi:10.3390/ijms26104662

296. Zweifel M, Matozan K, Dahinden C, Schaffner T, Mohacsi P. Eotaxin/CCL11 Levels Correlate With Myocardial Fibrosis and Mast Cell Density in Native and Transplanted Rat Hearts. Transplantation Proceedings. 2010 Sep;42(7):2763–6. doi:10.1016/j.transproceed.2010.05.152

297. Huaux F, Gharaee-Kermani M, Liu T, Morel V, McGarry B, Ullenbruch M, et al. Role of Eotaxin-1 (CCL11) and CC chemokine receptor 3 (CCR3) in bleomycin-induced lung injury and fibrosis. Am J Pathol. 2005 Dec;167(6):1485–96. doi:10.1016/S0002-9440(10)61235-7 PubMed PMID: 16314464; PubMed Central PMCID: PMC1613185.

298. Carulli MT, Ong VH, Ponticos M, Shiwen X, Abraham DJ, Black CM, et al. Chemokine receptor CCR2 expression by systemic sclerosis fibroblasts: Evidence for autocrine regulation of myofibroblast differentiation. Arthritis & Rheumatism. 2005 Dec;52(12):3772–82. doi:10.1002/art.21396

299. Xu J, Lin SC, Chen J, Miao Y, Taffet GE, Entman ML, et al. CCR2 mediates the uptake of bone marrow-derived fibroblast precursors in angiotensin II-induced cardiac fibrosis. Am J Physiol Heart Circ Physiol. 2011 Aug;301(2):H538-547. doi:10.1152/ajpheart.01114.2010 PubMed PMID: 21572015; PubMed Central PMCID: PMC3154672.

300. Wang L, Feng J, Deng Y, Yang Q, Wei Q, Ye D, et al. CCAAT/Enhancer-Binding Proteins in Fibrosis: Complex Roles Beyond Conventional Understanding. Research. 2022 Jan;2022:2022/9891689. doi:10.34133/2022/9891689

301. Li X, Sun M, Men S, Shi Y, Ma L, An Y, et al. The Inflammatory Transcription Factor C/EBPβ Plays a Critical Role in Cardiac Fibroblast Differentiation and a Rat Model of Cardiac Fibrosis Induced by Autoimmune Myocarditis. Int Heart J. 2018 Nov 30;59(6):1389–97. doi:10.1536/ihj.17-446

302. Hu B, Wu Z, Nakashima T, Phan SH. Mesenchymal-specific deletion of C/EBPβ suppresses pulmonary fibrosis. Am J Pathol. 2012 Jun;180(6):2257–67. doi:10.1016/j.ajpath.2012.02.010 PubMed PMID: 22503555; PubMed Central PMCID: PMC3378850.

303. Ramji DP, Foka P. CCAAT/enhancer-binding proteins: structure, function and regulation. Biochem J. 2002 Aug 1;365(Pt 3):561–75. doi:10.1042/BJ20020508 PubMed PMID: 12006103; PubMed Central PMCID: PMC1222736.

304. Hu B, Wu Z, Jin H, Hashimoto N, Liu T, Phan SH. CCAAT/Enhancer-Binding Protein β Isoforms and the Regulation of α-Smooth Muscle Actin Gene Expression by IL-1β. The Journal of Immunology. 2004 Oct 1;173(7):4661–8. doi:10.4049/jimmunol.173.7.4661

305. Sterken BA, Ackermann T, Müller C, Zuidhof HR, Kortman G, Hernandez-Segura A, et al. C/EBPβ isoform-specific regulation of migration and invasion in triple-negative breast cancer cells. NPJ Breast Cancer. 2022 Jan 18;8(1):11. doi:10.1038/s41523-021-00372-z PubMed PMID: 35042889; PubMed Central PMCID: PMC8766495.

306. Buck M, Chojkier M. C/EBPβ Associates With Caspase 8 Complex Proteins and Modulates Apoptosis in Hepatic Stellate Cells. Journal of Clinical Gastroenterology. 2007 Nov;41(Supplement 3):S295–9. doi:10.1097/MCG.0b013e31814927d5

307. Tie Y, Zhai C, Zhang Y, Qin X, Yu F, Li H, et al. CCAAT /enhancer-binding protein β overexpression alleviates myocardial remodelling by regulating angiotensin-converting enzyme-2 expression in diabetes. J Cellular Molecular Medi. 2018 Mar;22(3):1475–88. doi:10.1111/jcmm.13406

308. Tie Y, Lin Z, Zhang M, Ren B, Han D, Li K, et al. Targeting C/EBPβ to Suppress Myocardial Fibrosis in Hypertensive Heart Disease: Role of the ACE2/Ang-(1-7) Pathway. J Cell Mol Med. 2026 Apr;30(7):e71139. doi:10.1111/jcmm.71139 PubMed PMID: 41958066; PubMed Central PMCID: PMC13066493.

309. Vachhani P, Tan P, Watson AM, Wu SJ, Baker R, Cheung S, et al. A phase I / IIa trial of PXS-5505, a novel pan-lysyl oxidase inhibitor, in advanced myelofibrosis. Haematologica. 2025 Apr 17. doi:10.3324/haematol.2024.287231 PubMed PMID: 40241543.

310. Chaudhari N, Findlay AD, Stevenson AW, Clemons TD, Yao Y, Joshi A, et al. Topical application of an irreversible small molecule inhibitor of lysyl oxidases ameliorates skin scarring and fibrosis. Nat Commun. 2022 Sep 22;13(1):5555. doi:10.1038/s41467-022-33148-5

311. Pinnell SR. Molecular Defects in the Ehlers-Danlos Syndrome. J Invest Dermatol. 1982 Jul;79(s1):90s–2s. doi:10.1111/1523-1747.ep12545860

312. Vater CA, Harris ED, Siegel RC. Native cross-links in collagen fibrils induce resistance to human synovial collagenase. Biochemical Journal. 1979 Sep 1;181(3):639–45. doi:10.1042/bj1810639

313. Kagan HM. Intra- and extracellular enzymes of collagen biosynthesis as biological and chemical targets in the control of fibrosis. Acta Tropica. 2000 Oct;77(1):147–52. doi:10.1016/S0001-706X(00)00128-5

314. Payne SH. The utility of protein and mRNA correlation. Trends Biochem Sci. 2015 Jan;40(1):1–3. doi:10.1016/j.tibs.2014.10.010 PubMed PMID: 25467744; PubMed Central PMCID: PMC4776753.

315. Derynck R, Zhang YE. Smad-dependent and Smad-independent pathways in TGF-beta family signalling. Nature. 2003 Oct 9;425(6958):577–84. doi:10.1038/nature02006 PubMed PMID: 14534577.